1994-12

Single and dual burn maneuvers for low-earth-orbit maintenance

Hernandez, Andrew A.

Monterey, California. Naval Postgraduate School

NAVAL POSTGRADUATE SCHOOL
Monterey, California

THESIS

SINGLE AND DUAL BURN MANEUVERS FOR LOW-EARTH-ORBIT MAINTENANCE

by

Andrew A. Hernandez

December 1994

Thesis Advisor: I. M. Ross

Approved for public release; distribution is unlimited

REPORT DOCUMENTATION PAGE

Form Approved OMB No. 0704

1. AGENCY USE ONLY *(Leave blank)*	2. REPORT DATE DECEMBER 1994	3. REPORT TYPE AND DATES COVERED Master's Thesis, Final

4. TITLE AND SUBTITLE
SINGLE AND DUAL BURN MANEUVERS FOR LOW EARTH ORBIT MAINTENANCE

5. FUNDING NUMBERS

6. AUTHOR(S) Hernandez, Andrew A.

7. PERFORMING ORGANIZATION NAME(S) AND ADDRESS(ES)
Naval Postgraduate School
Monterey CA 93943-5000

8. PERFORMING ORGANIZATION REPORT NUMBER

9. SPONSORING/MONITORING AGENCY NAME(S) AND ADDRESS(ES)

10. SPONSORING/MONITORING AGENCY REPORT NUMBER

11. SUPPLEMENTARY NOTES The views expressed in this thesis are those of the author and do not reflect the official policy or position of the Department of Defense or the U.S. Government.

12a. DISTRIBUTION/AVAILABILITY STATEMENT Approved for public release; distribution unlimited

12b. DISTRIBUTION CODE

13. ABSTRACT *(maximum 200 words)*Optimal control theory suggests maintaining an orbital altitude band for Low- Earth-Orbiting (LEO) satellites using periodic thrusting than forced Keplerian motion, i.e. a trajectory obtained by thrust-drag cancellation. Designing guidance algorithms for orbit maintenance is complicated by the nonlinearities associated with orbital motion. An algorithm developed previously using thrusters firing significantly off the direction of motion successfully maintains an orbital band, but is very inefficient. This thesis develops two different control strategies based on the osculating orbital parameters, taking a conservative approach to keeping within altitude limitations. Thrust is in the local horizontal plane, along the direction of flight. Single and dual burn maneuvers are considered for various bandwidths and thruster sizes. The dual burn strategy is somewhat close to a Hohmann transfer. The specified orbital band is generally maintained, with some cases slightly exceeding the upper limit. Propellant consumption for both maneuvers is significantly better than previous methods. This thesis shows that forward firing thrusters can be used with osculating orbital parameters to obtain efficiencies within forced Keplerian motion values.

14. SUBJECT TERMS Forced Keplerian Trajectory, thrust-to-drag ratio, ballistic coefficient, eccentricity, orbital decay.

15. NUMBER OF PAGES 100

16. PRICE CODE

17. SECURITY CLASSIFICATION OF REPORT	18. SECURITY CLASSIFICATION OF THIS PAGE	19. SECURITY CLASSIFICATION OF ABSTRACT	20. LIMITATION OF ABSTRACT
UNCLASSIFIED	UNCLASSIFIED	UNCLASSIFIED	UL

Approved for public release; distribution is unlimited.

Single and Dual Burn Maneuvers for Low-Earth-Orbit Maintenance

by

Andrew A. Hernandez
Lieutenant, United States Navy
B.S., University of Florida, 1986

Submitted in partial fulfillment
of the requirements for the degree of

MASTER OF SCIENCE IN ASTRONAUTICAL ENGINEERING

from the

NAVAL POSTGRADUATE SCHOOL
December 1994

Author: [redacted]
Andrew A. Hernandez

Approved by: [redacted]
I. M. Ross, Thesis Advisor

[redacted]
K. T. Alfriend, Second Reader

[redacted]
Daniel J. Collins, Chairman
Department of Aeronautics and Astronautics

ABSTRACT

Optimal control theory suggests maintaining an orbital altitude band for Low-Earth-Orbiting (LEO) satellites using periodic thrusting than forced Keplerian motion, i.e. a trajectory obtained by thrust-drag cancellation. Designing guidance algorithms for orbit maintenance is complicated by the nonlinearities associated with orbital motion. An algorithm developed previously using thrusters firing significantly off the direction of motion successfully maintains an orbital band, but is very inefficient. This thesis develops two different control strategies based on the osculating orbital parameters, taking a conservative approach to keeping within altitude limitations. Thrust is in the local horizontal plane, along the direction of flight. Single and dual burn maneuvers are considered for various bandwidths and thruster sizes. The dual burn strategy is somewhat close to a Hohmann transfer. The specified orbital band is generally maintained, with some cases slightly exceeding the upper limit. Propellant consumption for both maneuvers is significantly better than previous methods. This thesis shows that forward firing thrusters can be used with osculating orbital parameters to obtain efficiencies within forced Keplerian motion values.

TABLE OF CONTENTS

I. INTRODUCTION

The rising cost of placing a satellite in orbit is creating a higher emphasis on minimization of non-payload mass to facilitate more payload items, and thus capability, on a single vehicle. Reducing the mass of propellant required to maintain a desired orbit has the additional benefits for the program in that it also reduces the size and mass of the tanks needed to store it. Spacecraft configuration, orbit requirements and thruster control logic dictate propellant consumption. The propellant mass required for orbital maintenance is significantly higher for a Low-Earth Orbiting (LEO) satellite than a geosynchronous one because of the significant effects of atmospheric drag on the orbit.

Consider the problem of maintaining a spacecraft within a prescribed orbital band in LEO (see Figure 1). The conceptually simplest thruster control logic is that of a Forced Keplerian Trajectory (FKT), where the thrust cancels drag. While this method is easy to visualize it is difficult to implement because of technological restrictions on drag estimation, thrust vectoring and thrust magnitude adjustments. Although Ross and Melton, using optimal control theory, show that an FKT is not an optimal maneuver for propellant consumption [Ref. 1], it is a good baseline to measure other methods.

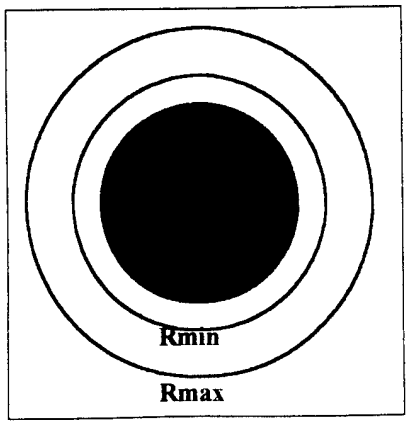

Figure 1. Orbit Radial Bandwidth

The Hohmann transfer between the lower and upper radial bands is another method of thruster control. Two thruster burn sequences are used in this scheme. The

change in velocity imparted at the lower altitude in the first sequence places the satellite in an elliptic transfer orbit that has an apogee of the maximum radius, while the one at the upper altitude circularizes the orbit. Both thrust sequences are in the direction of flight.

Gottlieb's Eccentricity Intercept Targeting and Guidance (EITAG) [Ref. 2] program computes thruster burn duration and timing based on the relationship between eccentricity, *e*, and semi-major axis, *a*, as shown in Figure 2. It integrates forward from the current *e-a* pair and backward from the desired *e-a* pair. A two burn routine reboosts the satellite to the desired circular orbit. The first burn achieves the intersection point of the two curves. The vehicle coasts until it reaches the required position in this intermediate orbit that enables the second burn to move the satellite along the final curve.

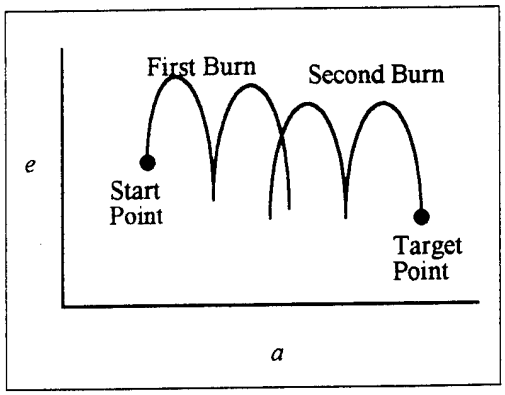

Figure 2. Eccentricity Versus Semi-major Axis

In order to maintain a radial band Pauls [Ref. 3] and Wilsey [Ref. 4] developed a single burn control logic based on orbital radius, specific energy and a thruster cant angle (the angle the thrust vector makes with respect to the local horizontal). While the method successfully controls the radial band it causes the satellite to consume at least three times the propellant of the FKT benchmark.

Since orbital parameters are derived from the radius and its changes, in this thesis a control strategy is developed using the osculating (instantaneous) perigee and apogee radii for a single burn with the thruster firing in the local horizontal plane along the direction of motion. A dual burn logic, using the single burn strategy as the first burn and the flight path angle as the control variable for the second burn, is also explored.

II. FORMULA DEVELOPMENT

A. DEVELOPMENT OF THE EQUATIONS OF MOTION

Assuming the satellite is a non-lifting (blunt) body simplifies analysis in that drag is the only uncontrollable nonconservative force being considered. Specifying planar motion, the initial orbit as circular, defining the problem as a two-body problem and neglecting all other possible perturbations facilitates ease of formulation. The orbital dynamics can be considered in a polar coordinate system as shown in Figure 3.

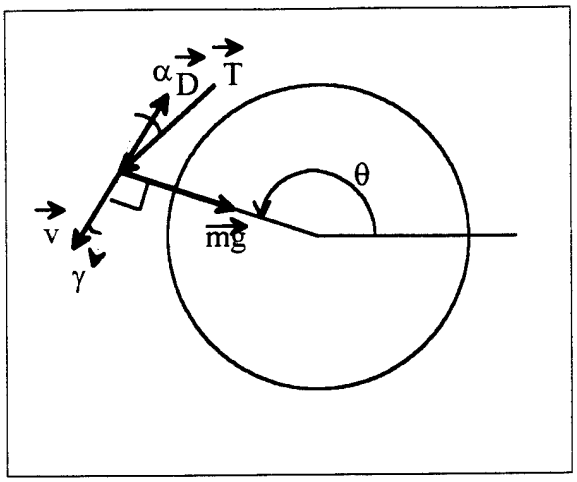

Figure 3. Orbital Coordinate System

The equations of motion are

$$a_r = \sum \frac{F_r}{m} \tag{1}$$

$$a_t = \sum \frac{F_t}{m} \tag{2}$$

where a_r and a_t are the radial and transverse components of the inertial acceleration, ΣF_r and ΣF_t are the sums of the respective forces, and m is the satellite mass. Drag and thrust can be broken into components

$$D_r = -D\sin\gamma \tag{3a}$$

$$D_t = -D\cos\gamma \tag{3b}$$

$$T_r = T\sin\alpha \tag{4a}$$

$$T_t = T\cos\alpha \tag{4b}$$

where γ is the flight path angle (the angle between the transverse axis and the velocity vector) and α is the thruster elevation angle (the angle between the transverse axis and the thrust vector). Expressing the equations of motion in polar coordinates and substituting in Equations 3 and 4 yields

$$\ddot{r} - \dot{\theta}^2 r = -\frac{\mu}{r^2} + \frac{D_r}{m} + \frac{T_r}{m} \tag{5}$$

$$\ddot{\theta} r + 2\dot{\theta}\dot{r} = \frac{D_t}{m} + \frac{T_t}{m} \tag{6}$$

where μ is the geocentric gravitational constant and θ is the angular position of the satellite as depicted in Figure 3.

B. NONDIMENSIONALIZATION OF THE EQUATIONS OF MOTION

It is useful to nondimensionalize the equations of motion listed above in order to limit the effects of computational errors when dealing with large numbers. This also allows better analysis of the effects of the variation of parameters.

1. Definitions

Base units in mass, length and time are required to nondimensionalize the problem. The base mass, m_b, is the initial mass of the satellite. The base length, r_b, is the initial semi-major axis of the actual orbit. Since the satellite travels above and below the center

of the desired radial band the initial satellite position is at the upper limit of the bandwidth. The base time, t_b, is the period of the initial orbit

$$t_b = 2\pi\sqrt{\frac{r_b^3}{\mu}} \tag{7}$$

The nondimensionalized mass, radius and time are thus

$$\bar{m} = \frac{m}{m_b} \tag{8}$$

$$\bar{r} = \frac{r}{r_b} \tag{9}$$

$$\bar{t} = \frac{t}{t_b} \tag{10}$$

2. Equation Nondimensionalization

The satellite's position variables and their derivatives are nondimensionalized using the base units

$$\dot{r} = \frac{dr}{dt} = \frac{d(r_b\bar{r})}{d(t_b\bar{t})} = \frac{r_b d\bar{r}}{t_b d\bar{t}} = \frac{r_b}{t_b}\bar{r}' \tag{11}$$

$$\ddot{r} = \frac{d^2r}{dt^2} = \frac{d}{dt}\left(\frac{dr}{dt}\right) = \frac{d}{dt}\left(\frac{r_b}{t_b}\bar{r}'\right) = \frac{r_b}{r_t}\frac{d}{d(t_b\bar{t})}(\bar{r}') = \frac{r_b}{t_b^2}\frac{d\bar{r}'}{d\bar{t}} = \frac{r_b}{t_b^2}\bar{r}'' \tag{12}$$

$$\theta = \bar{\theta} \tag{13}$$

$$\dot{\theta} = \frac{d\theta}{dt} = \frac{d\bar{\theta}}{d(t_b\bar{t})} = \frac{d\bar{\theta}}{t_b d\bar{t}} = \frac{1}{t_b}\bar{\theta}' \tag{14}$$

$$\ddot{\theta} = \frac{d^2\theta}{dt^2} = \frac{d}{dt}\left(\frac{d\theta}{dt}\right) = \frac{d}{dt}\left(\frac{1}{t_b}\bar{\theta}'\right) = \frac{1}{t_b}\frac{d}{d(t_b\bar{t})}\left(\bar{\theta}'\right) = \frac{1}{t_b^s}\frac{d\bar{\theta}'}{d\bar{t}} = \frac{1}{t_b^2}\bar{\theta}'' \tag{15}$$

where primes represent a differentiation with respect to nondimensionalized time. Substituting these equations and Equations 3 and 4 into the equations of motion yields

$$\frac{r_b}{t_b^2}\bar{r}'' - \left(\frac{1}{t_b}\bar{\theta}'\right)^2 r_b\bar{r} = -\frac{\mu}{(r_b\bar{r})^2} - \frac{D\sin\gamma}{m_b\bar{m}} + \frac{T\sin\alpha}{m_b\bar{m}} \tag{16}$$

$$\frac{1}{t_b^2}\bar{\theta}'' r_b\bar{r} + 2\frac{1}{t_b}\bar{\theta}'\frac{r_b}{t_b}\bar{r}' = -\frac{D\cos\gamma}{m_b\bar{m}} + \frac{T\cos\alpha}{m_b\bar{m}} \tag{17}$$

Rearranging terms

$$\bar{r}'' = \bar{\theta}'^2\bar{r} - \frac{t_b^2}{r_b^3}\frac{\mu}{\bar{r}^2} - \frac{t_b^2}{r_b m_b}\frac{D\sin\gamma}{\bar{m}} + \frac{t_b^2}{r_b m_b}\frac{T\sin\alpha}{\bar{m}} \tag{18}$$

$$\bar{\theta}'' = -2\frac{\bar{\theta}'\bar{r}'}{\bar{r}} - \frac{t_b^2}{r_b m_b}\frac{D\cos\gamma}{\bar{m}\bar{r}} + \frac{t_b^2}{r_b m_b}\frac{T\cos\alpha}{\bar{m}\bar{r}} \tag{19}$$

Substituting in Equation 7 for the base time the equations become

$$\bar{r}'' = \bar{\theta}'^2\bar{r} - \left(\frac{2\pi}{\bar{r}}\right)^2 - \frac{t_b^2}{r_b m_b}\frac{D\sin\gamma}{\bar{m}} + \frac{t_b^2}{r_b m_b}\frac{T\sin\alpha}{\bar{m}} \tag{20}$$

$$\bar{\theta}'' = -2\frac{\bar{\theta}'\bar{r}'}{\bar{r}} - \frac{t_b^2}{r_b m_b}\frac{D\cos\gamma}{\bar{m}\bar{r}} + \frac{t_b^2}{r_b m_b}\frac{T\cos\alpha}{\bar{m}\bar{r}} \tag{21}$$

3. Nondimensionalization of Nonconservative Forces

The nonconservative forces (thrust and drag) are to be nondimensionalized by multiplying and dividing by the base units required to remove the dimensions.

a. Nondimensionalized Thrust

Nondimensionalized thrust is defined by

$$\overline{T} = \frac{t_b^2}{r_b m_b} T \tag{22}$$

b. Nondimensionalized Drag

Nondimensionalized drag is given as

$$\overline{D} = \frac{t_b^2}{r_b m_b} D \tag{23}$$

4. Nondimensionalization of Other Parameters

The drag the satellite encounters depends solely on the atmosphere the orbit passes through. Drag is defined by

$$D = \frac{1}{2}\rho A C_D v^2 \tag{24}$$

where ρ is the atmospheric density, A is the effective surface area of the vehicle, C_D is the drag coefficient associated with the spacecraft, and v is the instantaneous velocity. An exponentially decaying density is a common atmospheric model and is given by

$$\rho = \rho_o e^{-\frac{1}{H}(r - r_{ref})} \tag{25}$$

where ρ_o is the density at r_{ref}, the reference altitude, and H is the atmospheric scale height. Nondimensionalized scale height is defined as

$$\overline{\beta} = \frac{r_b}{H} \tag{26}$$

A base density is defined as

$$\rho_b = \rho_o \tag{27}$$

The nondimensionalized density is

$$\bar{\rho} = \frac{\rho}{\rho_o} = \frac{\rho_o}{\rho_o} e^{-\frac{\bar{\beta} H}{r_b} \frac{1}{H}(r - r_{ref})} = e^{-\bar{\beta}\left(\bar{r} - \frac{r_{ref}}{r_b}\right)} \tag{28}$$

The ballistic coefficient is defined as

$$B = \frac{m_b}{AC_d} \tag{29}$$

thus the nondimensionalized ballistic coefficient is

$$\bar{B} = \frac{B}{\rho_b r_b} = \frac{m_b}{AC_d \rho_b r_b} \tag{30}$$

The spacecraft's velocity is

$$v^2 = \dot{r}^2 + r^2 \dot{\theta}^2 \tag{31}$$

and is nondimensionalized using Equations 9, 11 and 14 to

$$v^2 = \left(\frac{r_b}{t_b}\bar{r}'\right)^2 + (r_b \bar{r})^2 \left(\frac{1}{t_b}\bar{\theta}'\right)^2 = \frac{r_b^2}{t_b^2}\left(\bar{r}'^2 + \bar{r}^2 \bar{\theta}'^2\right) = \frac{r_b^2}{t_b^2}\bar{v}^2 \tag{32}$$

The nondimensionalized thrust-to-drag ratio is

$$\bar{T}_D = \frac{\bar{T}}{\bar{D}_o} \tag{33}$$

where $\bar{D}_o$ is the nondimensionalized drag for the FKT orbit. The change in mass is given by

$$\dot{m} = -\frac{T}{I_{sp}g} \tag{34}$$

Nondimensionalizing yields

$$\bar{m}' = \dot{m}\frac{t_b}{m_b} = -\frac{T}{I_{sp}g}\frac{\bar{T}m_b r_b}{Tt_b^2}\frac{t_b}{m_b} = -\frac{\bar{T}r_b}{I_{sp}gt_b} \tag{35}$$

5. Nondimensionalized Equations

Substituting Equations 22 through 32 into the equations of motion produces

$$\bar{r}'' = \bar{\theta}'^2\bar{r} - \left(\frac{2\pi}{\bar{r}}\right)^2 - \frac{e^{-\bar{\beta}\left(\bar{r}-\frac{r_{ref}}{r_b}\right)}\bar{v}^2\sin\gamma}{2\bar{m}\bar{B}} + \frac{\bar{T}\sin\alpha}{\bar{m}} \tag{36}$$

$$\bar{\theta}'' = -2\frac{\bar{\theta}'\bar{r}'}{\bar{r}} - \frac{e^{-\bar{\beta}\left(\bar{r}-\frac{r_{ref}}{r_b}\right)}\bar{v}^2\cos\gamma}{2\bar{m}\bar{r}\bar{B}} + \frac{\bar{T}\cos\alpha}{\bar{m}\bar{r}} \tag{37}$$

III. COMPUTER MODEL DEVELOPMENT

A. ORIGINAL DEVELOPMENT

The original program was developed by Pauls [Ref. 3], and modified by Wilsey [Ref. 4] and Gardner [Ref. 5]. It was FORTRAN based, and simulated the motion of a spacecraft in orbit by utilizing a fourth-order Runge-Kutta numerical integration routine. Wilsey [Ref. 4] nondimensionalized the equations and used four state variables to reduce the two second order equations of motion to four first order equations; Gardner [Ref. 5] redefined the variables and added the mass to the state variables and the mass equation as a first order differential integrated by the Runge-Kutta routine.

B. STATE VARIABLE DEFINITIONS

Maintaining a four element state vector based on the position variables and leaving the mass as a separate issue, the state vector is defined as

$$x_1 = r \tag{38}$$

$$x_2 = \dot{r} = \dot{x}_1 \tag{39}$$

$$x_3 = \theta \tag{40}$$

$$x_4 = \dot{\theta} = \dot{x}_3 \tag{41}$$

Their nondimensionalized counterparts are

$$\bar{x}_1 = \bar{r} \tag{42}$$

$$\bar{x}_2 = \bar{r}' = \bar{x}_1' \tag{43}$$

$$\bar{x}_3 = \bar{\theta} \tag{44}$$

$$\bar{x}_4 = \bar{\theta}' = \bar{x}_3' \tag{45}$$

C. NONDIMENSIONALIZED STATE VARIABLE EQUATIONS OF MOTION

Rewriting the equations of motion (Equations 38 and 39) by substituting in the nondimensionalized state variables, Equations 42 through 45, yields

$$\bar{x}_2' = \bar{x}_1\bar{x}_4^2 - \left(\frac{2\pi}{\bar{x}_1}\right)^2 - \frac{e^{-\bar{\beta}\left(\bar{r}-\frac{r_{ref}}{r_b}\right)}\bar{v}^2\sin\gamma}{2\bar{m}\bar{B}} + \frac{\bar{T}\sin\alpha}{\bar{m}} \tag{46}$$

$$\bar{x}_4' = -\frac{2\bar{x}_4\bar{x}_2}{\bar{x}_1} - \frac{e^{-\bar{\beta}\left(\bar{r}-\frac{r_{ref}}{r_b}\right)}\bar{v}^2\cos\gamma}{2\bar{m}\bar{x}_1\bar{B}} + \frac{\bar{T}\cos\alpha}{\bar{m}\bar{x}_1} \tag{47}$$

The flight path angle, γ, is dependent on the radial and tangential components of the velocity vector and can be expressed in terms of the state variables

$$\sin\gamma = \frac{\bar{x}_2}{\bar{v}} \tag{48}$$

$$\cos\gamma = \frac{\bar{x}_1\bar{x}_4}{\bar{v}} \tag{49}$$

Thus the equations appear in the computer program as

$$\bar{x}_1' = \bar{x}_2 \tag{50}$$

$$\bar{x}_2' = \bar{x}_1\bar{x}_4^2 - \frac{4\pi^2}{\bar{x}_1^2} - \frac{e^{-\bar{\beta}\left(\bar{r}-\frac{r_{ref}}{r_b}\right)}\bar{v}\bar{x}_2}{2\bar{m}\bar{B}} + \frac{\bar{T}\sin\alpha}{\bar{m}} \tag{51}$$

$$\bar{x}_3' = \bar{x}_4 \tag{52}$$

$$\bar{x}_4' = -\frac{2\bar{x}_4\bar{x}_2}{\bar{x}_1} - \frac{e^{-\bar{\beta}\left(\bar{r}-\frac{r_{ref}}{r_b}\right)}\bar{v}\bar{x}_4}{2\bar{m}\bar{B}} + \frac{\bar{T}\cos\alpha}{\bar{m}\bar{x}_1} \tag{53}$$

D. PROGRAM ORGANIZATION

The program, written in MATLAB, is broken into several functional subroutines to provide a fluid and logical flow of data through required calculations. Initialization of constants and variables is followed by the computation of drag at the Keplerian orbit radius and then the main program. Nondimensionalized velocity is computed in LEOVEL using the radial and tangential velocity components. The exponential term of drag is evaluated in LEODRAG. LEOLOCAL determines the individual pieces of the equations of motion for easy assimilation in LEOXDOT, where the derivatives of the nondimensionalized state variables are calculated. The Runge-Kutta is completed in LEORK4A, LEORK4B, LEORK4C, and LEORK4D, with the program recycling through from LEOVEL. After the RK4 routines have produced the new nondimensionalized state variables the propellant consumption for that step is computed, then the osculating orbital parameters are determined by LEOPARM1 and LEOPARM2. The thruster firing logic routine in effect is called (either LEOTFLPH alone or in combination with LEOTFLAP for the dual burn scenario) to determine whether or not the thruster is active during the upcoming step. A flowchart for the program is shown in Figure 4.

E. PROGRAM VALIDATION

All aspects of the code were verified since the program was written in a different language from the previous versions. The process Wilsey [Ref. 4] utilized was duplicated.

1. Initial Validation with No External Forces

With no atmospheric affects to hinder orbital motion the specific energy and angular momentum for both elliptic and circular orbits must remain constant. Results for

these values are shown in Figures 5 and 6 for the elliptic orbit, and Figures 7 and 8 for the circular orbit. Small fluctuations are impossible to see on the plots, so closer analysis is called for. Comparison of the output of the program to the initial values for these arguments, depicted in Figures 9 and 10 for the elliptic case and Figures 11 and 12 for the

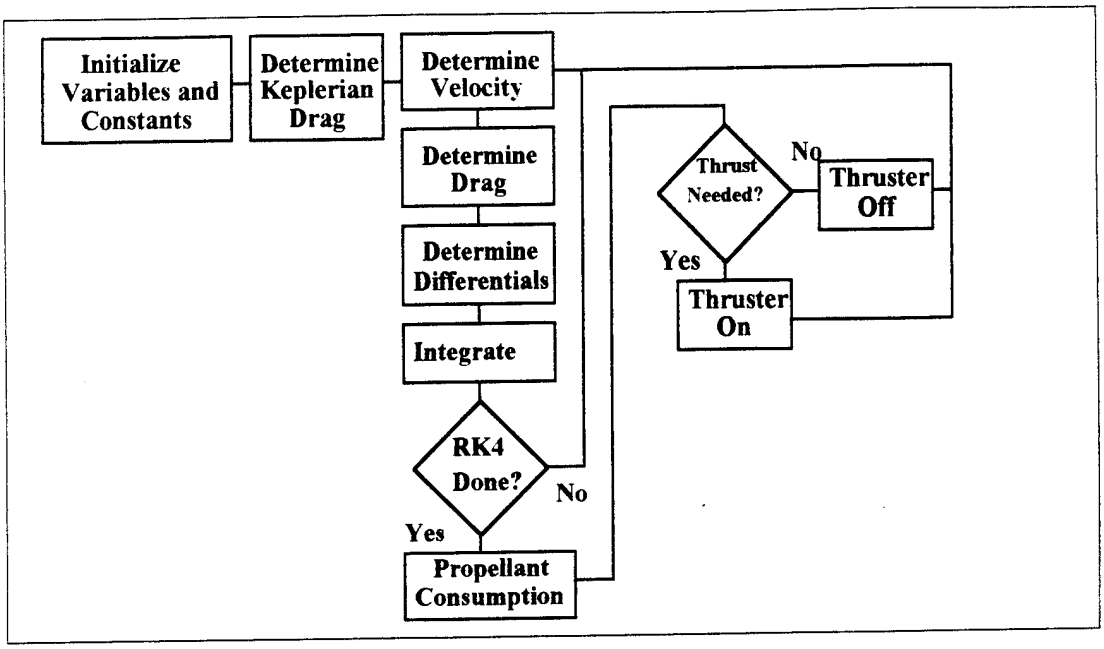

Figure 4. Program Flowchart

circular one, shows minor fluctuations on the order of 10^{-13} with respect to the base for the elliptic orbit and zero for the circular orbit. The fluctuations follow no discernible pattern and are of a relative magnitude that is known to be beneath MATLAB's computational limits and are viewed by the processor as near zero. This suggests they are computational noise generated by the numerous calculations of infinitesimal numbers, and the main body of the program is validated.

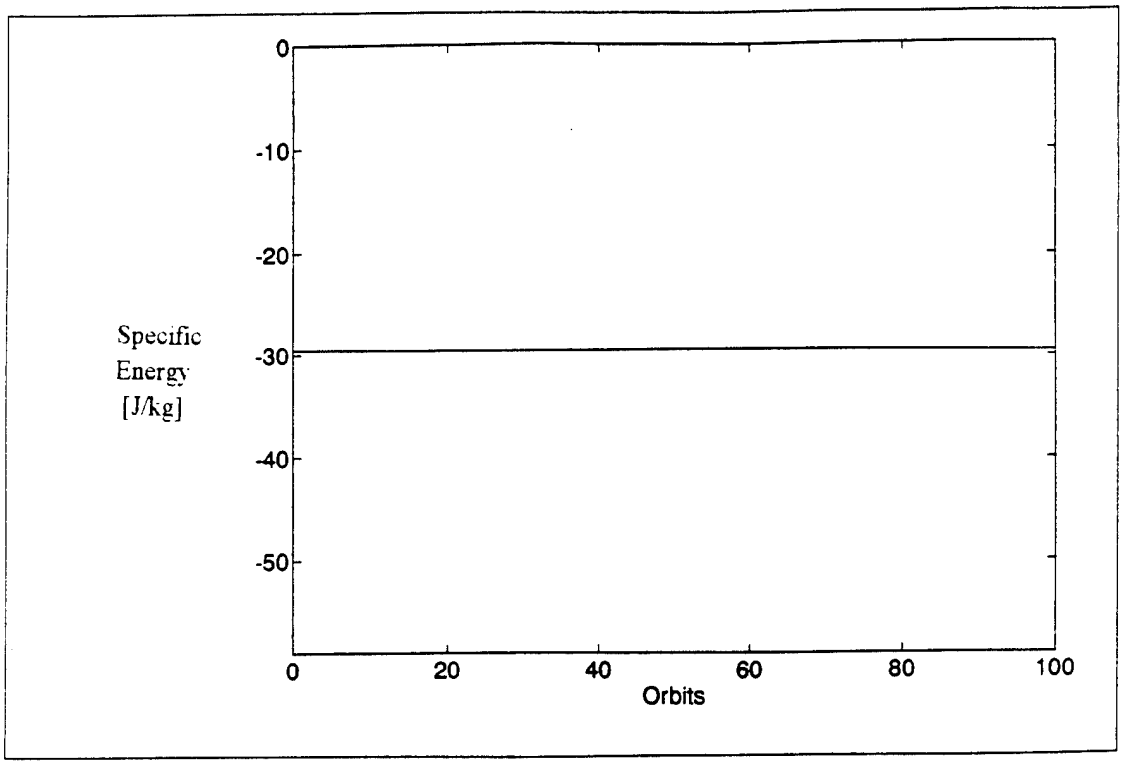

Figure 5. Specific Energy of a Drag Free Elliptic Orbit

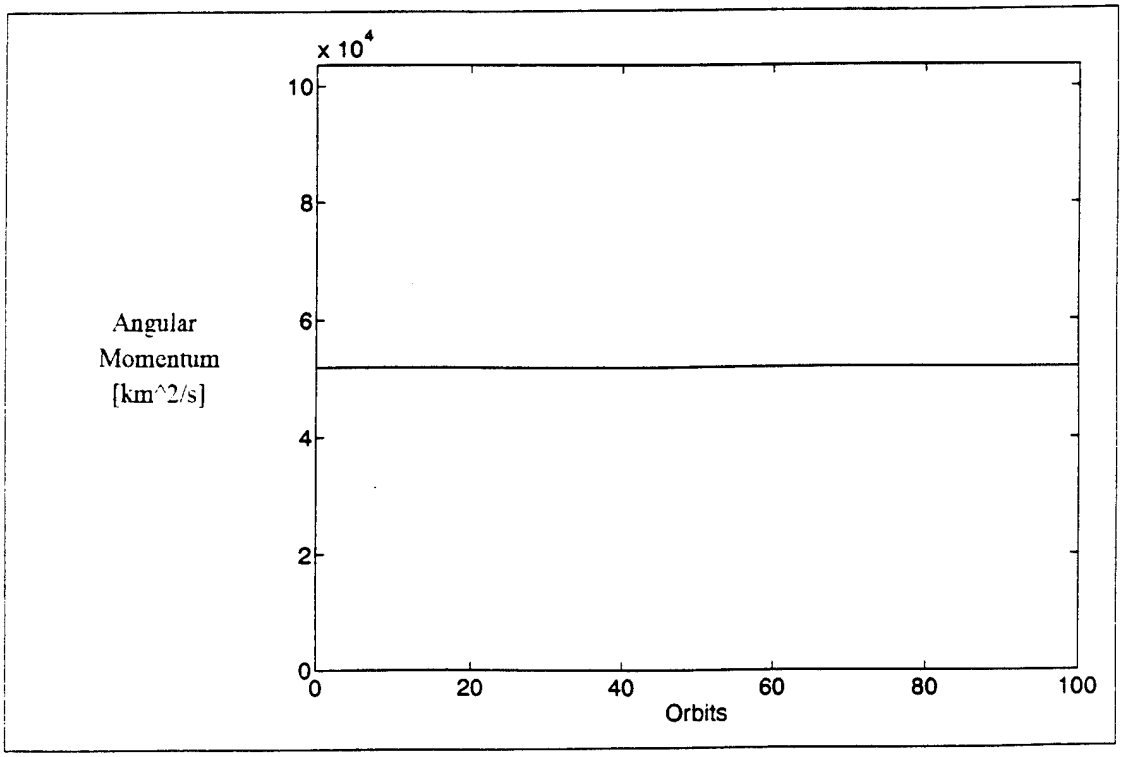

Figure 6. Angular Momentum of a Drag Free Elliptic Orbit

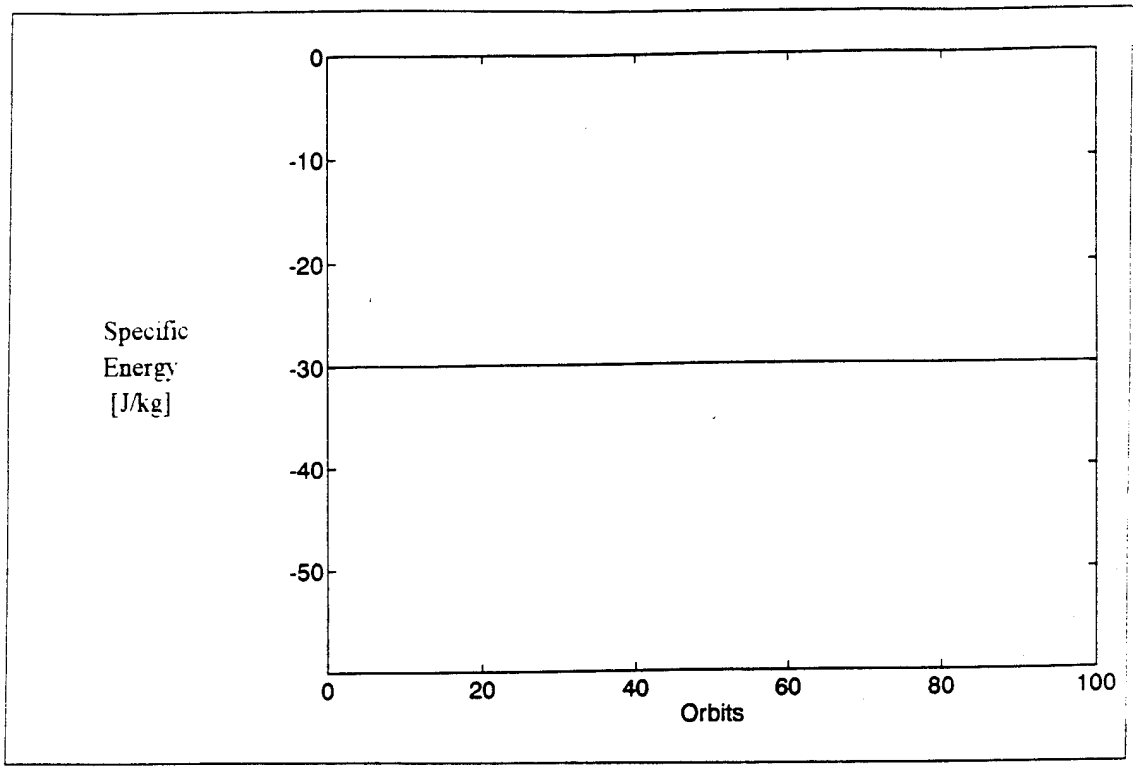

Figure 7. Specific Energy of a Drag Free Circular Orbit

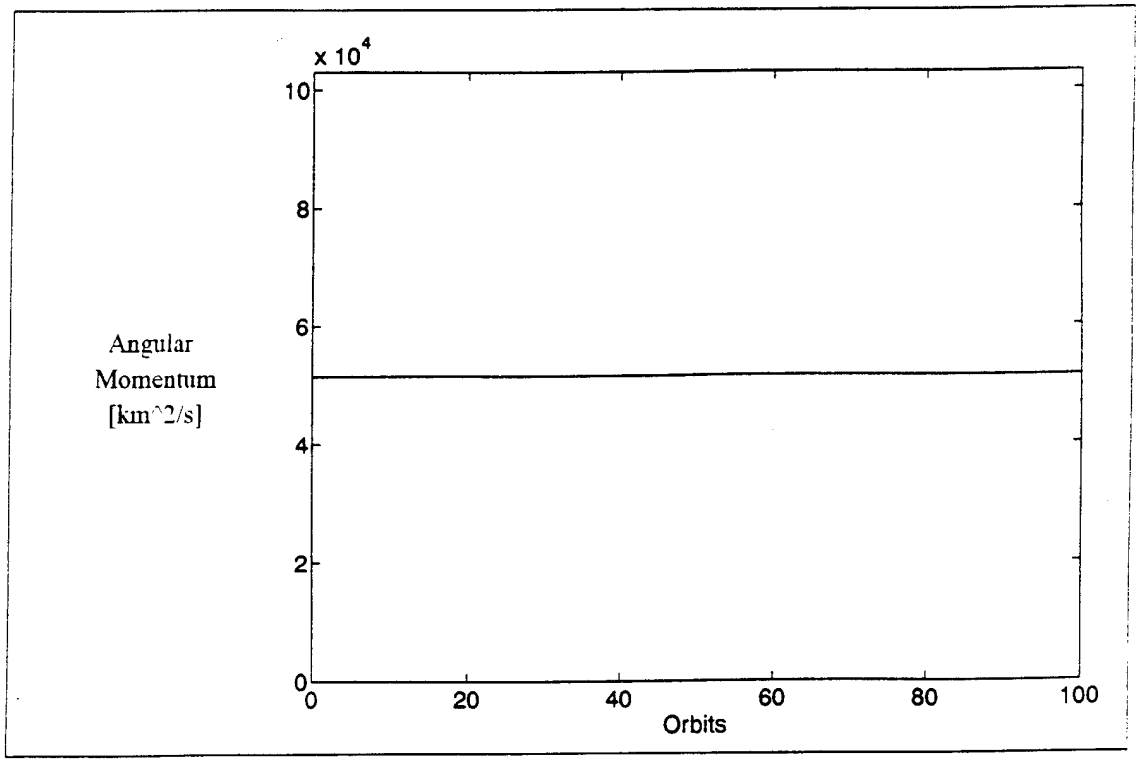

Figure 8. Angular Momentum of a Drag Free Circular Orbit

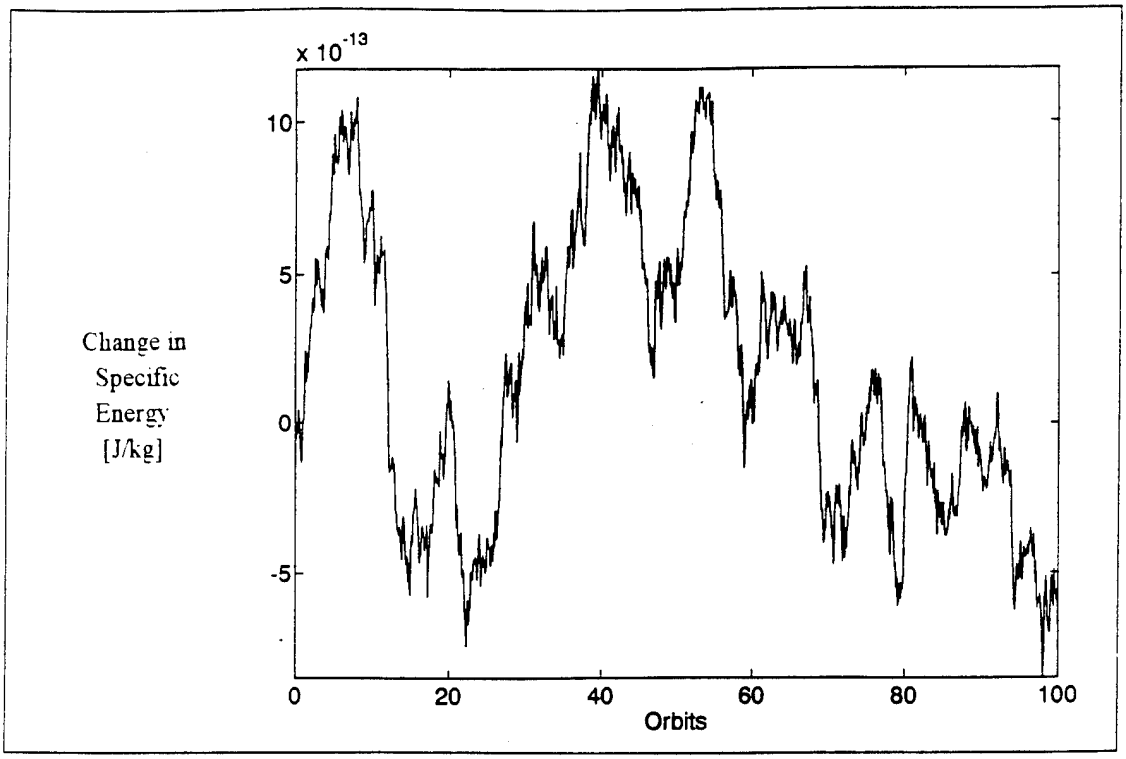

Figure 9. Change in Specific Energy of a Drag Free Elliptic Orbit

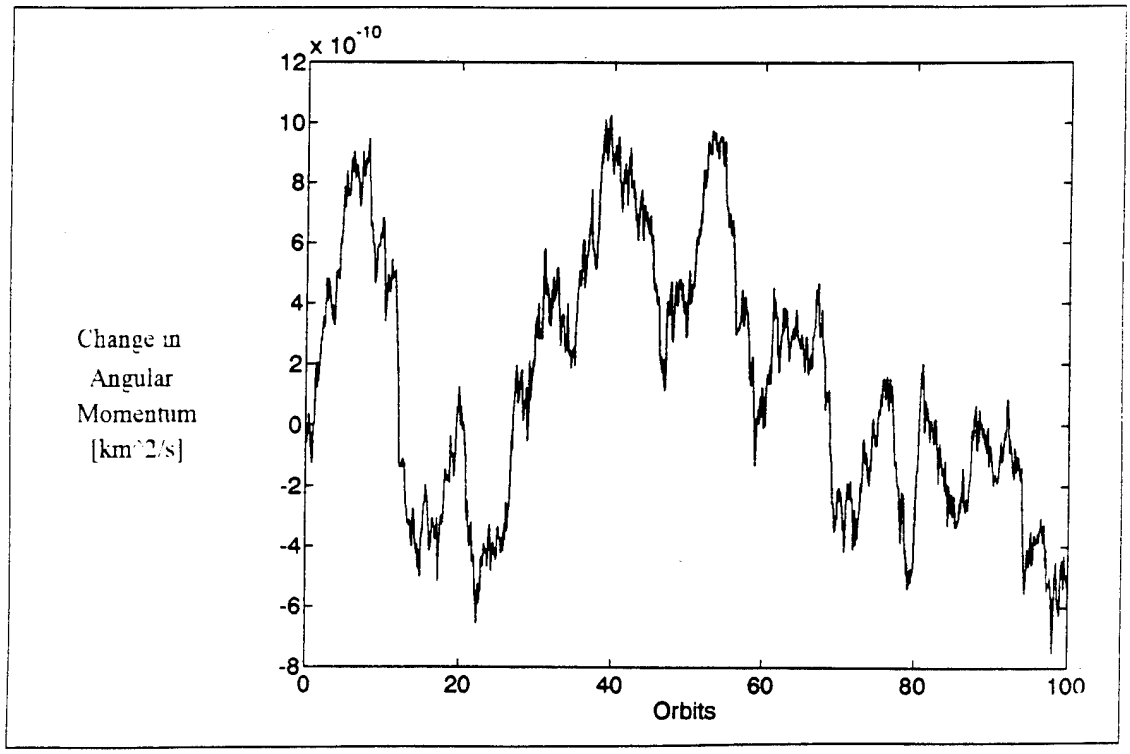

Figure 10. Change in Angular Momentum of a Drag Free Elliptic Orbit

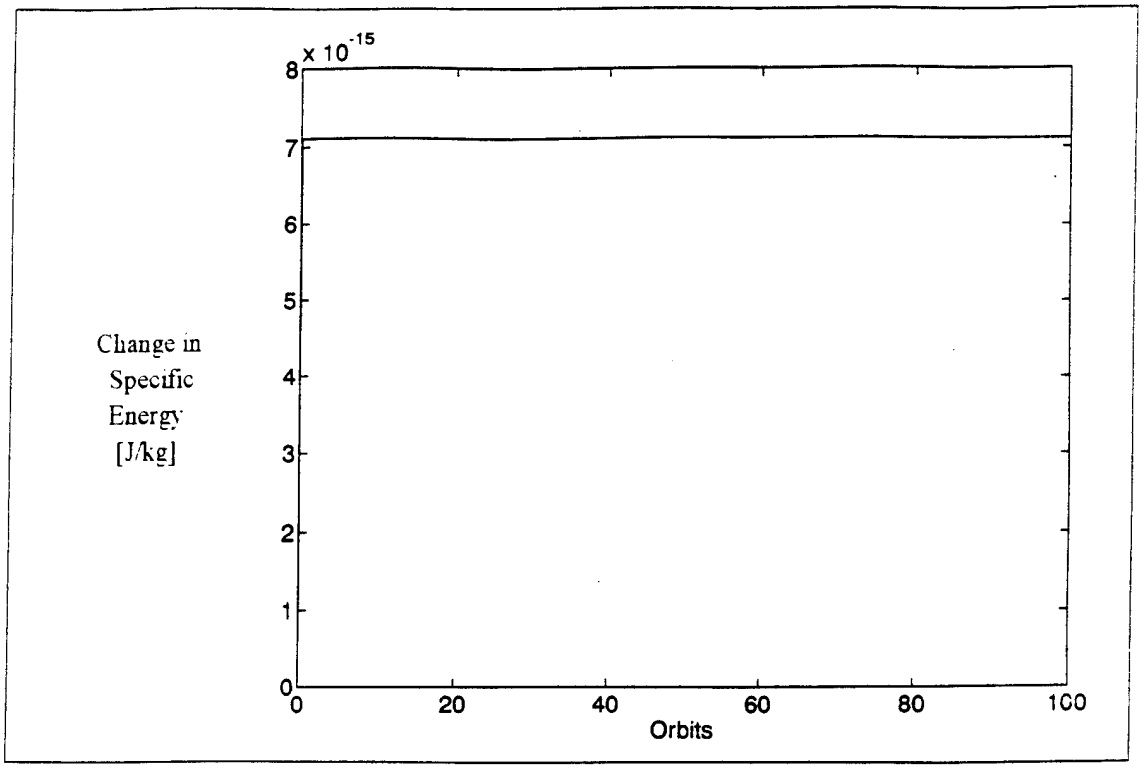

Figure 11. Change in Specific Energy of a Drag Free Circular Orbit

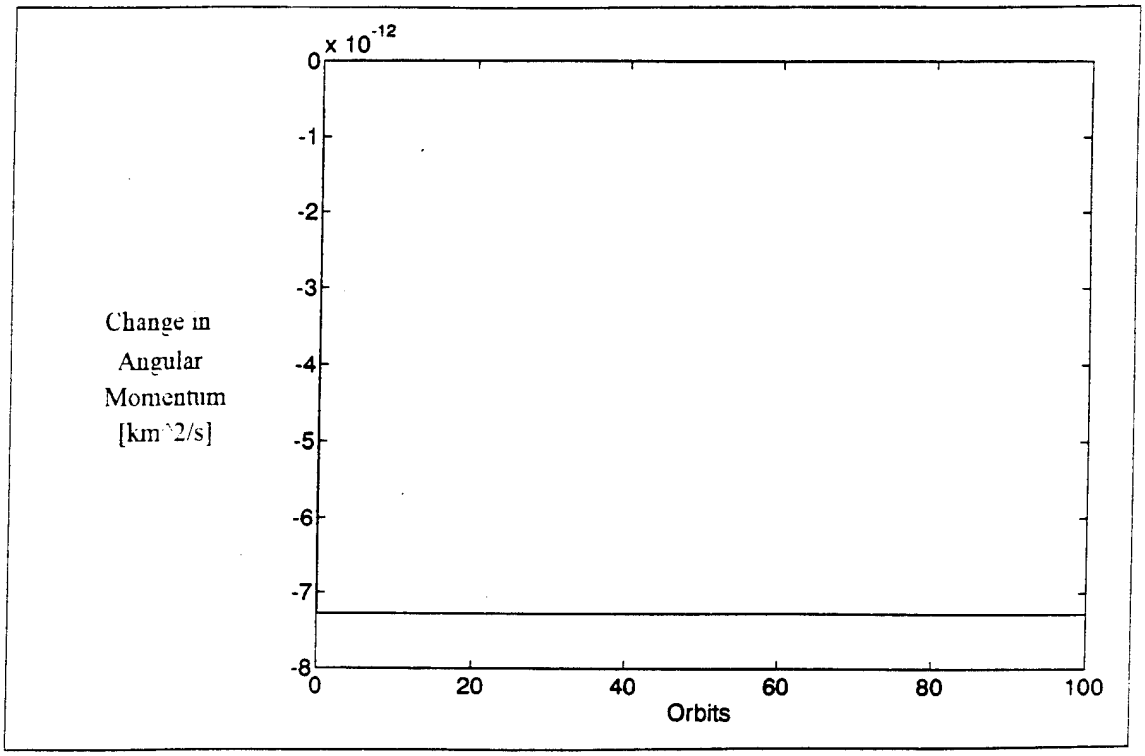

Figure 12. Change in Angular Momentum of a Drag Free Circular Orbit

2. Validation of Drag

The program was run using a constant atmospheric density model. The change in semi-major axis and velocity were compared with analytic values obtained by using equations from Wertz [Ref. 6] that approximate the changes for a satellite in a circular orbit experiencing drag

$$\Delta a = -2\pi \frac{AC_d}{m} \rho a^2 \tag{54}$$

$$\Delta v = \pi \frac{AC_d}{m} \rho a v \tag{55}$$

The equations were modified to facilitate ease of computation by making use of the definitions of the ballistic coefficient and its nondimensionalized counterpart, Equations 29 and 30, and noting that the mass and density are constant and that the initial semi-major axis is the base radius, to produce

$$\Delta a = -2\pi \frac{AC_d}{m_b} \rho_b a^2 \frac{m_b}{BAC_d} \frac{B}{\bar{B}\rho_b a} = -2\pi \frac{a}{\bar{B}} \tag{56}$$

$$\Delta v = \pi \frac{AC_d}{m_b} \rho_b a v \frac{m_b}{BAC_d} \frac{B}{\bar{B}\rho_b a} = \pi \frac{v}{\bar{B}} \tag{57}$$

A ten orbit test produced the computational values; the analytic values were calculated based on the computational semi-major axis and velocity at the start of each orbit. Percent differences were computed for both the change and the element. The results of the test, shown in Table 1, show that the percent difference in all cases is less than six-tenths of one percent, and the drag routine is validated.

ORBIT	% ΔSMA DIFFERENCE	%SMA DIFFERENCE	%ΔV DIFFERENCE	%V DIFFERENCE
1	-0.0063	-0.0158	0.0251	0.0316
2	0.0063	0.0158	0.0881	0.1105
3	0.0188	0.0474	0.1511	0.1895
4	0.0314	0.079	0.2141	0.2685
5	0.0439	0.1106	0.2772	0.3474
6	0.0565	0.1422	0.3404	0.4261
7	0.0696	0.1739	0.4033	0.5047
8	0.0817	0.2055	0.4661	0.5829
9	0.0942	0.2371	0.5285	0.6605
10	0.1068	0.2688	0.5903	0.7373

Table 1. Percent Difference in Change and Values for SMA and Velocity

IV. DEVELOPMENT OF THE ORBIT MAINTENANCE PROCEDURE

Ross and Melton [Ref. 1] demonstrated the non-optimality of a Forced Keplerian Trajectory with respect to propellant consumption. Pauls [Ref. 3] and Wilsey [Ref. 4] showed the adequacy, but non-optimality of a single, off axis burn controlled by radius and specific energy. A different method of control must be considered in order to approach optimality while maintaining the required orbital band. A review of orbital mechanics and Wilsey's [Ref. 4] plots for radius and eccentricity suggested a potential solution.

A. THRUSTER CANT ANGLE

A firing thruster imparts energy to the satellite at the expense of propellant, thus maximizing the energy gained while minimizing the burn time will reduce propellant consumption. The energy equation for an orbital body is

$$\varepsilon = \frac{v^2}{2} - \frac{\mu}{r} \tag{58}$$

The second term of the equation dominates, and orbital energy is negative. As the radius decreases the second term grows, and the energy increases negatively. Increasing the radius decreases the magnitude of the energy. Zeleny [Ref. 7] notes that Equation 58 can be expressed as

$$\varepsilon = \frac{1}{2}\vec{v} \bullet \vec{v} - \frac{\mu}{r} \tag{59}$$

The change in specific energy with respect to time is

$$\frac{d\varepsilon}{dt} = \vec{v} \bullet \frac{d\vec{v}}{dt} + \frac{\mu}{r^2}\frac{dr}{dt} = va\cos(\gamma - \xi) + \frac{\mu}{r^2}\frac{dr}{dt} \tag{60}$$

where ξ is the angle between the acceleration vector and the tangential axis. Thrust is larger than drag because a thrust equal to drag would require a FKT to maintain orbit. Figure 13 shows the results at two different thruster cant angles. If the cant angle is small, the velocity will not move radically above the tangential axis, and the second term of

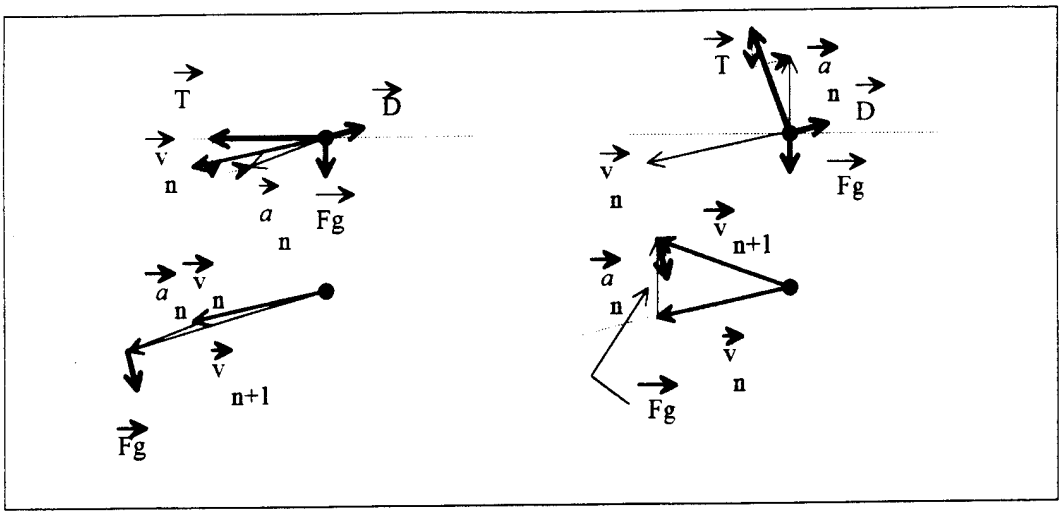

Figure 13. Resulting Velocities at Two Thruster Cant Angles

Equation 60 will be very small in comparison with the first term. If the cant angle is high the initial response will be reduced, since both terms are small. A sufficiently long burn would place the velocity and the thrust almost in the same direction, but the objective is to reduce burn times. The maximum change of orbital energy is obtained when the velocity and acceleration are nearly parallel. For decay of a circular orbit due to drag the flight path angle remains small, between 0° and -1°, provided the initial altitude, bandwidth (separation between maximum and miniumum radii) and vehicle configuration are sufficient to preclude extreme affects. If the path becomes elliptic, or the thruster is small and the bandwidth larger than the thruster can achieve in one orbit, the flight path angle may vary between 1° and -1°. Setting the thruster cant angle, α, equal to zero enables the satellite to sufficiently handle both positive and negative flight path angles with equal ability, more so than setting it 1° to either side. To achieve the same change in energy a

thruster firing at a significantly larger angle would have to fire longer, consuming more propellant. The thruster cant angle is therefore set at zero.

B. ECCENTRICITY CONTROL

The imposition of a maximum and minimum radius limits the eccentricity the orbit may obtain without having a portion of the orbit exceed either boundary. If the eccentricity surpasses the limit, the thruster control logic, whatever it may be, will be forced to fire the thrusters more often than if the eccentricity remains within orbital bandwidth requirements. The limiting eccentricity is given by

$$e_{\max} = \frac{R\max - R\min}{R\max + R\min} \tag{61}$$

For a thruster control logic to be remotely close to optimal it must avoid allowing the osculating eccentricity exceeding the maximum value.

C. SINGLE BURN THRUST CONTROL LOGIC

Since the orbital parameters of interest are based on the radius, orbital angle and their respective rates of change, and since the desired outcome is the maintenance of a prespecified orbital band by limiting the eccentricity, the control logic utilizes these values to obtain the desired results.

1. Thruster Firing Criteria

Acknowledging that the satellite would descend beneath the minimum radius if the thruster was not fired prior to reaching it dictates a burn start before the lower radial limit is reached. Atmospheric density profile, orbital bandwidth, thruster capacity and cant angle, and satellite configuration all play a role in how far the vehicle drops from thruster initiation until the radius ceases to decrease. Starting the burn when the osculating perigee radius drops below the minimum radius will at worst delay the time until the satellite passes the minimum value or cause the satellite to begin to climb well before the lower radial limit is reached. Any result in between the two is reasonably acceptable and the thruster firing criteria is established.

2. Thruster Turn Off Criteria

Gottlieb [Ref. 2] shows the relationship between semi-major axis, a, and eccentricity, e, during thrusted flight. If the thruster is allowed to fire until either portion of the a-e pair is beyond its limiting value the satellite will in all likelihood either exceed the bandwidth restrictions or require excessive burns to maintain it. Turning the thruster off when the osculating apogee radius exceeds the maximum radius implies that the orbital radius will never exceed the maximum value. This is mainly because the effect drag will have on reducing the apogee radius, and partly due to the change in apogee for any given instant being small enough so that the osculating apogee does not significantly exceed the limit. The error in overshooting the upper limit is small considering the second factor, and the thruster turn off criteria is established. Figure 14 is the logic flowchart for the single burn maneuver.

3. Resulting Orbit

Since the thrusts occur based on the osculating perigee falling below the minimum limit the satellite may not be at a perigee position when the thruster is activated. Additionally, the velocity change will not necessarily correspond to that of a Hohmann transfer. Changes in the perigee radius and apogee radius may occur simultaneously. Raising the instantaneous radius by increasing the apogee radius is the primary intent of the burn, but changes in the perigee radius are also important. Raising the perigee radius along with the apogee radius places the satellite in a more desirable orbit because it increases the time it takes for the perigee radius to decay below the minimum limit, increasing the period between burns.

The change in perigee radius can be determined from analysis of the semi-major axis, eccentricity, angular momentum and specific energy. Zeleny [Ref. 7] states the change in eccentricity and angular momentum from a change in velocity are

$$de = \frac{1}{\mu^2 e}(h^2 d\varepsilon + 2\varepsilon h dh) \tag{62}$$

$$\vec{dh} = \vec{r} \times \vec{dv} \tag{63}$$

where h is the angular momentum. The angular momentum is

$$\vec{h} = \vec{r} \times \vec{v} \tag{64}$$

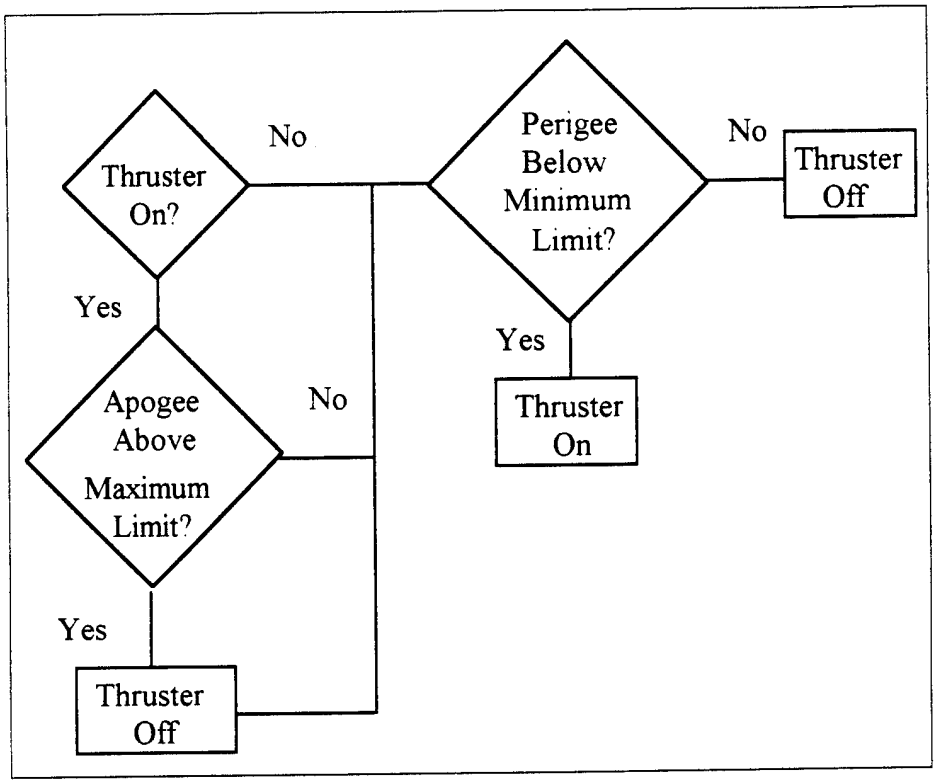

Figure 14. Single Burn Maneuver Thruster Control Flow

and thus

$$h = rv \sin\left(\frac{\pi}{2} - \gamma\right) = rv \cos\gamma \tag{65}$$

The change in angular momentum can be expressed as

$$dh = ra\cos\xi \tag{66}$$

Substituting Equations 58, 60, 65 and 66 into Equation 62 yields

$$de = \frac{h}{e\mu^2}[rv^2 a\cos\gamma\cos(\gamma-\xi) + \frac{\mu v^2}{r}\cos\gamma$$

$$+rv^2 a\cos\xi - 2\mu a\cos\xi] \tag{67}$$

Since all the angles in this equation are zero or approximately zero, and the terms outside the brackets are positive, the sign of the equation can be determined from

$$\text{sign}(de) = \text{sign}\left[2a(rv^2-\mu) + \frac{\mu v^2}{r}\right] \tag{68}$$

Zeleny [Ref. 7] states that the change in semi-major axis is

$$da = \frac{\mu}{2\varepsilon^2}d\varepsilon \tag{69}$$

The perigee radius is defined as

$$r_p = a(1-e) \tag{70}$$

so its change is

$$dr_p = (1-e)da - ade \tag{71}$$

From Equation 68 the change in eccentricity varies from positive to negative. As the velocity increases with a burn, the change in eccentricity is more likely to become positive,

and attempt to reduce the change in perigee radius. Eccentricity is generally very small, and changes to it even smaller for any given instant in time. The change in semi-major axis is not small, in comparison. The first term in Equation 71 is on the order of the change in semi-major axis while the second term is significantly smaller. The overall result is a positive change in the perigee radius, placing the satellite in a much more desirable, but still eccentric, orbit.

D. DUAL BURN CONTROL LOGIC

The single burn strategy described above leaves the satellite in an elliptic orbit. If the perigee radius has not been sufficiently raised, drag will soon lower it beneath the minimum limit and the thruster will fire again. Reducing the eccentricity by conducting a second burn as the satellite approaches apogee could result in an increase in the period of radius boosting burns, potentially saving propellant. The objective of the second burn is to decrease eccentricity, but not necessarily make the orbit circular.

1. Thruster Firing Criteria

As the satellite approaches apogee the thruster must fire to increase both the semi-major axis and the perigee radius. The flight path angle, γ, is positive during the perigee to apogee transition, and decreases as the vehicle nears apogee. Waiting for the flight path angle to become negative before initiating thrust could raise the apogee radius, placing the satellite on a path that exceeds the maximum radial limit. Firing the thruster when it drops below a minimum positive value seems to be the prudent course of action. An arbitrary value was selected for the firing criteria, and adjusted until it minimized eccentricity for the smallest thruster-bandwidth combination. Using the resulting firing angle with larger thrusters and bands yielded higher than desired eccentricities. More powerful thrusters change the path quicker, and should require less time to reduce the eccentricity. Larger bandwidths increase the maximum allowable eccentricity, producing boost orbits with a correspondingly lower velocity at apogee. Longer burns are required at the smaller velocity to raise it to a value close to that of a circular orbit at the apogee radius. Modifying the base flight path firing angle by a ratio of the bandwidth-to-thrust

ratio proved insufficient. Using the square of the bandwidth in the numerator of the ratio produced more favorable, but not perfect, results.

2. Thruster Turn Off Criteria

If the thruster fires too long the apogee radius will rise, and the path potentially exceed the upper radial limits. If the burn is too short the perigee radius will not be increased sufficiently to affect its decay-to-minimum time. Controlling the end of the burn by comparing the perigee radius to the radius is insufficient because it does not consider the effects on the apogee radius, and the burn might be long. Examination of the flight path path angle proves more interesting.

The tangent of the flight path angle is given by

$$\zeta = \tan\gamma = \frac{\dot{r}}{r\dot{\theta}} \tag{72}$$

Its rate of change is

$$d\zeta = \frac{d\dot{r}}{r\dot{\theta}} - \frac{\dot{r}\,dr}{r^2\dot{\theta}} - \frac{\dot{r}\,d\dot{\theta}}{r\dot{\theta}^2} = \frac{1}{r\dot{\theta}}\left(\ddot{r} - \frac{\dot{r}^2}{r} - \frac{\dot{r}\ddot{\theta}}{\dot{\theta}}\right) \tag{73}$$

Near apogee, with no thrust, the values of the variables inside the expression are

$$r >> 0 \tag{74a}$$

$$\dot{r} \rightarrow 0^+ \tag{74b}$$

$$\ddot{r} < 0 \tag{74c}$$

$$\dot{\theta} > 0 \tag{74d}$$

$$\ddot{\theta} < 0 \tag{74e}$$

and the change in the tangent of the flight path angle is negative. The thruster, as seen from the equations of motion, changes the rates in Equations 74c and 74e to positive values. Since radial velocity is approximately zero, the radial acceleration changes govern Equation 73, eventually causing $d\zeta$ to become positive.

Continuous thrusting at the chosen cant angle increases both r and v. At apogee thrusting has more affect on velocity than radius. The result is that the orbit tends to circularize, then, as shown previously, the semi-major axis increases, and the orbit becomes elliptic again. This ties in with the change the flight path angle undergoes, and thus when it begins to increase, the eccentricity has reached a minimum. The thruster cut off criteria is determined. Figure 15 depicts the flowpath for the second burn in the dual burn thruster control logic.

3. Resulting Orbit

The resulting orbit will be nearly circular and at or near the maximum radial limit. Since the perigee radius is almost equal to the apogee radius, the decay pattern should allow for more time between boosting burns.

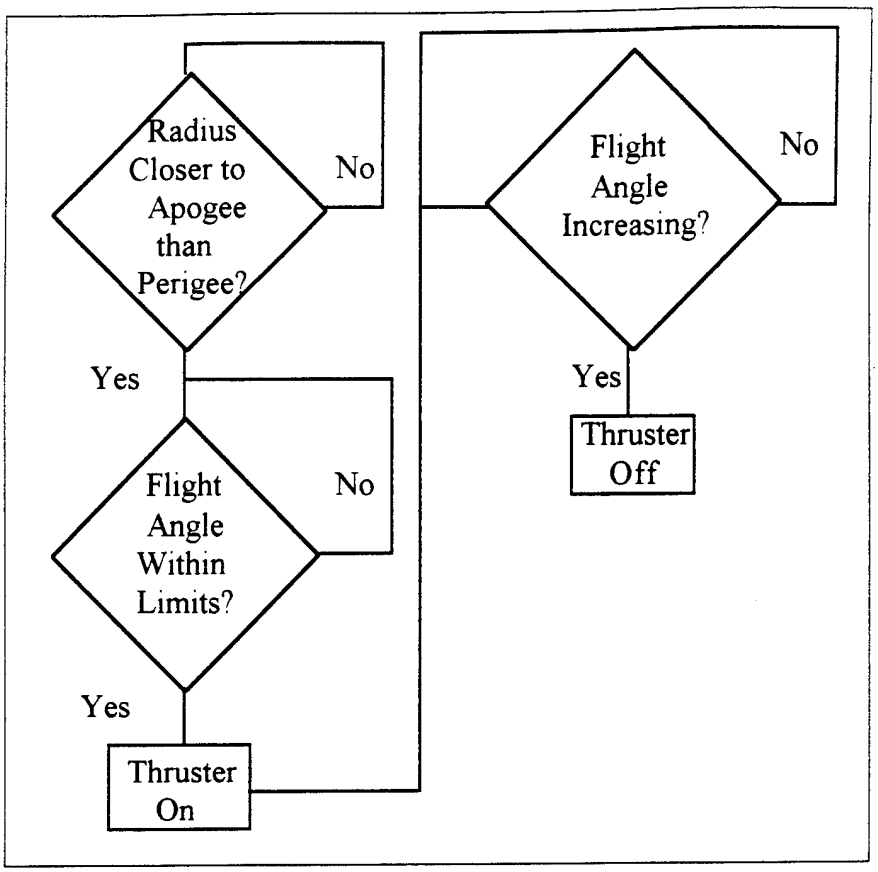

Figure 15. Dual Burn Strategy Second Burn Logic

V. ANALYSIS AND RESULTS

The satellite is initially positioned at the upper radius limit, as though a launch vehicle had placed it there. FKT analysis is done at the lower limit, midband, and the initial radius. Configuration changes are limited to the thruster sizing and the limited effects on nondimensionalization caused by the different starting altitudes. The following parameters were used in all cases:

Midband Radius:	R_e + 260 km
Cant Angle:	0°
Ballistic Coefficient:	150 kg/m^2
Scale Height:	46.9 km
Specific Impulse:	300 s
Initial Mass:	20,000 kg
Base Density Altitude:	250 km
Base Density:	7.248 x 10^{-11} kg/m^3
Density Factor:	12.47

Bandwidths were selected as 2, 10, 25, and 75 km (0.3 x 10^{-3}, 1.5 x 10^{-3}, 3.8 x 10^{-3}, and 11.2 x 10^{-3} distance units, respectively). Thruster sizes were limited to 40, 80, 160, 320, 640, and 1280 N. Table 2 shows the nondimensionalized counterparts to thruster size. The program is run for 100 orbits for the first three bandwidths, and 200 orbits for the last bandwidth. The equations of motion are updated 1000 times and the output sampled ten times per orbit.

A. SINGLE BURN STRATEGY

1. Band Maintenance

Pauls [Ref. 3] and Wilsey [Ref. 4] demonstrated that their single burn control logic did not permit forward-firing thrusters to maintain an orbital band. The ability of the selected Thruster Firing Control Logic (TFCL) to keep the satellite in a bandwidth at all must first, therefore, be established. Initial runs demonstrated that the logic successfully maintained the radius between two boundaries. Having shown the capacity to constrain

the position, the TFCL had to be evaluated on its ability to hold specified limits. Variations in bandwidth and thrust magnitude were applied. Figures 16 through 39 show the radius versus orbit. The TFCL kept the vehicle at or above the minimum radius regardless of the band and thruster size selected. Using thrusters smaller than 40 N could cause the path to drop under the limit. Staying beneath the upper radial limit depended on the thrust and the bandwidth, as well as the time step size. High thrust at small bandwidths caused the radius to exceed the maximum boundary. Table 3 summarizes the single burn band maintenance results.

Bandwidth [km]	Thrust [N]					
	40	80	160	320	640	1,280
	Nondimensionalized Thrust					
2	8.73	17.46	34.92	69.85	139.69	279.39
10	8.74	17.48	34.97	69.93	139.87	279.74
25	8.76	17.52	35.05	70.09	140.18	280.37
75	8.83	17.65	35.31	70.62	141.24	282.48

Table 2. Nondimentionalized Thrust by Bandwidth

Bandwidth [km]	Thrust [N]					
	40	80	160	320	640	1,280
2	SAT	SAT	SAT	+10%	+10%	+51%
10	SAT	SAT	SAT	SAT	+4%	+18%
25	SAT	SAT	SAT	SAT	SAT	+2%
75	SAT	SAT	SAT	SAT	SAT	SAT
SAT = Satisfactory Band Maintenance			+_% = _ % Above Maximum Radius Limit (Percent of Bandwith)			

Table 3. Single Burn Strategy Band Maintenance Summary

2. Orbital Path

The trajectory caused by the single burn, as expected, is generally elliptic. The orbital radius follows no immediately discernible pattern, and neither does the burn

pattern. In some instances TFCL causes the thruster to fire as the vehicle approaches apogee, inadvertently reducing the eccentricity of the orbit, as demonstrated in Figures 40 and 41. This is because the routine is only looking at the osculating perigee radius for firing criteria, not the vehicle's position relative to apogee or perigee. Since the orbit is not permitted to exceed the maximum eccentricity imposed by the radial limits, burns are required less frequently than by the Pauls-Wilsey method.

The method utilizes the full bandwidth during the course of the run, but does not use all available distance units on every opportunity. In the smaller bands, particularly the 2 km (0.3×10^{-3} distance units), the logic uses as little as half the available bandwidth. In cases with a larger minimum-maximum separation, approximately 90% of the band is used when burns occur.

B. DUAL BURN STRATEGY

1. Band Maintenance

Again the logic had to be tested to ensure it was capable of maintaining a band. Runs showed the dual burn maneuver kept the vehicle within radial limits. The new strategy was put through the same bandwidth-thruster variation sequence the single burn control method was. Plots of the resulting radius versus orbit are shown in Figures 42 through 65. Since the single burn strategy was used as the initial burn, the radius was not expected to, and did not, go below the minimum. The timing of the second burn did not always meet the needs of the particular osculating orbital elements, and periodically led to the upper radial limit being exceeded. Review of the burn initiation time, the flight path angle and the satellite's position with respect to apogee revealed thrusting began earlier than required. Thrust initiation for the second burn is based on a scaled flight path angle. The scaling ratio was too large, indicating the method favors the bandwidth over the thrust capacity more than it should. The use of a ratio was an arbitrary choice; other functions could well be the solution to the problem. Table 4 summarizes the dual burn maneuver results.

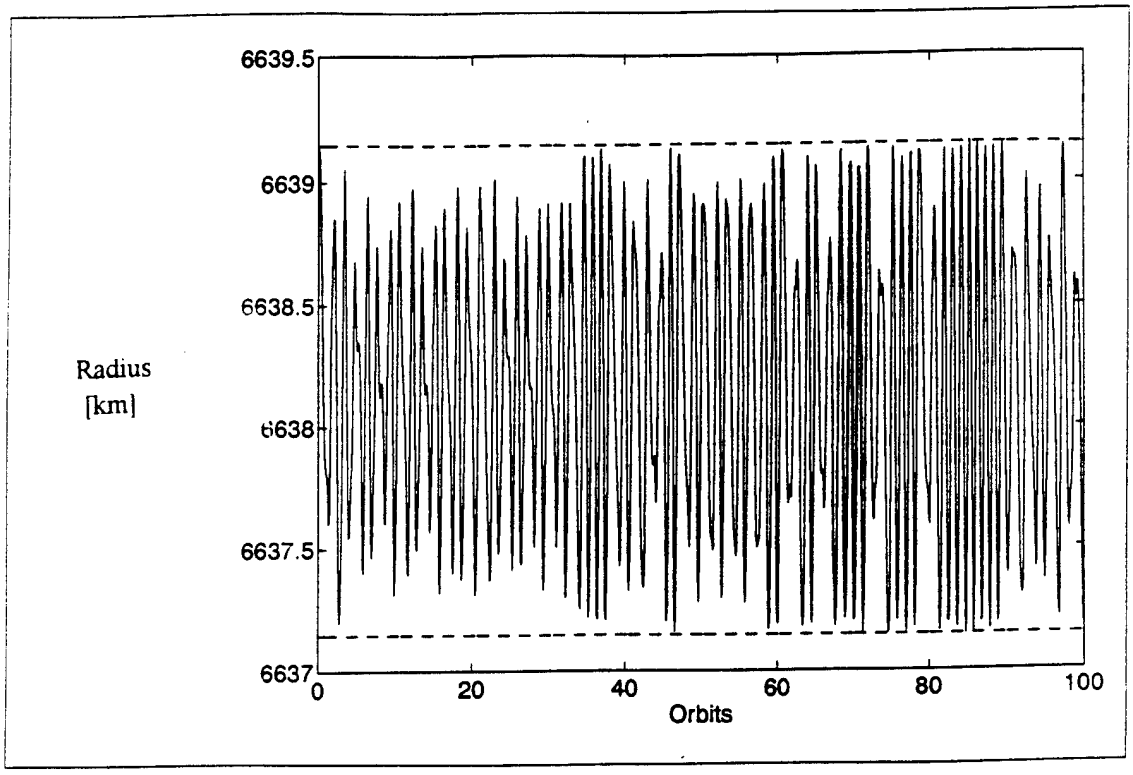

Figure 16. Single Burn Strategy Orbital Radius (2 km Bandwidth, 40 N Thrust)

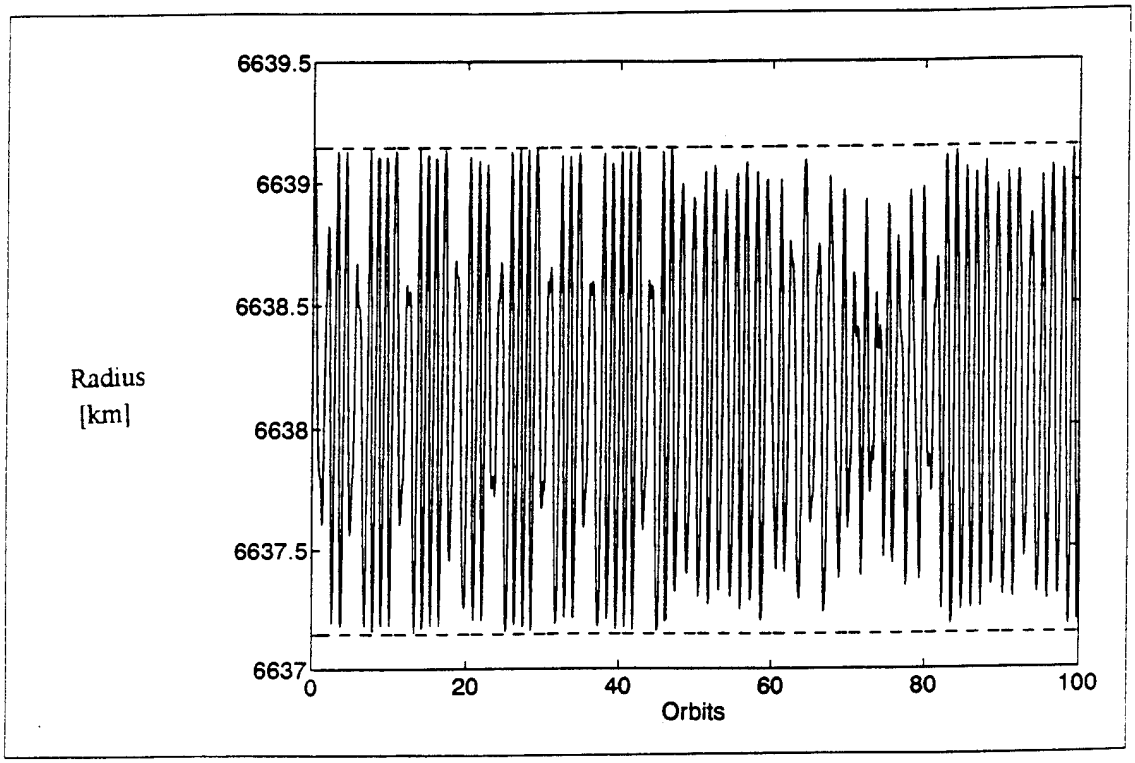

Figure 17. Single Burn Strategy Orbital Radius (2 km Bandwidth, 80 N Thrust)

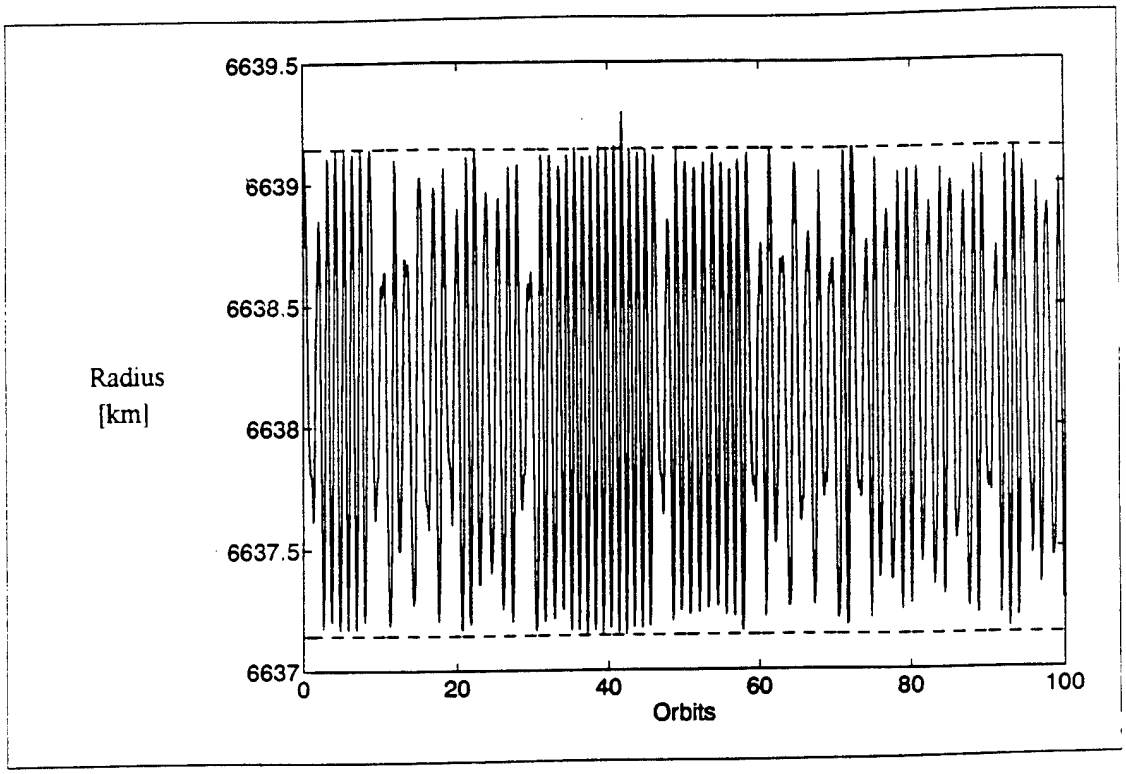

Figure 18. Single Burn Strategy Orbital Radius (2 km Bandwidth, 160 N Thrust)

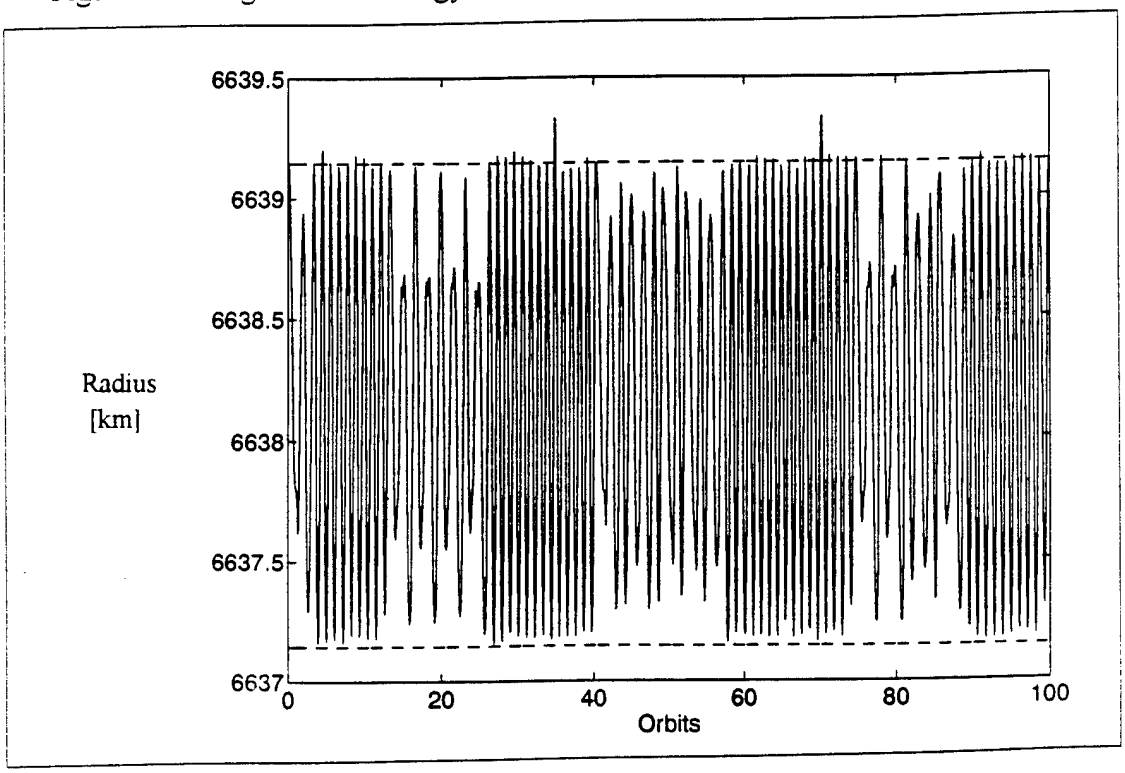

Figure 19. Single Burn Strategy Orbital Radius (2 km Bandwidth, 320 N Thrust)

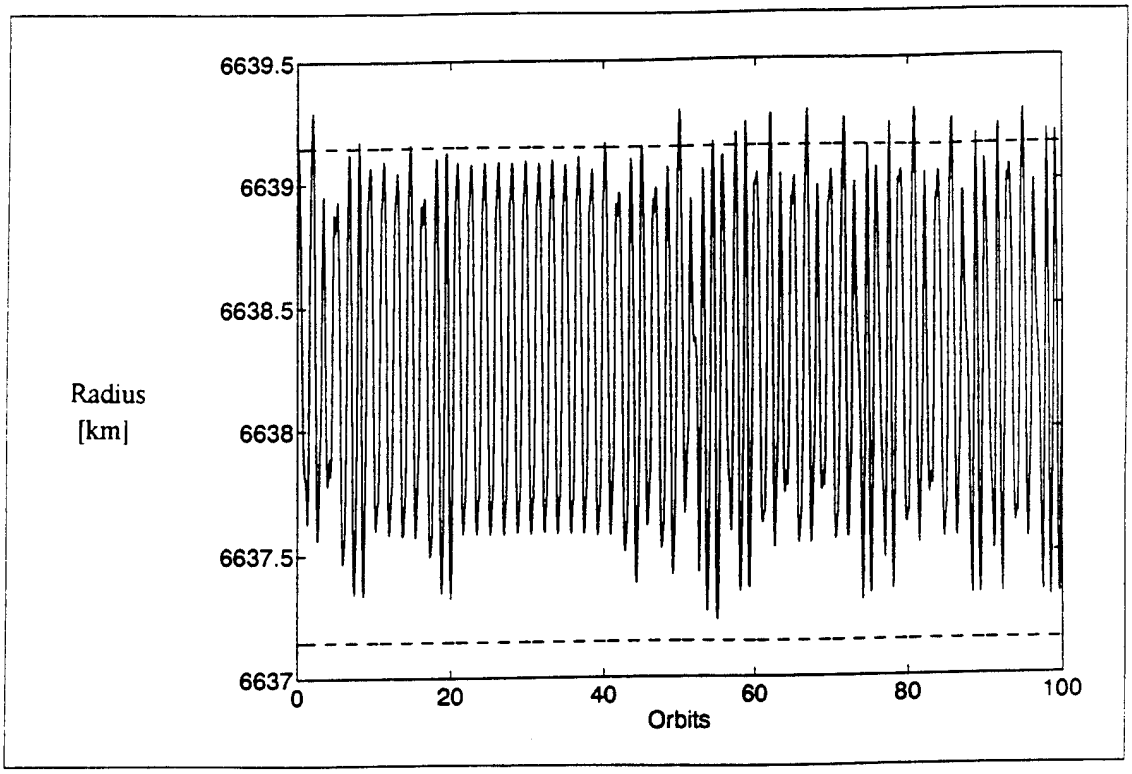

Figure 20. Single Burn Strategy Orbital Radius (2 km Bandwidth, 640 N Thrust)

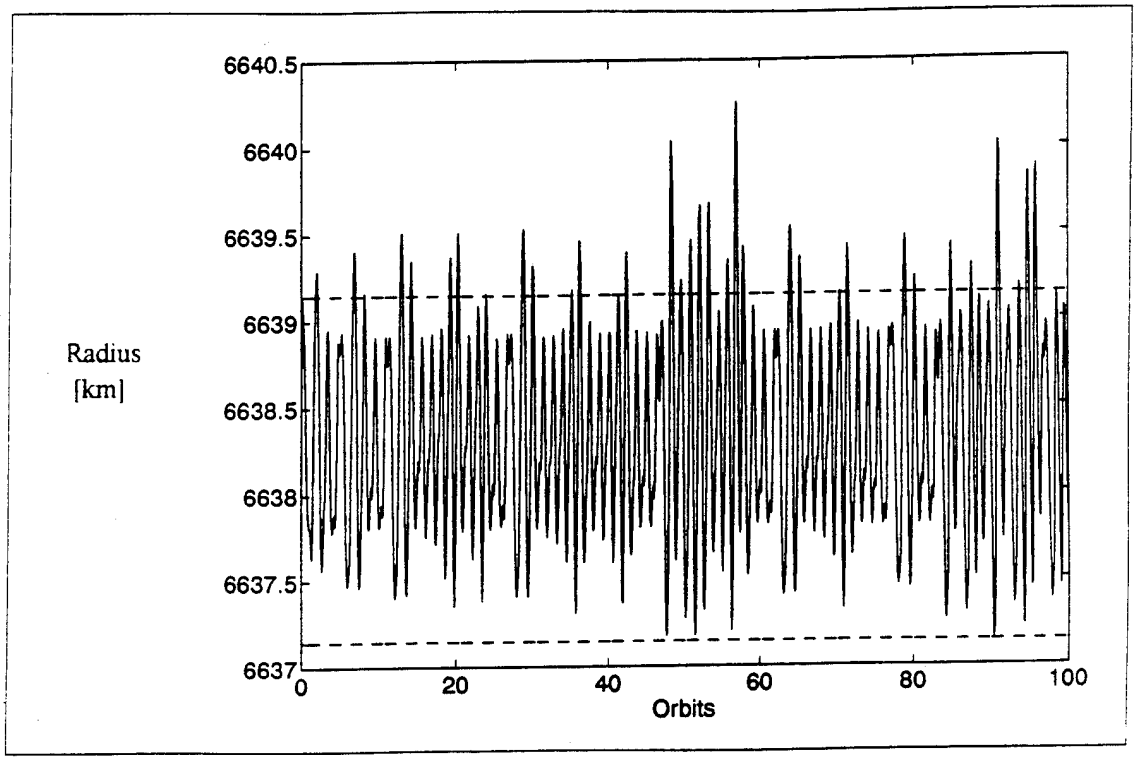

Figure 21. Single Burn Strategy Orbital Radius (2 km Bandwidth, 1280 N Thrust)

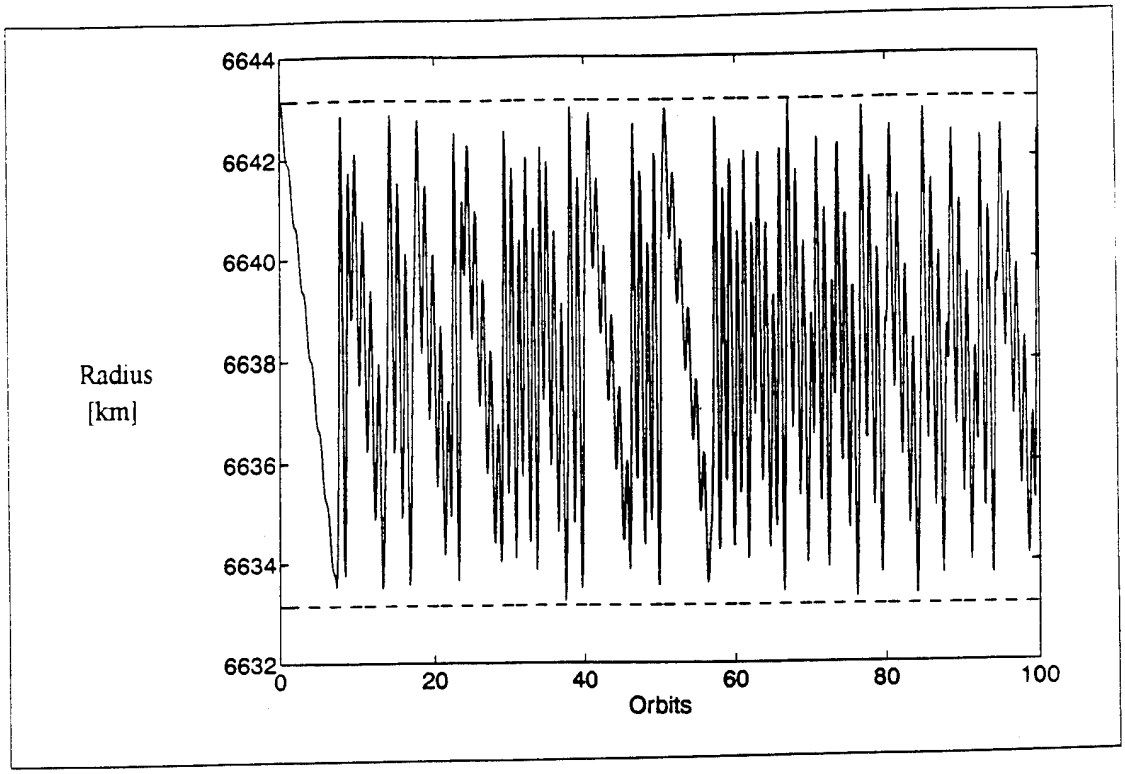

Figure 22. Single Burn Strategy Orbital Radius (10 km Bandwidth, 40 N Thrust)

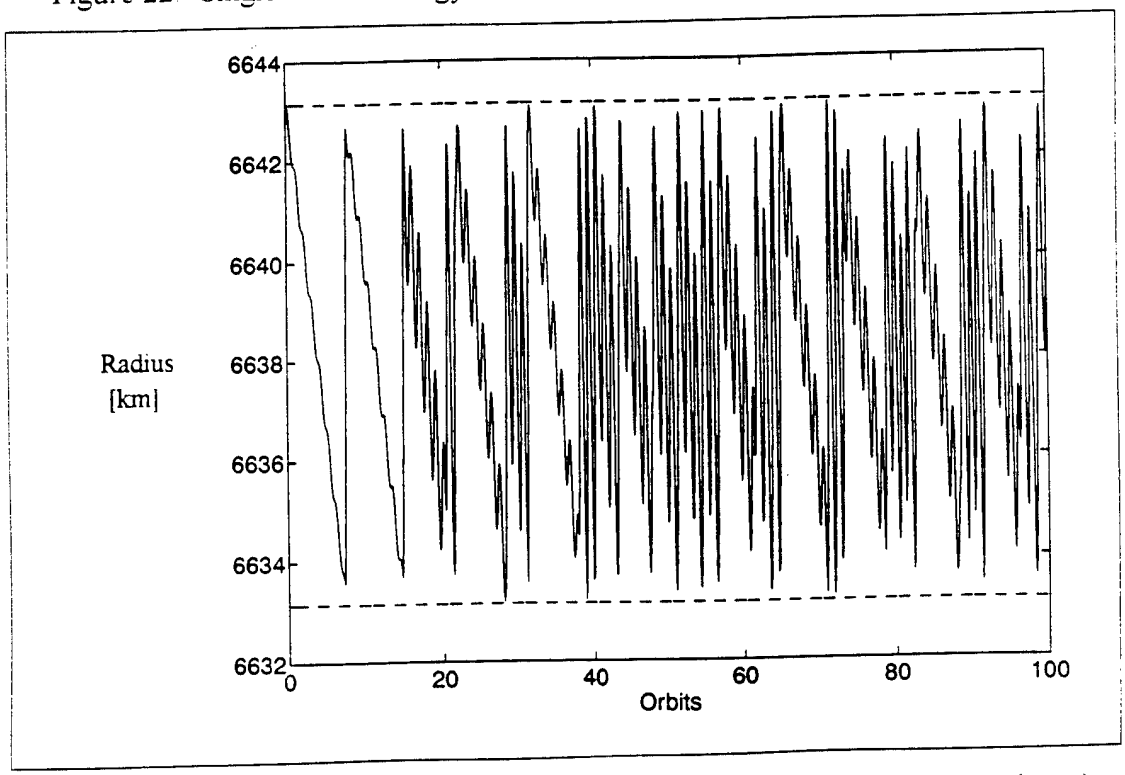

Figure 23. Single Burn Strategy Orbital Radius (10 km Bandwidth, 80 N Thrust)

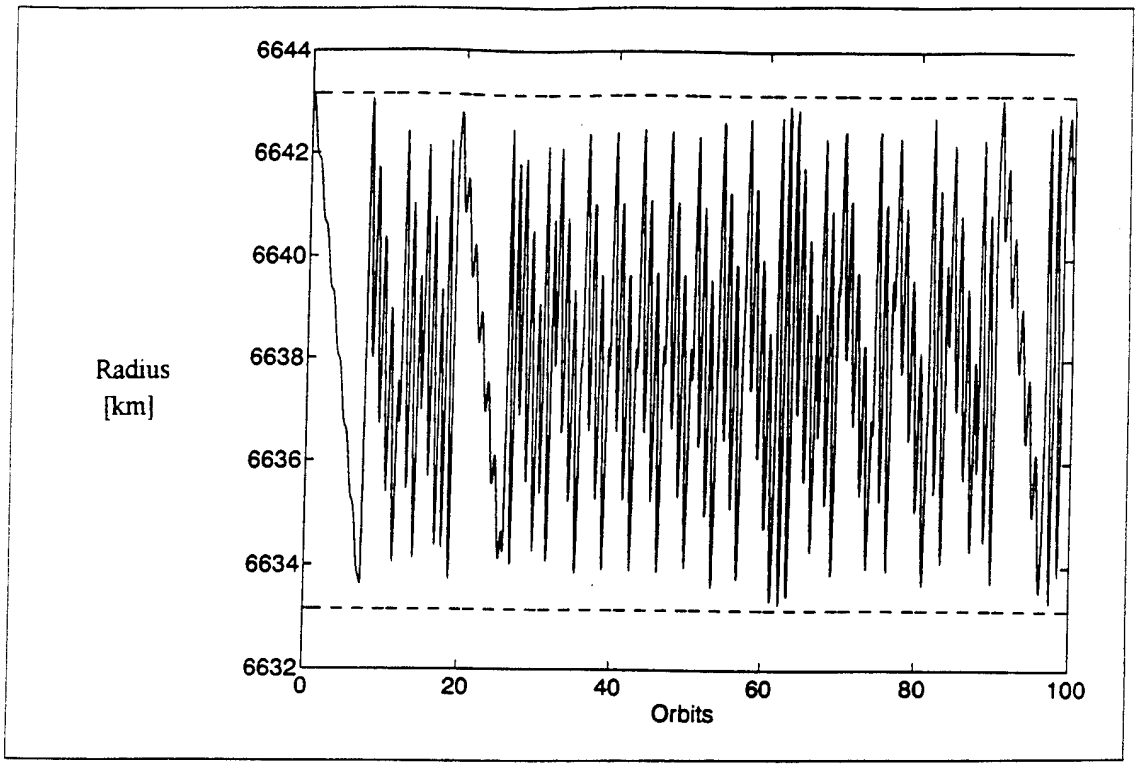

Figure 24 Single Burn Strategy Orbital Radius (10 km Bandwidth, 160 N Thrust)

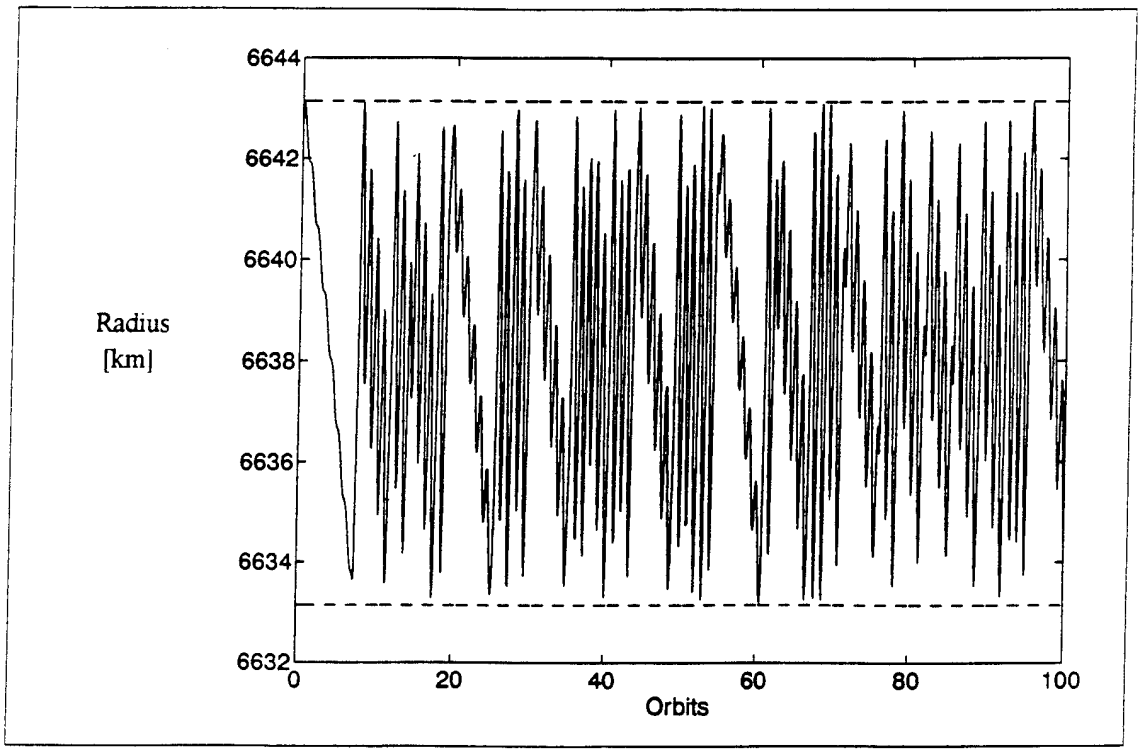

Figure 25 Single Burn Strategy Orbital Radius (10 km Bandwidth, 320 N Thrust)

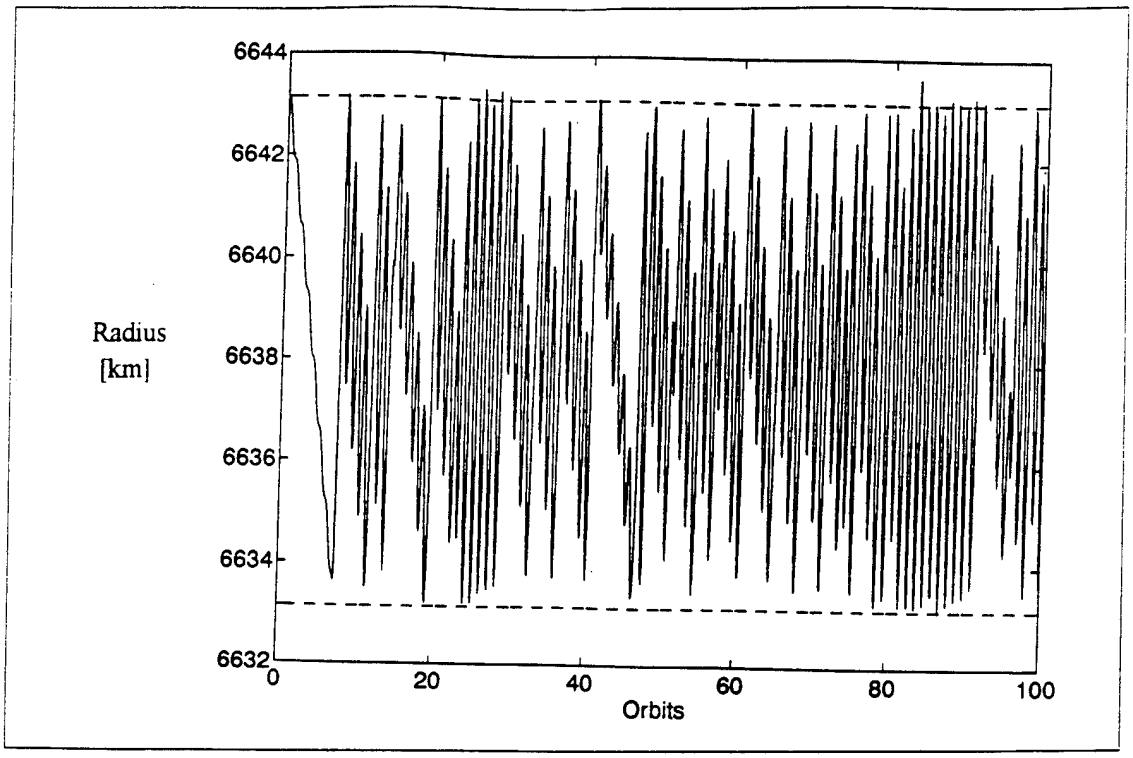

Figure 26. Single Burn Strategy Orbital Radius (10 km Bandwidth, 640 N Thrust)

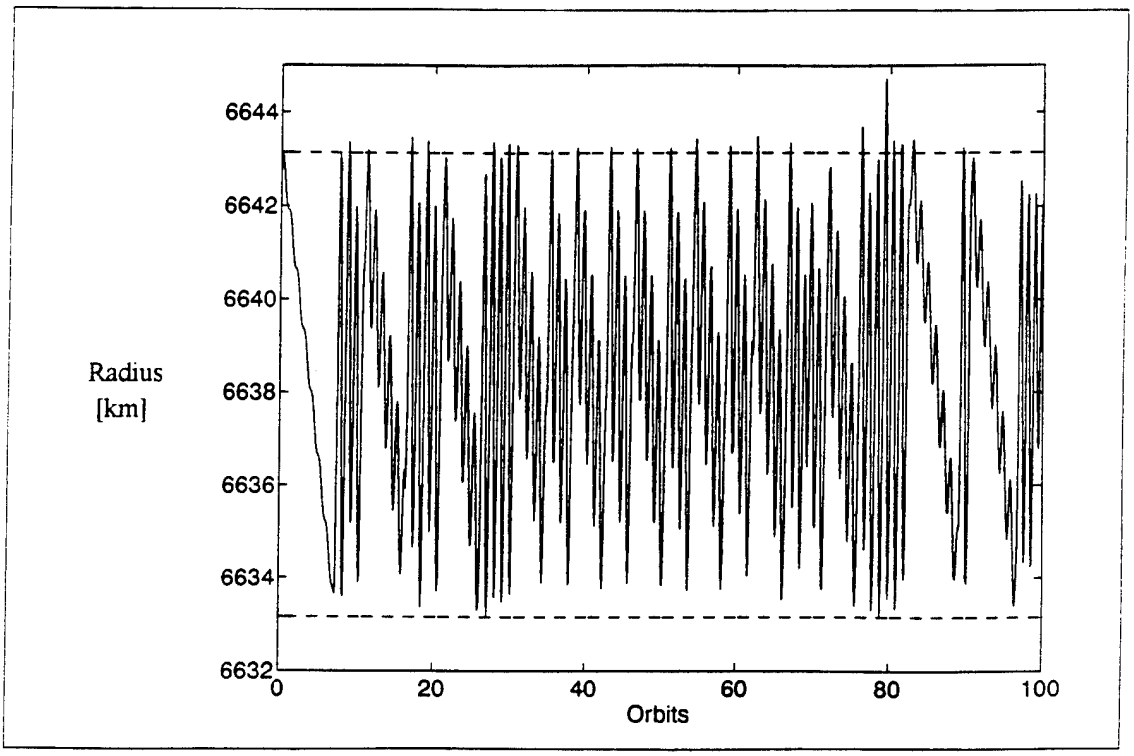

Figure 27. Single Burn Strategy Orbital Radius (10 km Bandwidth, 1280 N Thrust)

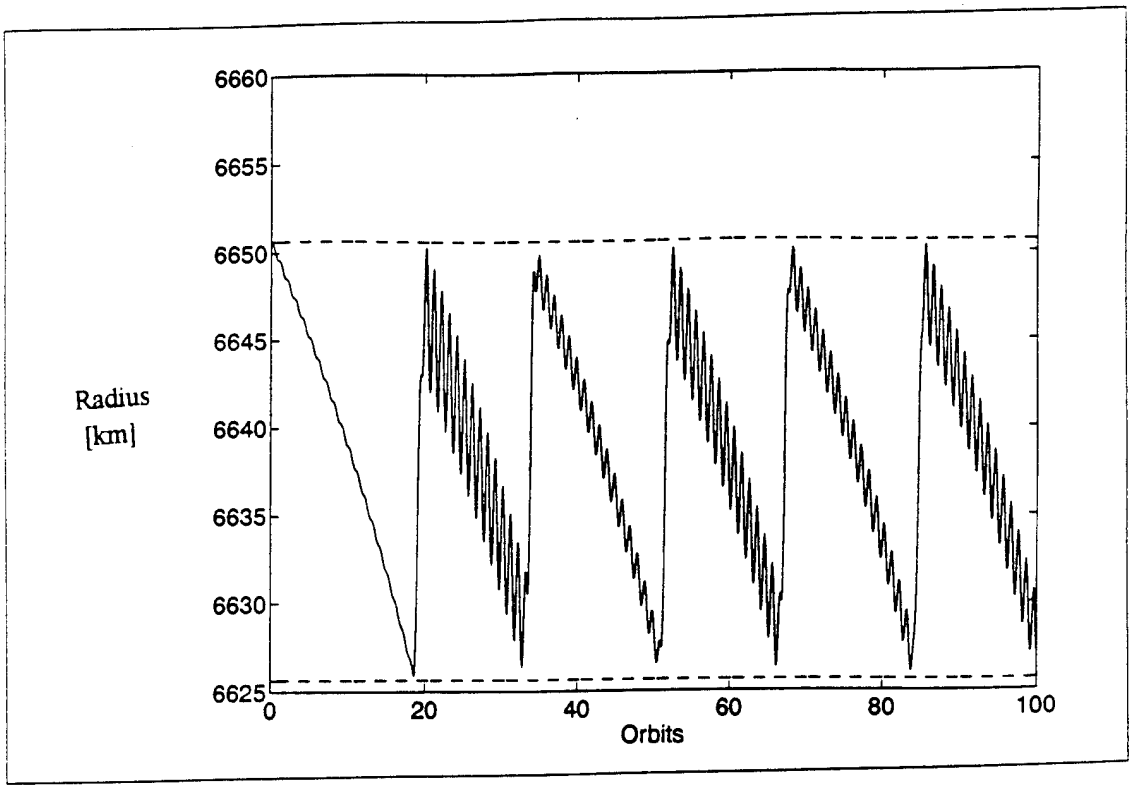

Figure 28. Single Burn Strategy Orbital Radius (25 km Bandwidth, 40 N Thrust)

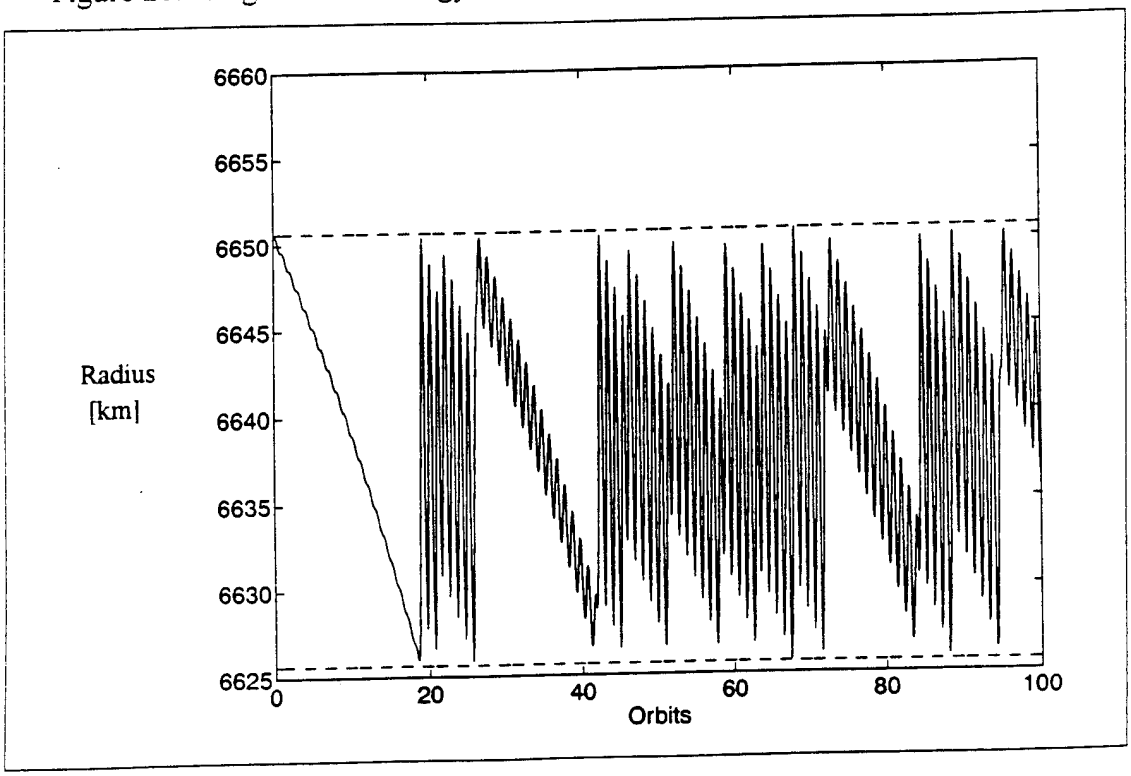

Figure 29. Single Burn Strategy Orbital Radius (25 km Bandwidth, 80 N Thrust)

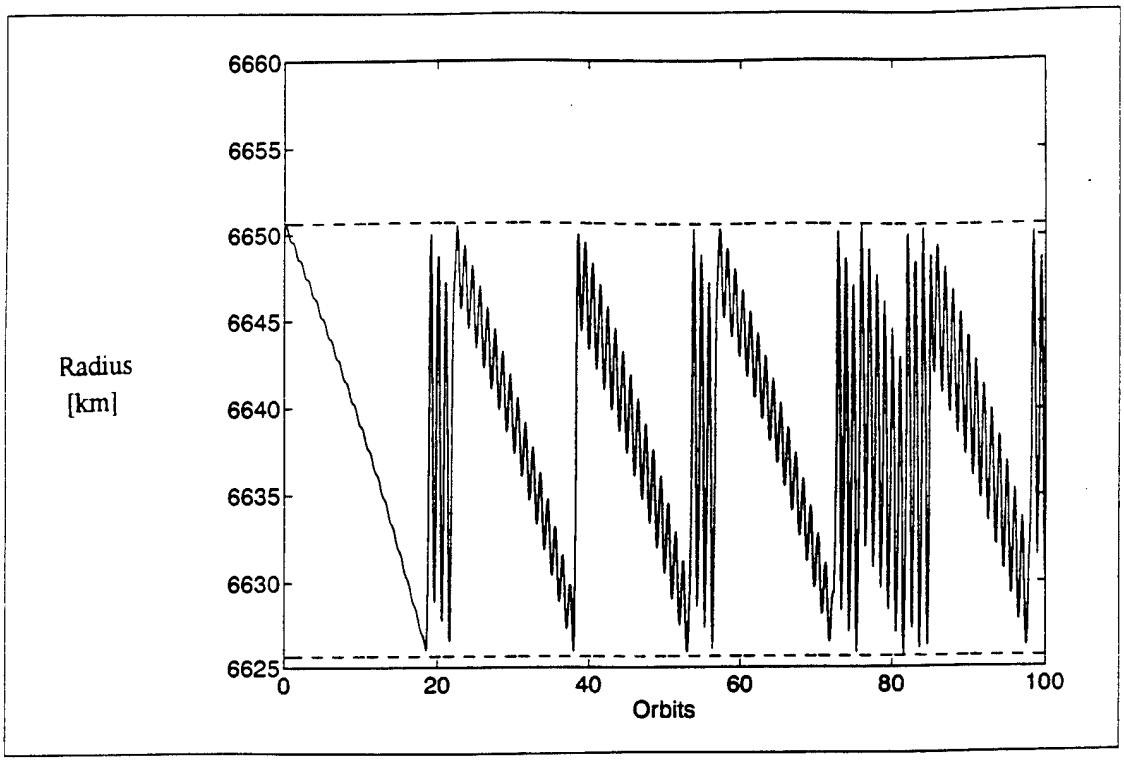

Figure 30. Single Burn Strategy Orbital Radius (25 km Bandwidth, 160 N Thrust)

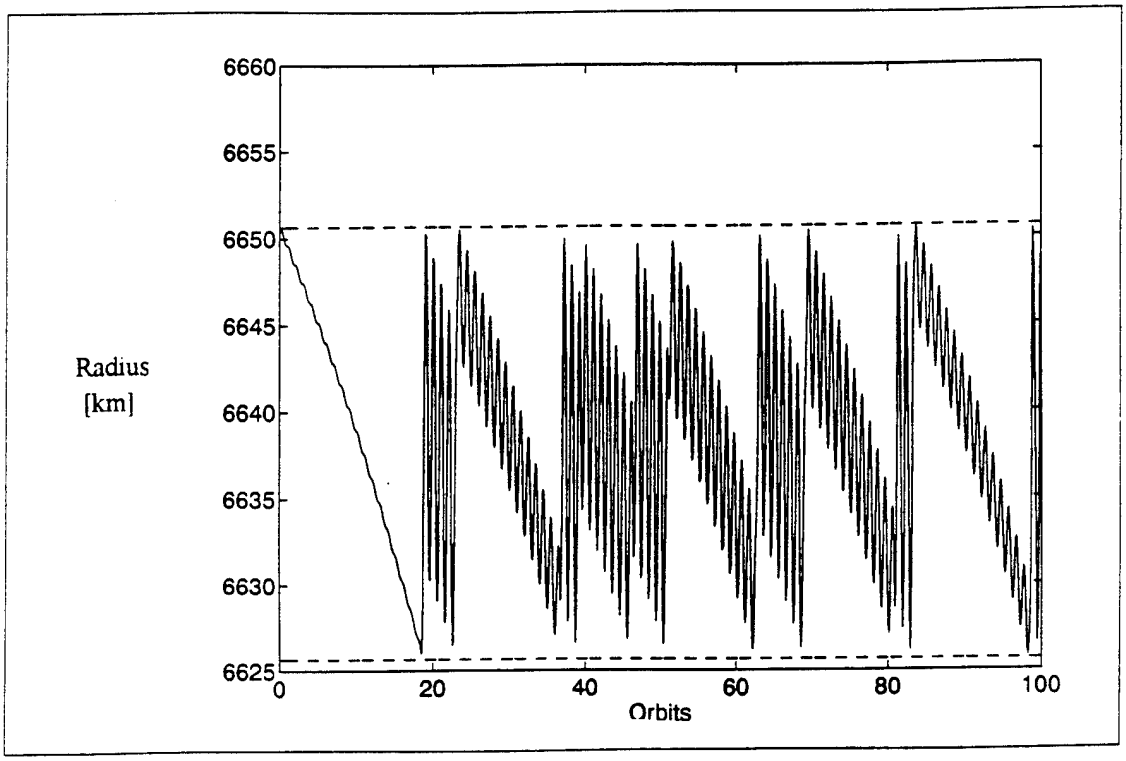

Figure 31. Single Burn Strategy Orbital Radius (25 km Bandwidth, 320 N Thrust)

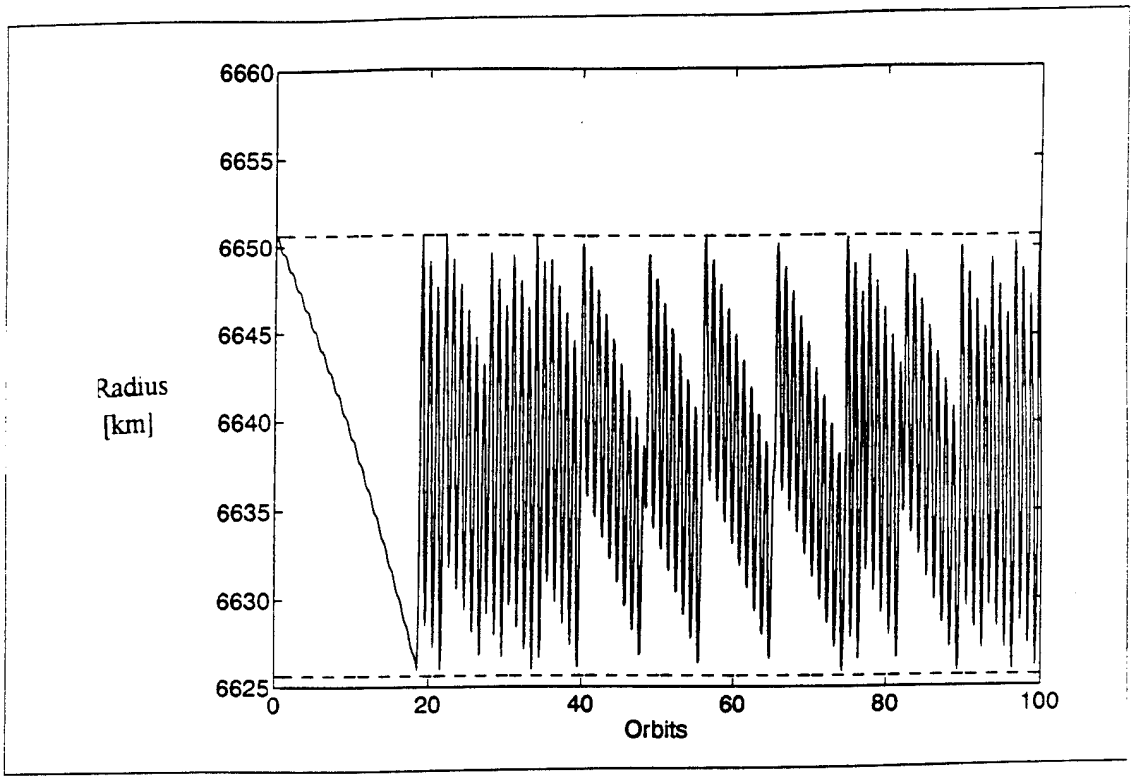

Figure 32. Single Burn Strategy Orbital Radius (25 km Bandwidth, 640 N Thrust)

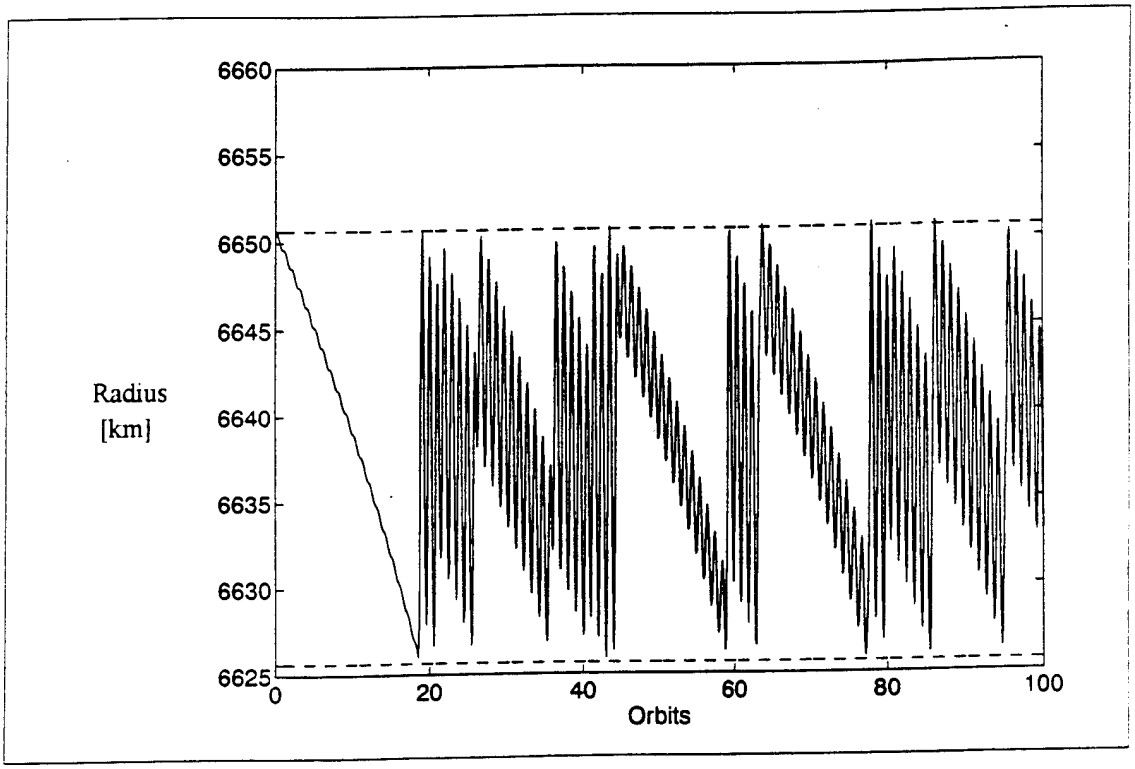

Figure 33. Single Burn Strategy Orbital Radius (25 km Bandwidth, 1280 N Thrust)

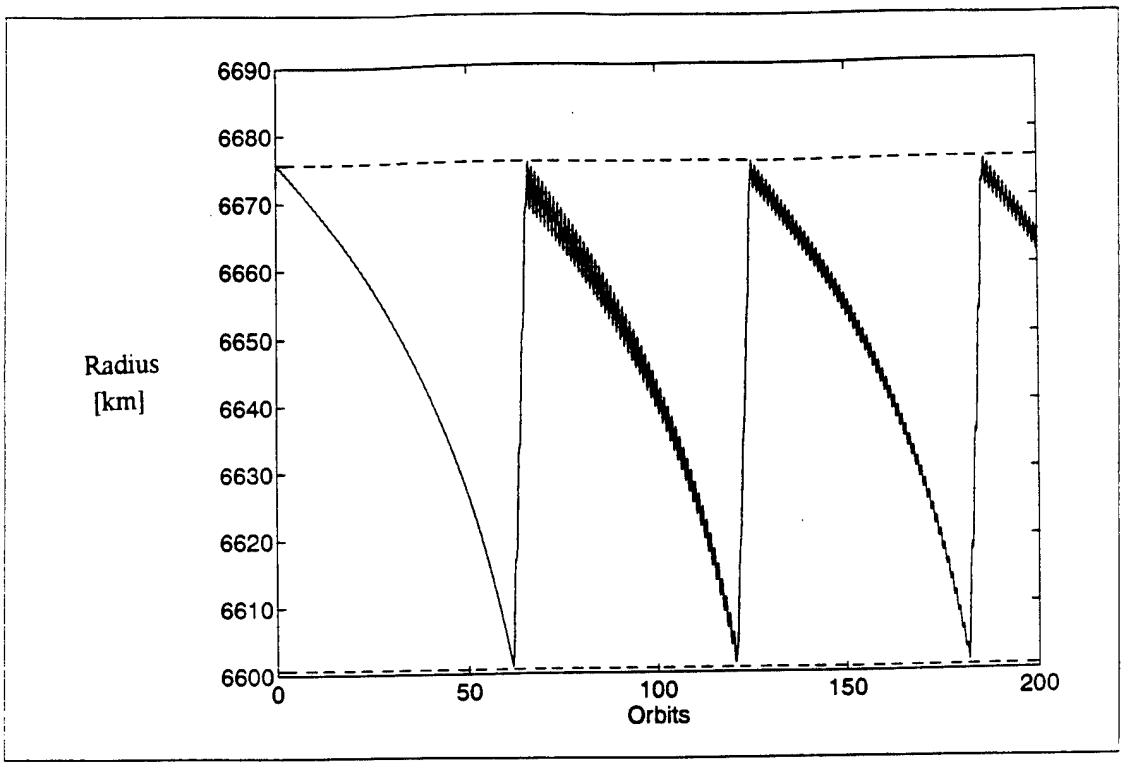

Figure 34. Single Burn Strategy Orbital Radius (75 km Bandwidth, 40 N Thrust)

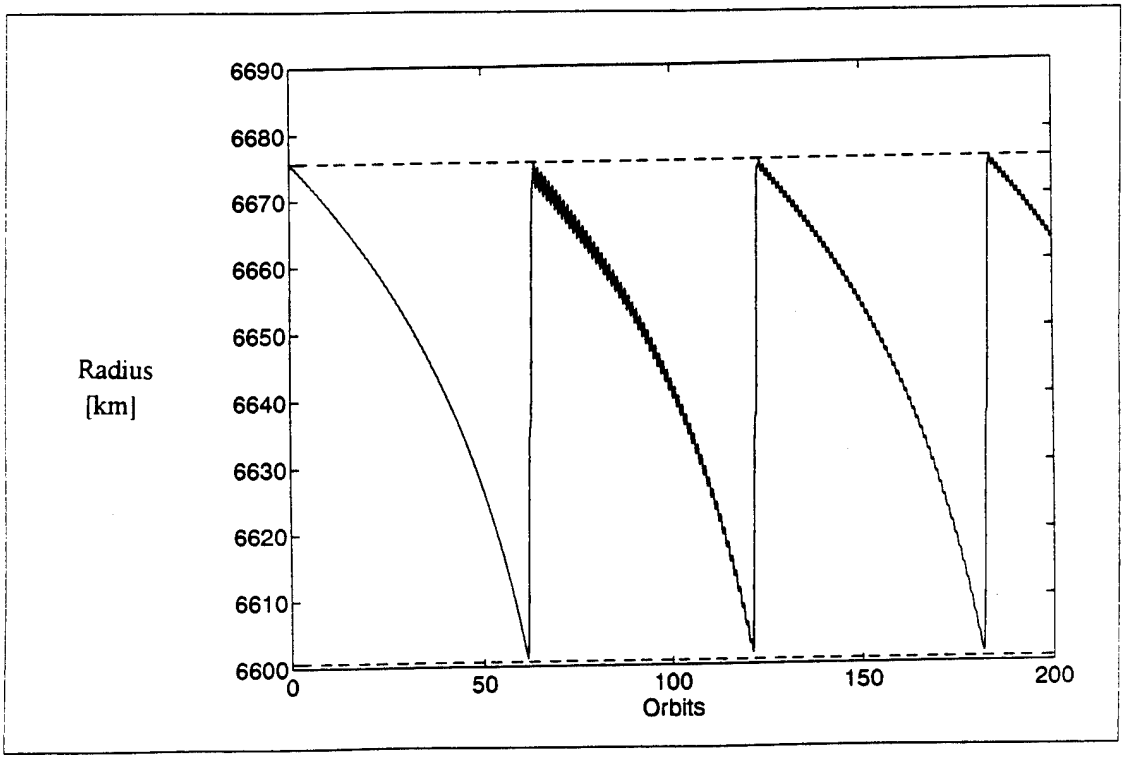

Figure 35. Single Burn Strategy Orbital Radius (75 km Bandwidth, 80 N Thrust)

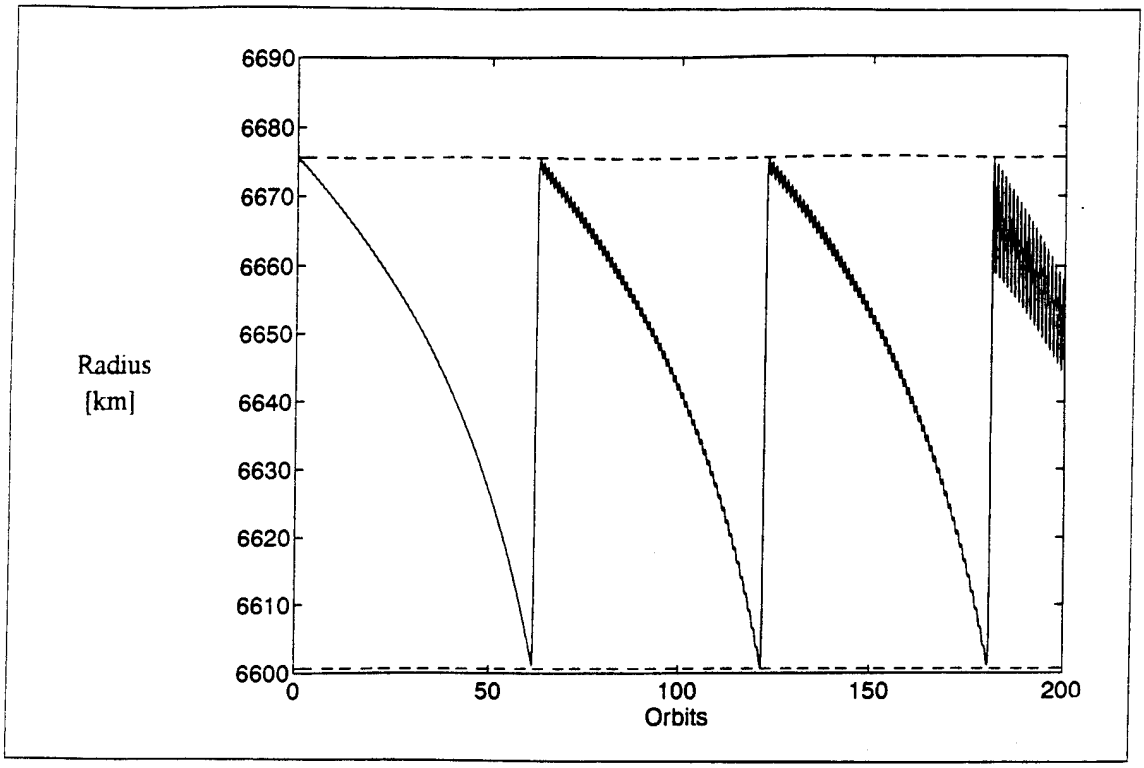

Figure 36. Single Burn Strategy Orbital Radius (75 km Bandwidth, 160 N Thrust)

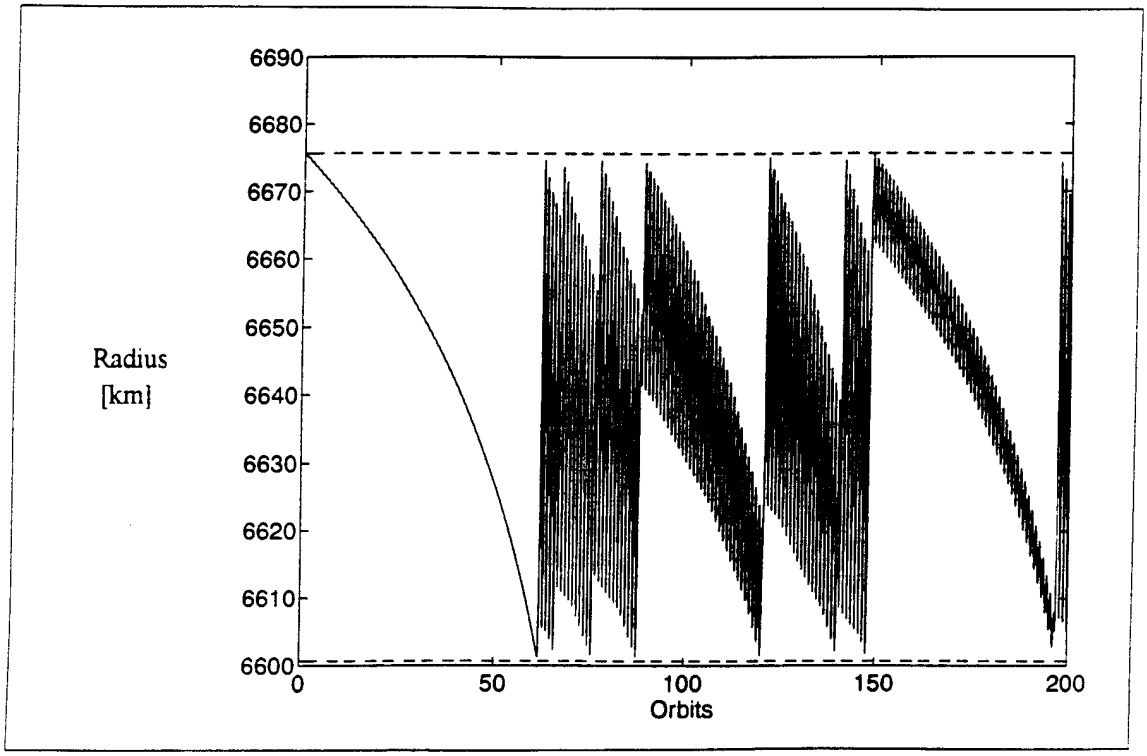

Figure 37 Single Burn Strategy Orbital Radius (75 km Bandwidth, 320 N Thrust)

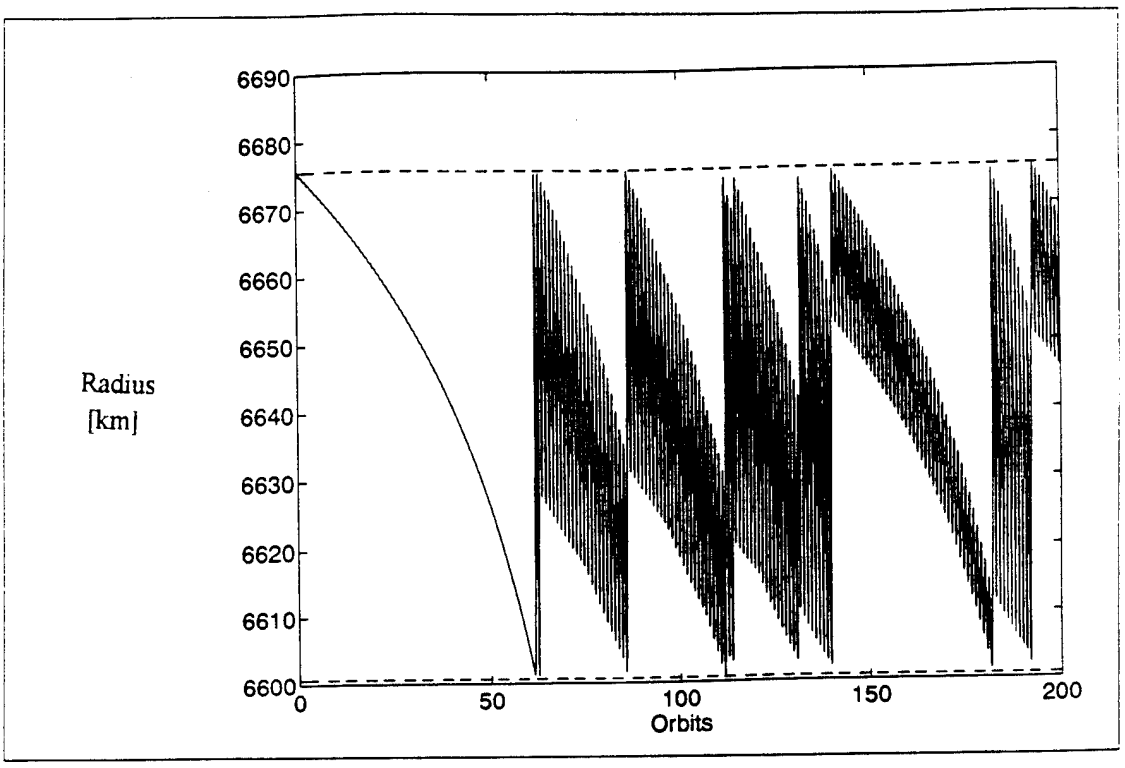

Figure 38 Single Burn Strategy Orbital Radius (75 km Bandwidth, 640 N Thrust)

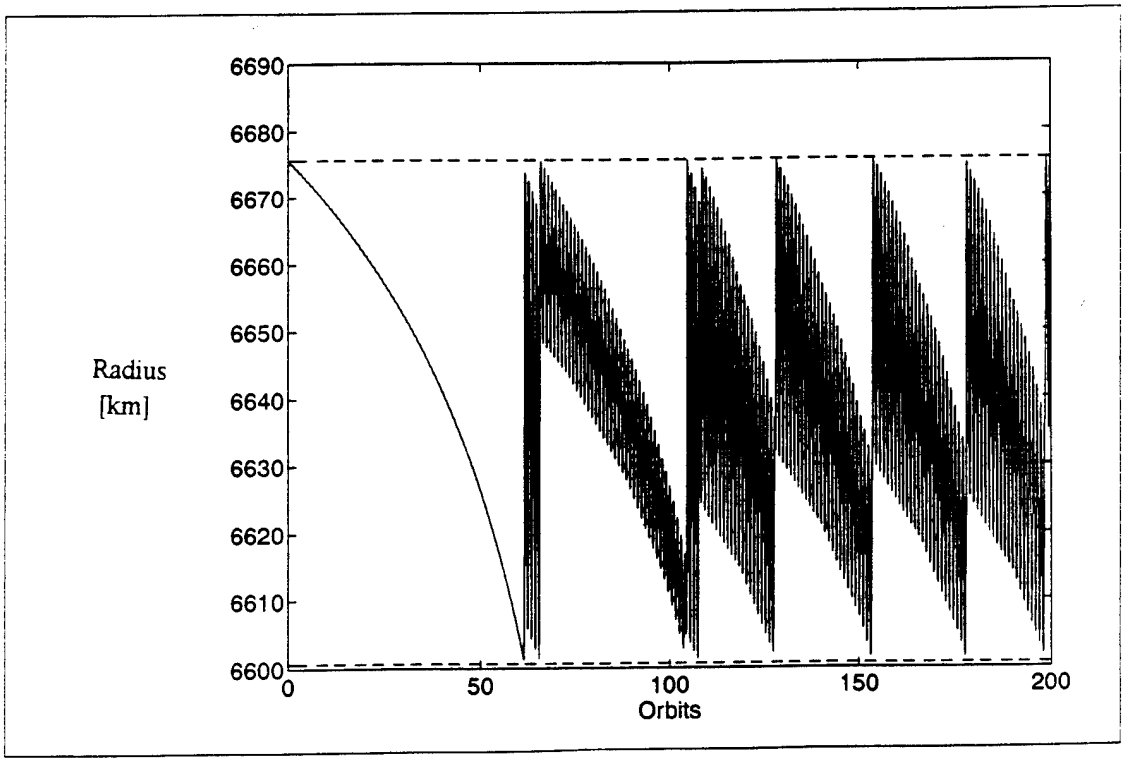

Figure 39 Single Burn Strategy Orbital Radius (75 km Bandwidth, 1280 N Thrust)

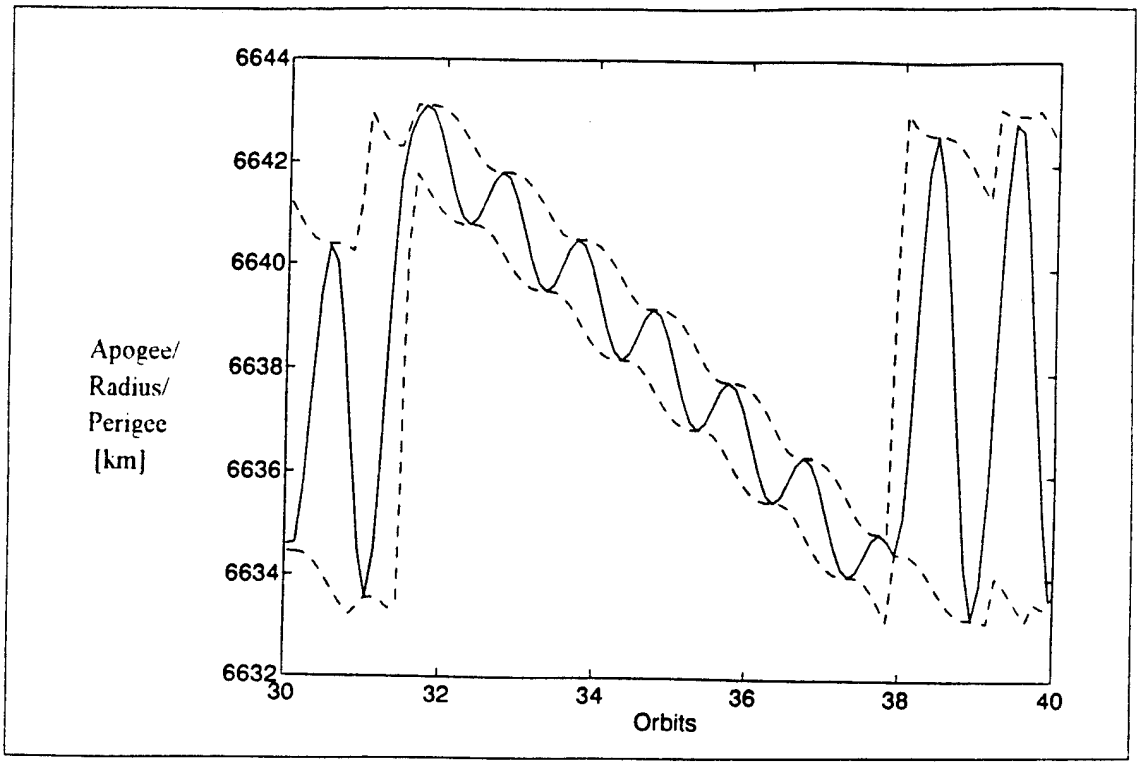

Figure 40 Apogee, Radius, and Perigee (10 km Bandwidth, 80 N Thrust)

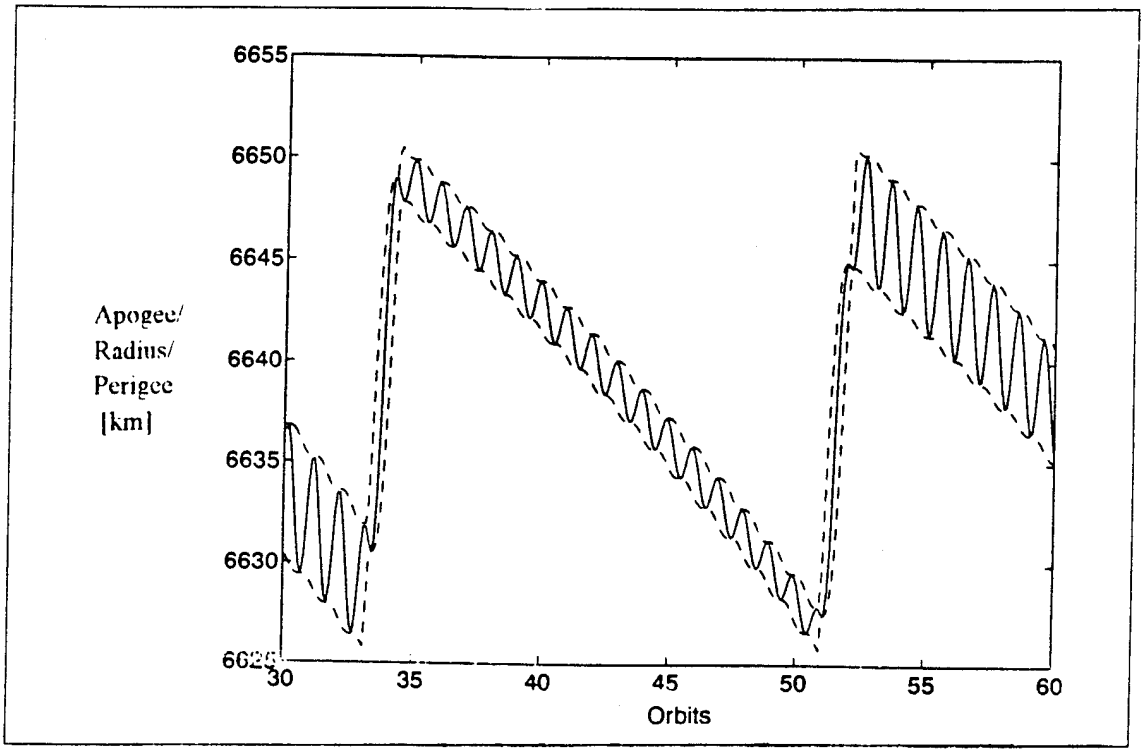

Figure 41. Apogee, Radius, and Perigee (25 km Bandwidth, 40 N Thrust)

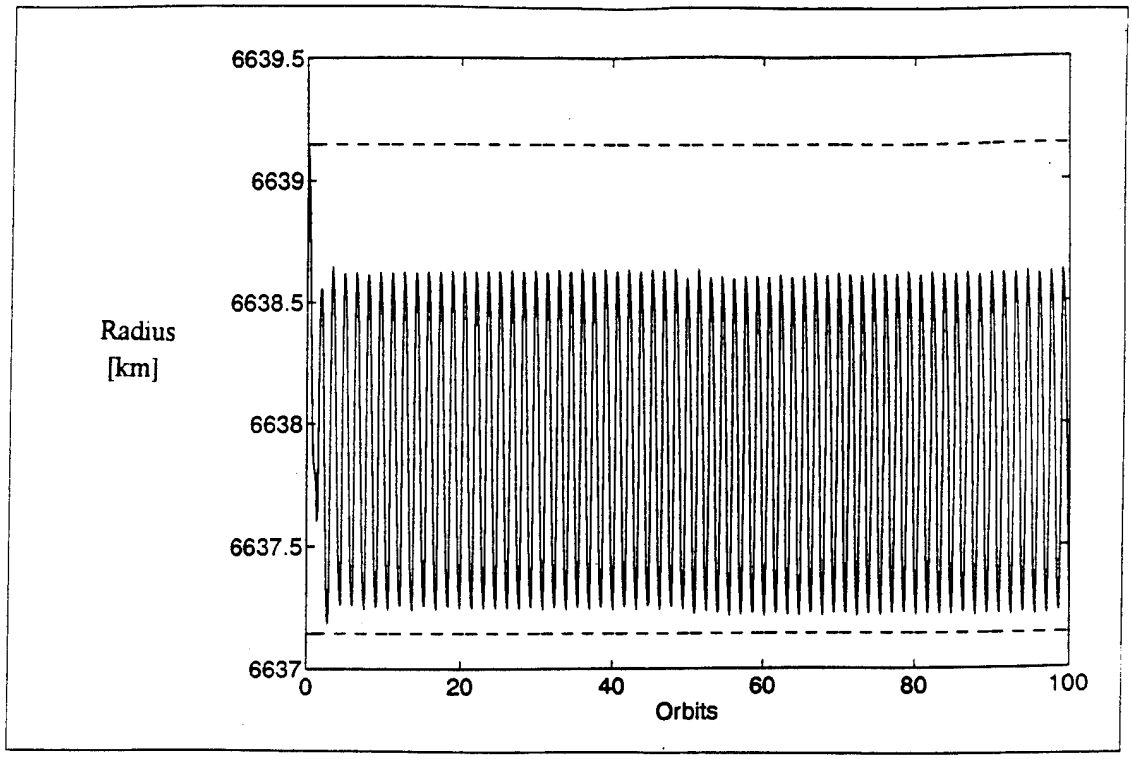

Figure 42. Dual Burn Strategy Orbtial Radius (2 km Bandwidth, 40 N Thrust)

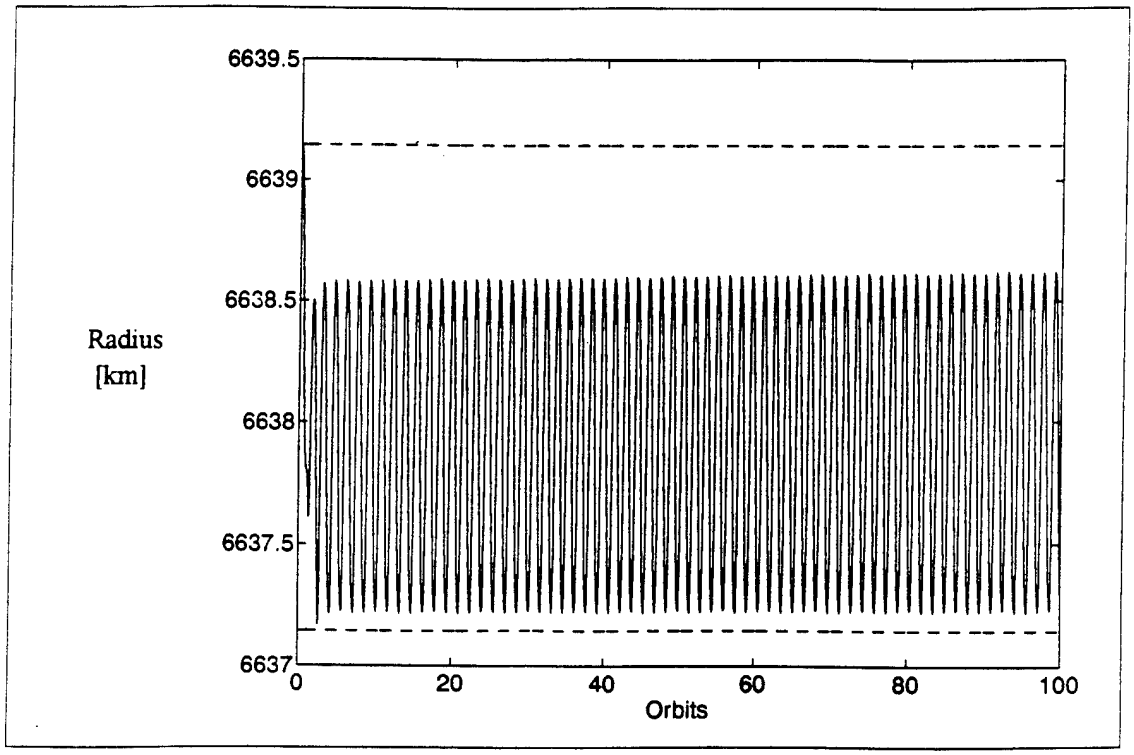

Figure 43. Dual Burn Strategy Orbital Radius (2 km Bandwidth, 80 N Thrust)

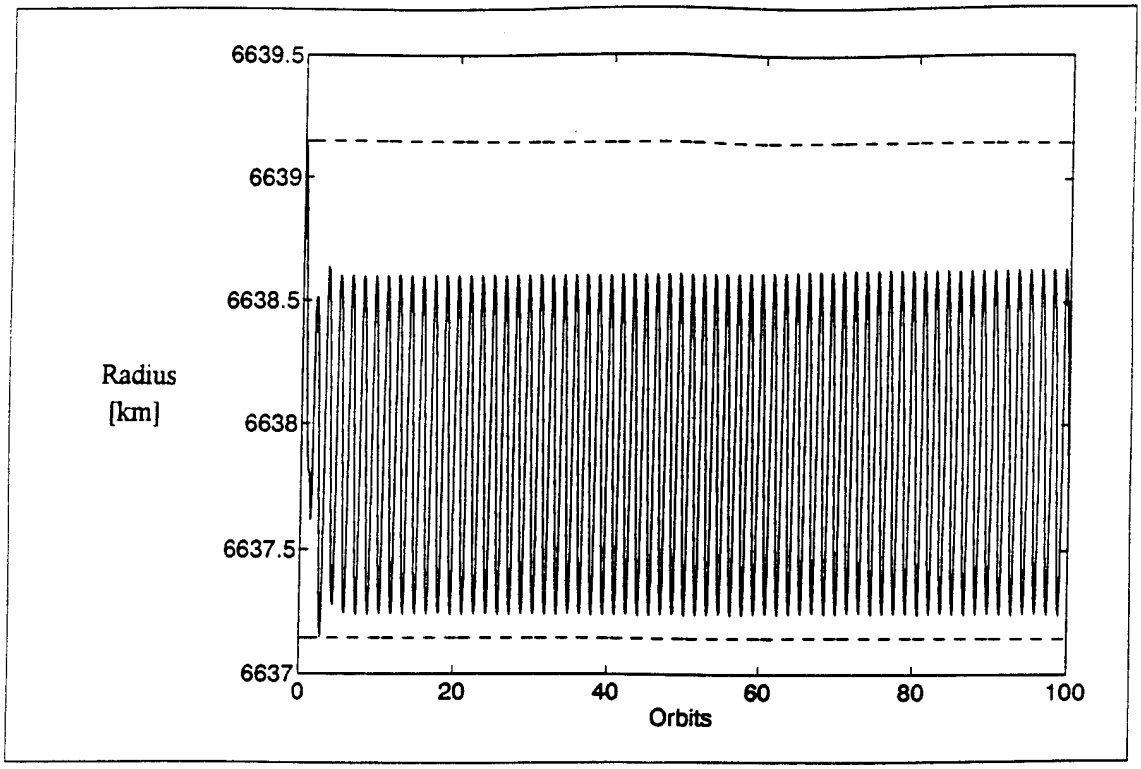

Figure 44. Dual Burn Strategy Orbital Radius (2 km Bandwidth, 160 N Thrust)

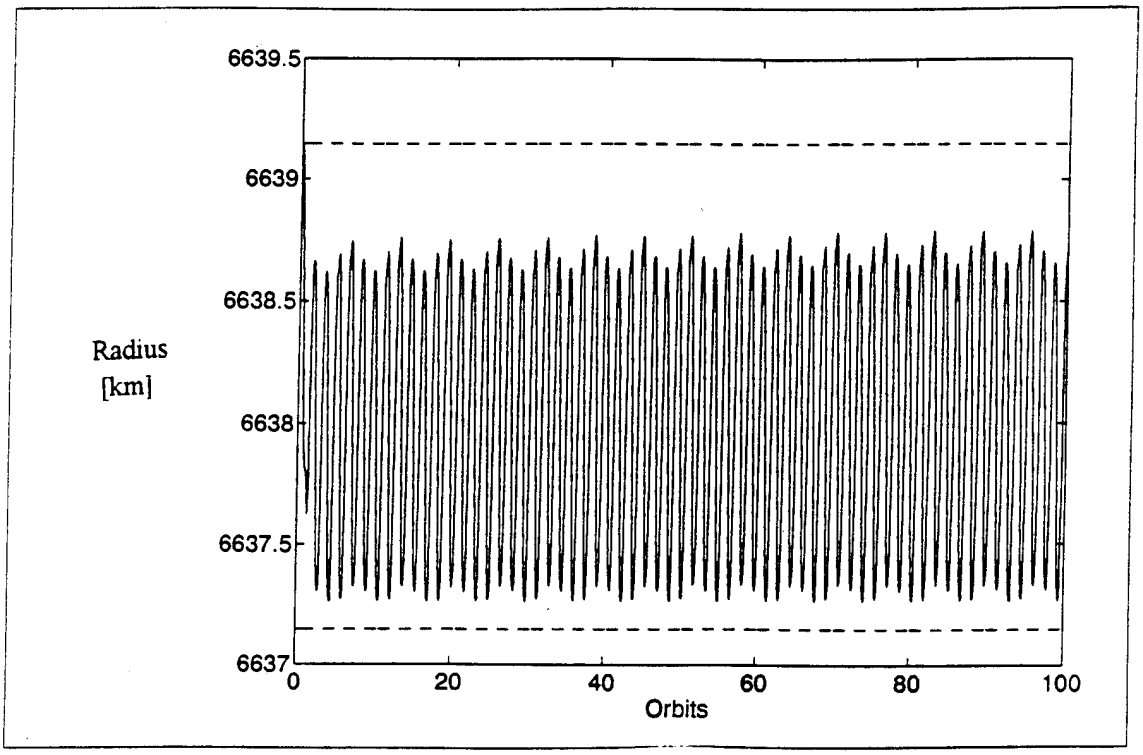

Figure 45. Dual Burn Strategy Orbital Radius (2 km Bandwidth, 320 N Thrust)

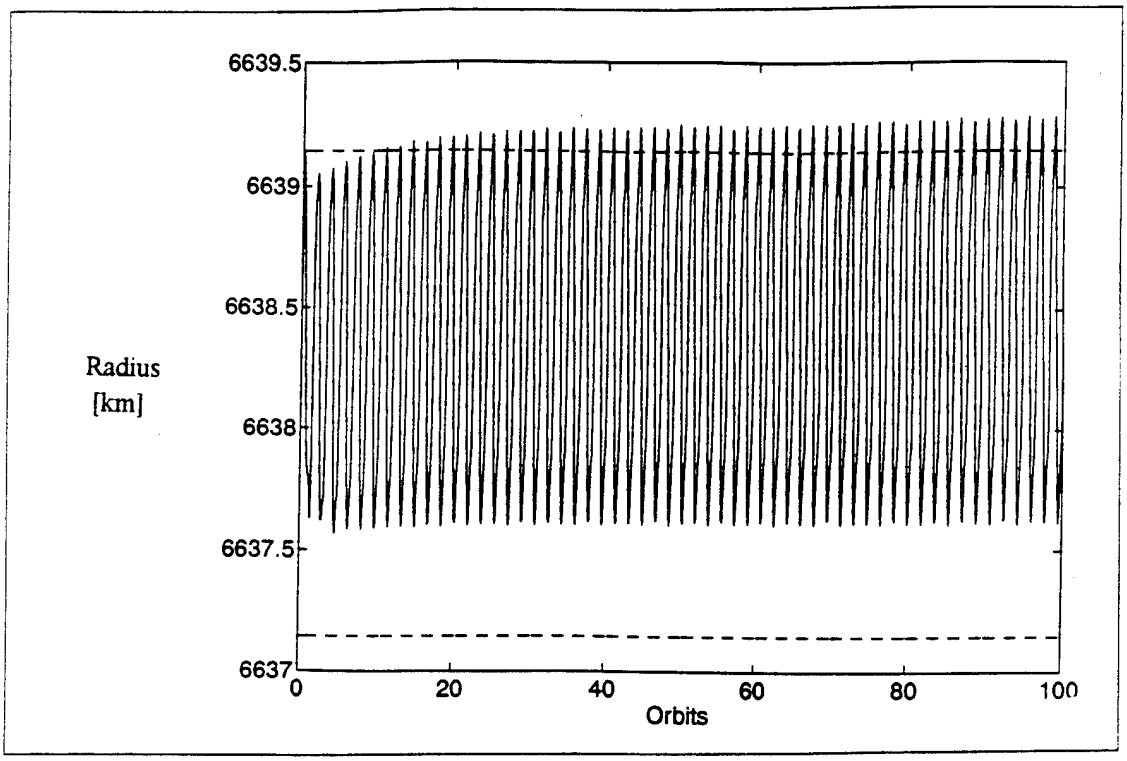

Figure 46. Dual Burn Strategy Orbital Radius (2 km Bandwidth, 640 N Thrust)

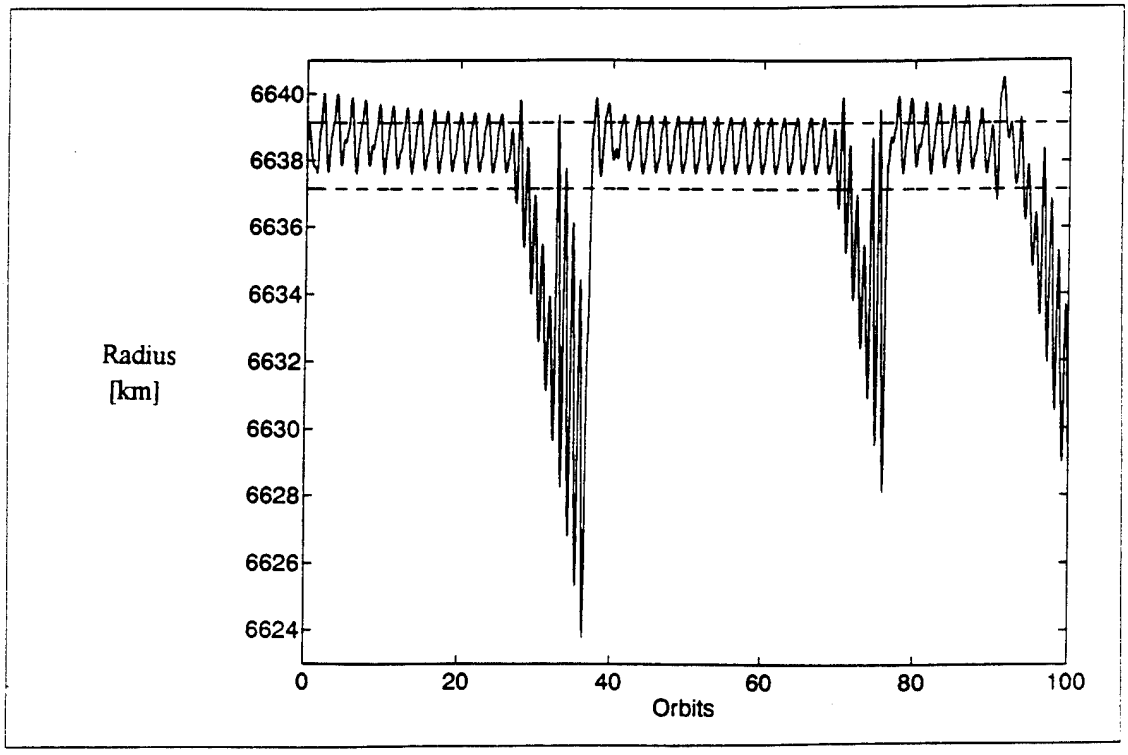

Figure 47. Dual Burn Strategy Orbital Radius (2 km Bandwidth, 1280 N Thrust)

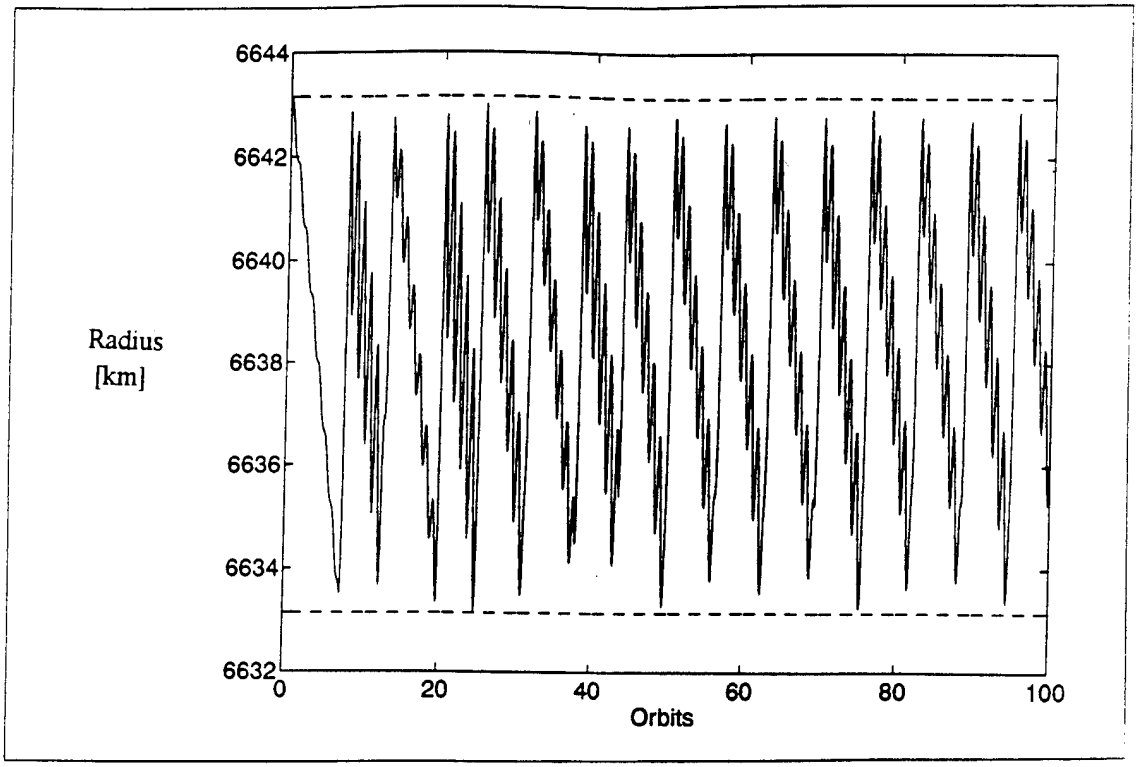

Figure 48. Dual Burn Strategy Orbital Radius (10 km Bandwidth, 40 N Thrust)

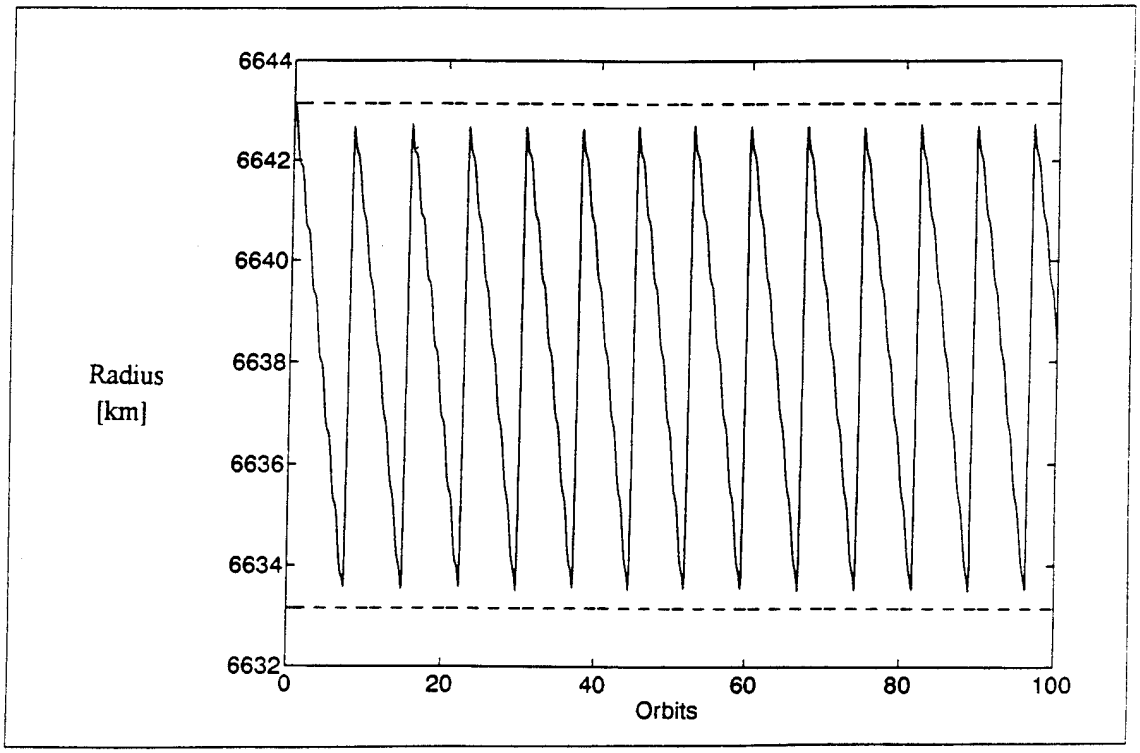

Figure 49. Dual Burn Strategy Orbital Radius (10 km Bandwidth, 80 N Thrust)

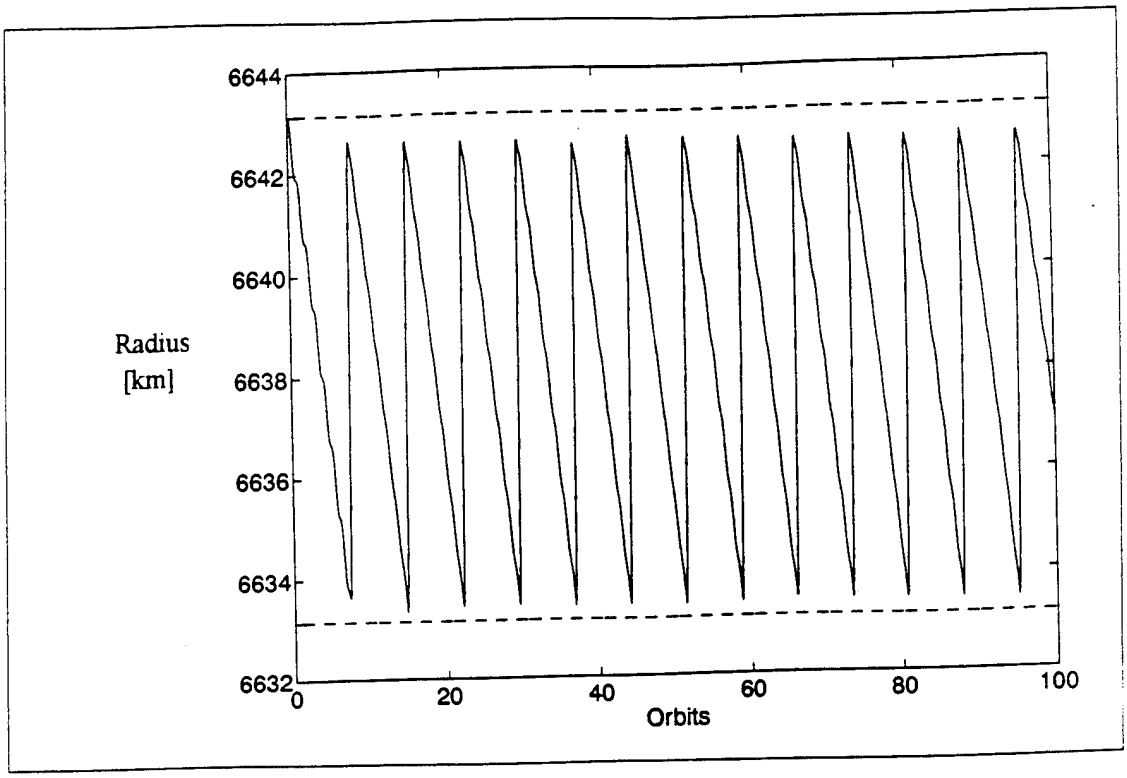

Figure 50. Dual Burn Strategy Orbital Radius (10 km Bandwidth, 160 N Thrust)

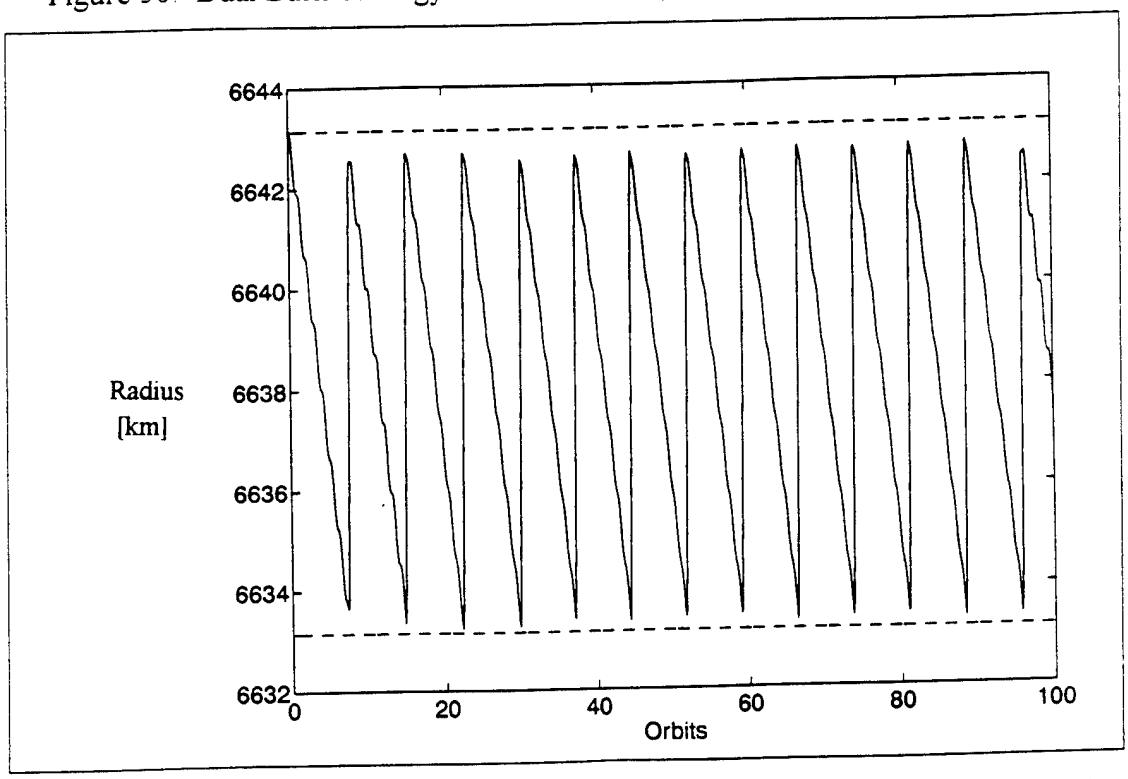

Figure 51. Dual Burn Strategy Orbital Radius (10 km Bandwidth, 320 N Thrust)

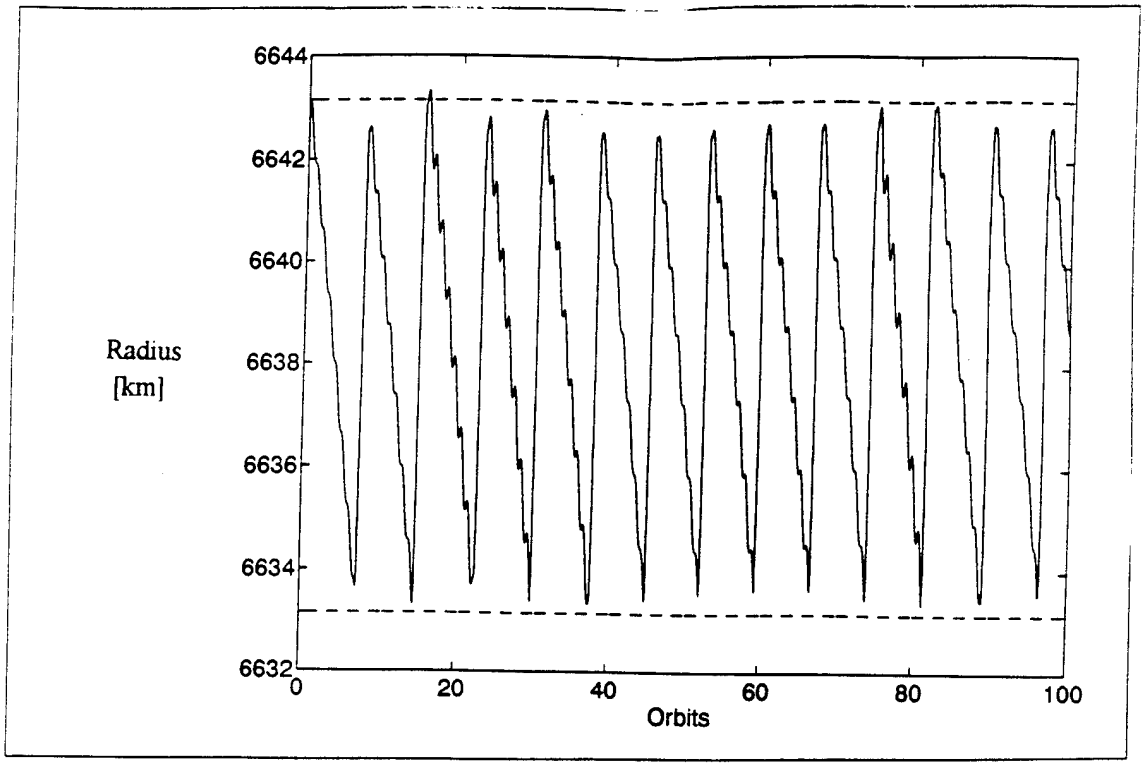

Figure 52. Dual Burn Strategy Orbital Radius (10 km Bandwidth, 640 N Thrust)

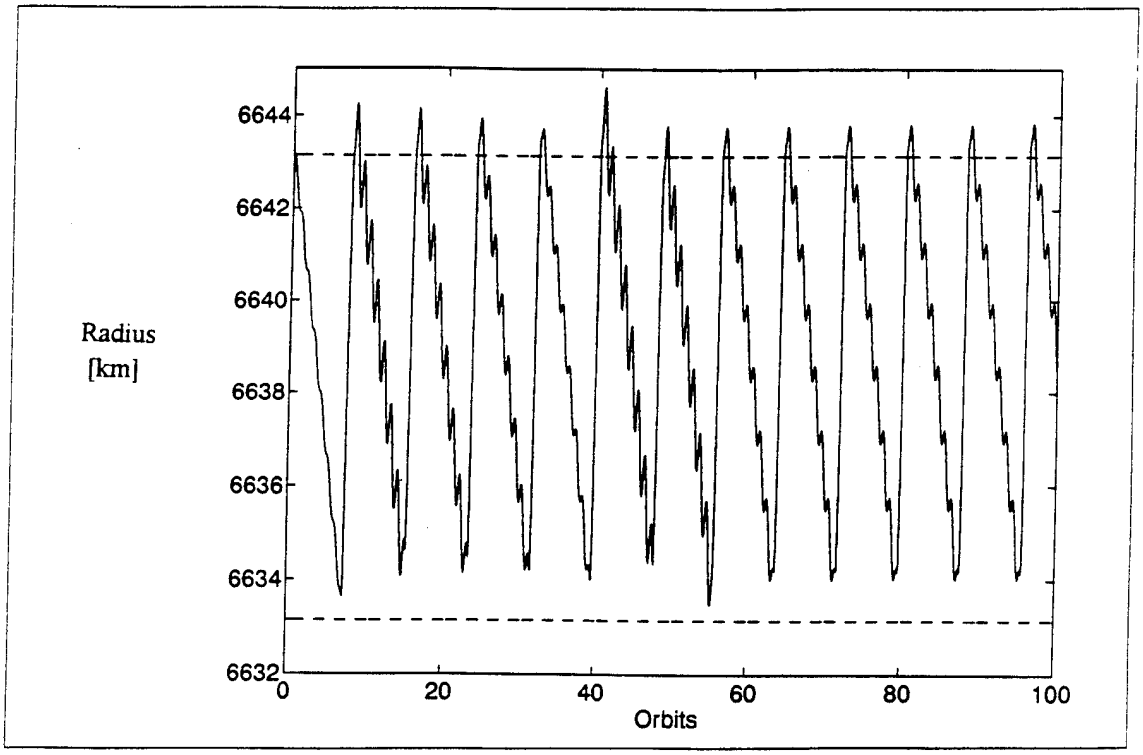

Figure 53. Dual Burn Strategy Orbital Radius (10 km Bandwidth, 1280 N Thrust)

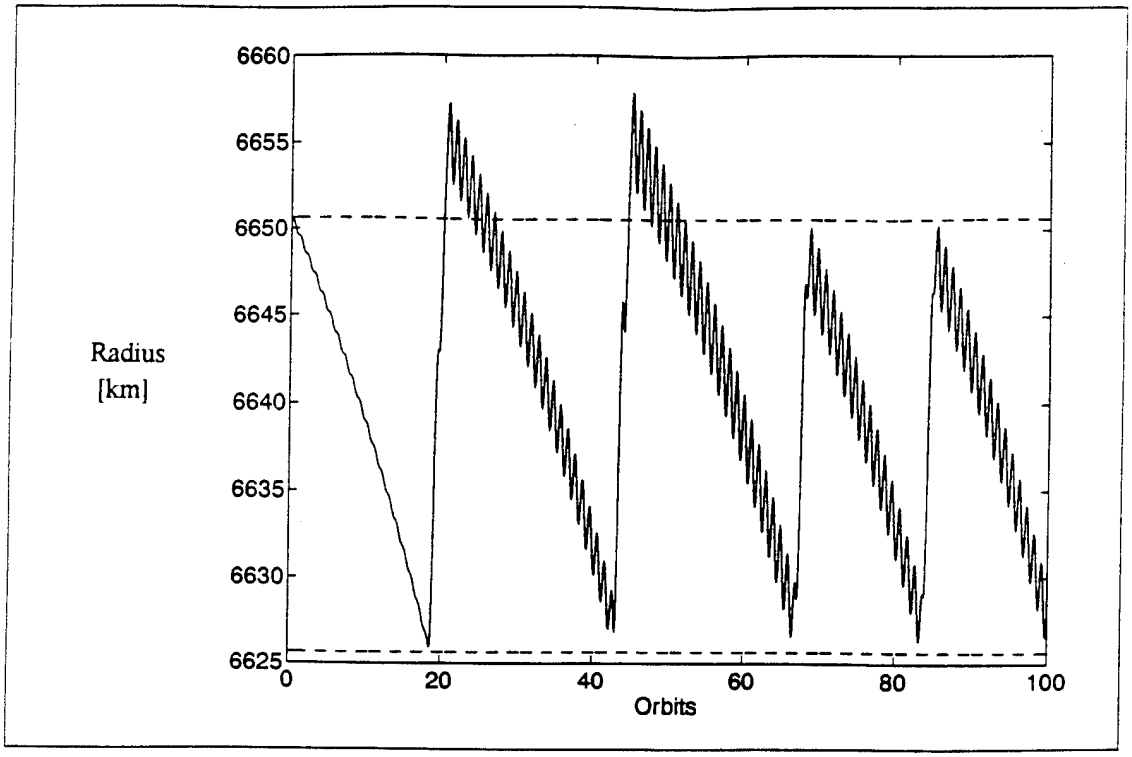

Figure 54. Dual Burn Strategy Orbital Radius (25 km Bandwidth, 40 N Thrust)

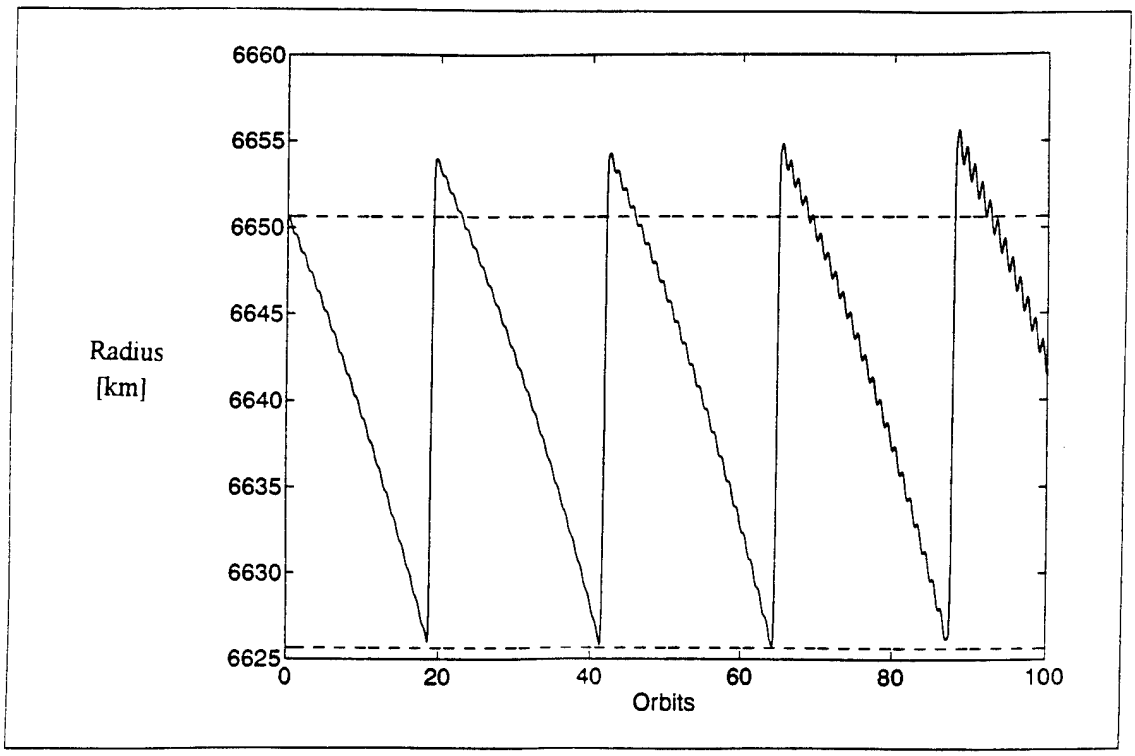

Figure 55. Dual Burn Strategy Orbital Radius (25 km Bandwidth, 80 N Thrust)

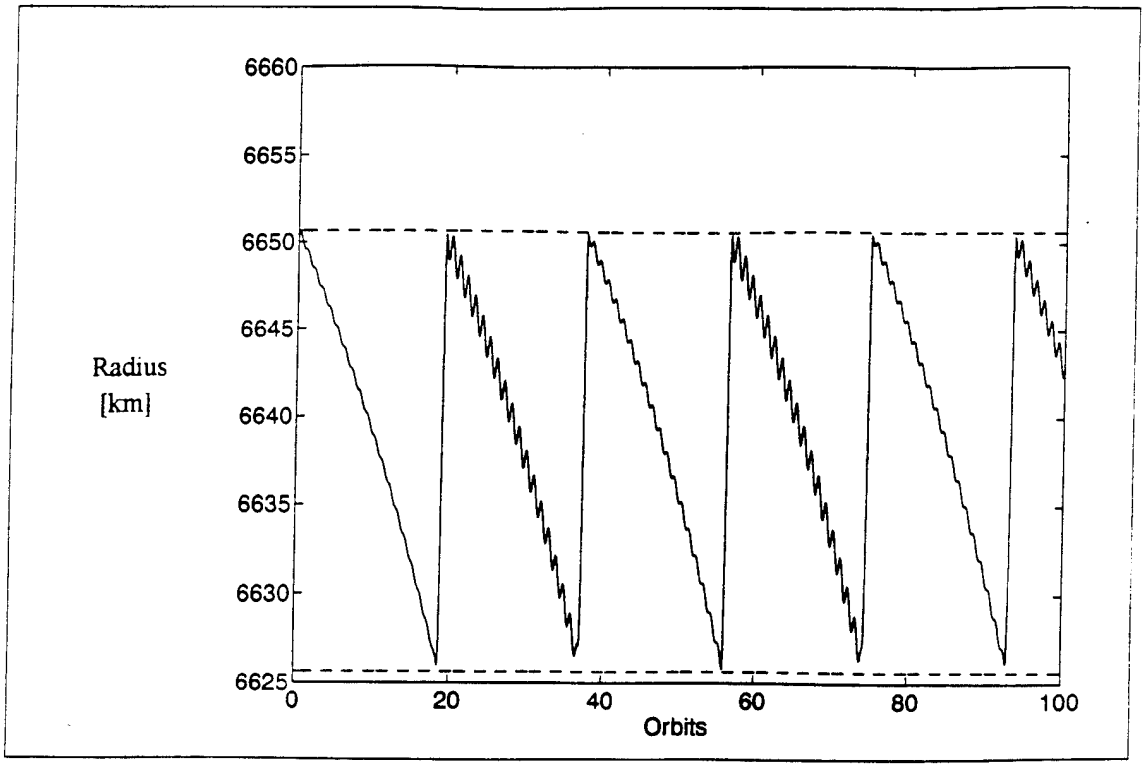

Figure 56. Dual Burn Strategy Orbital Radius (25 km Bandwidth, 160 N Thrust)

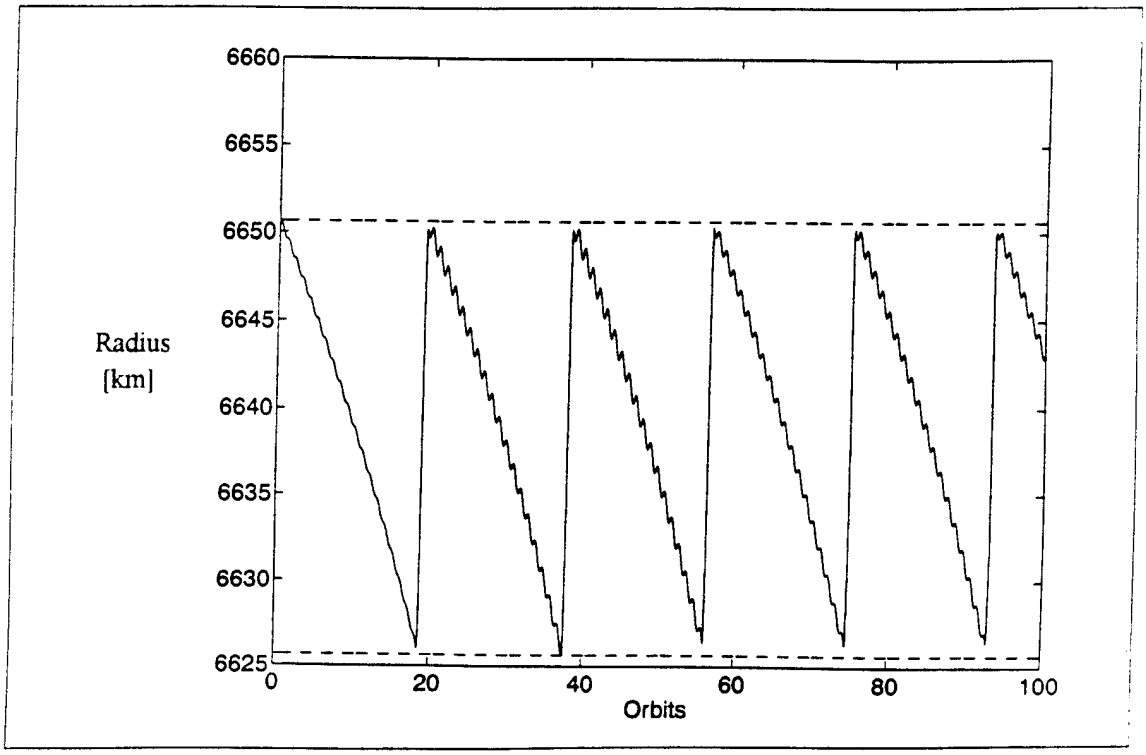

Figure 57. Dual Burn Strategy Orbital Radius (25 km Bandwidth, 320 N Thrust)

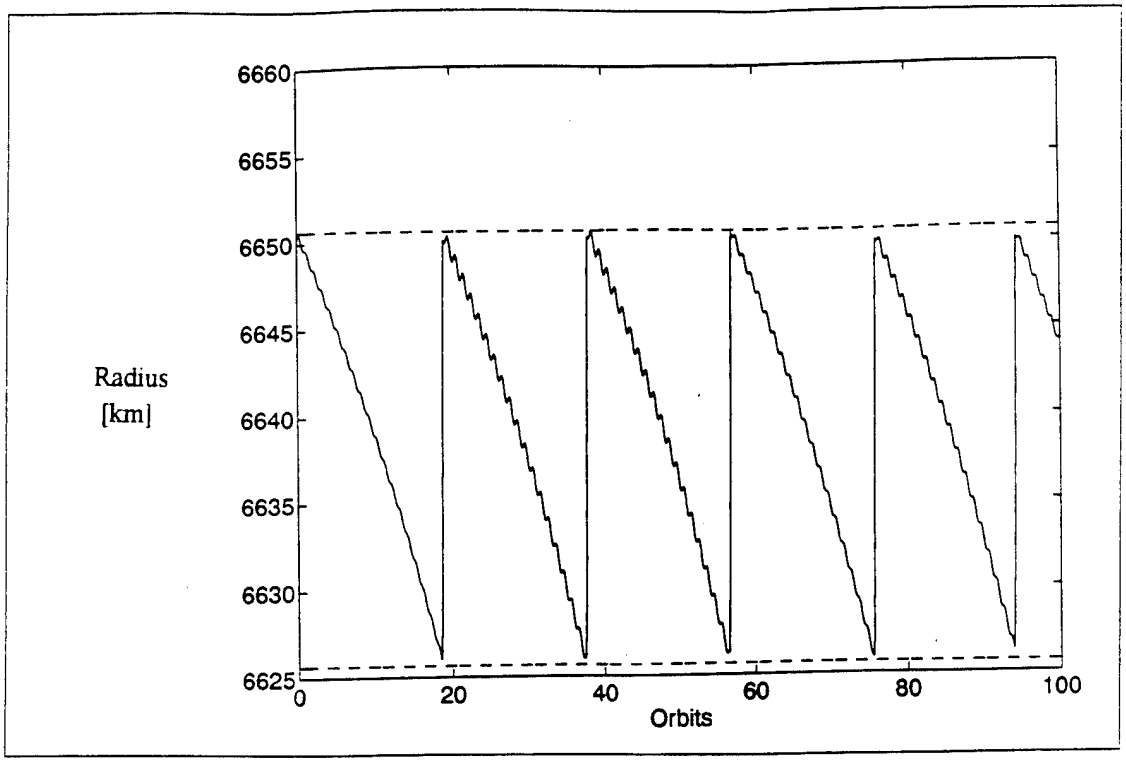

Figure 58. Dual Burn Strategy Orbital Radius (25 km Bandwidth, 640 N Thrust)

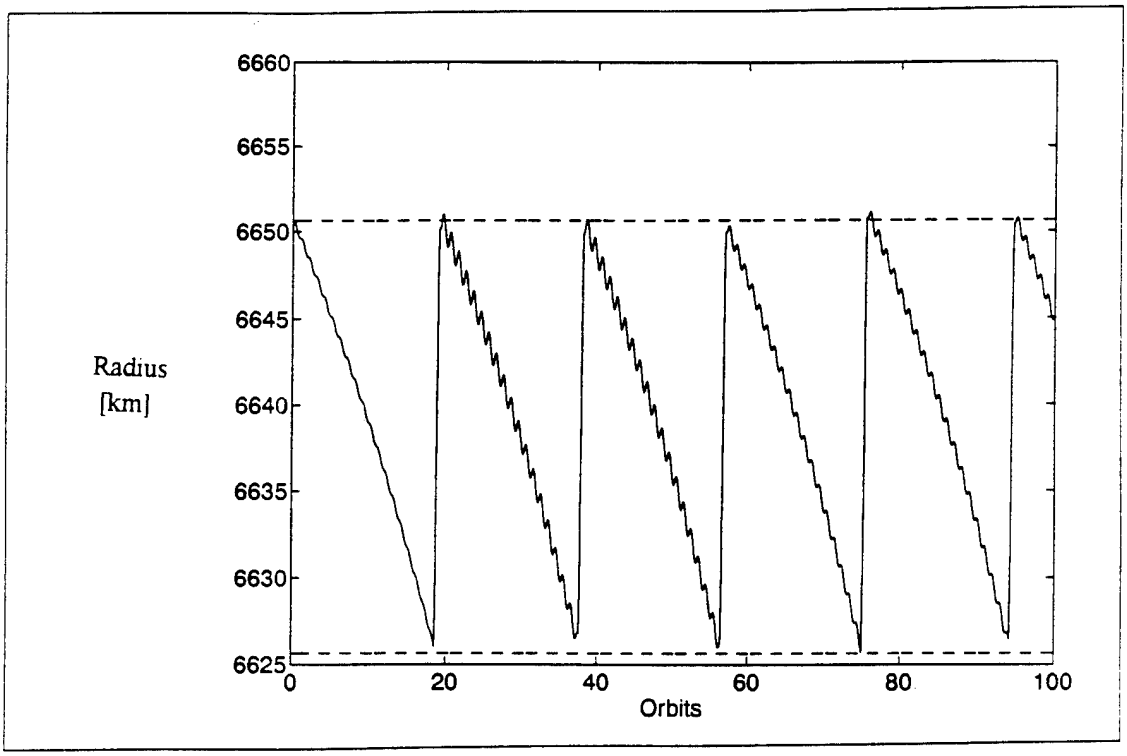

Figure 59. Dual Burn Strategy Orbital Radius (25 km Bandwidth, 1280 N Thrust)

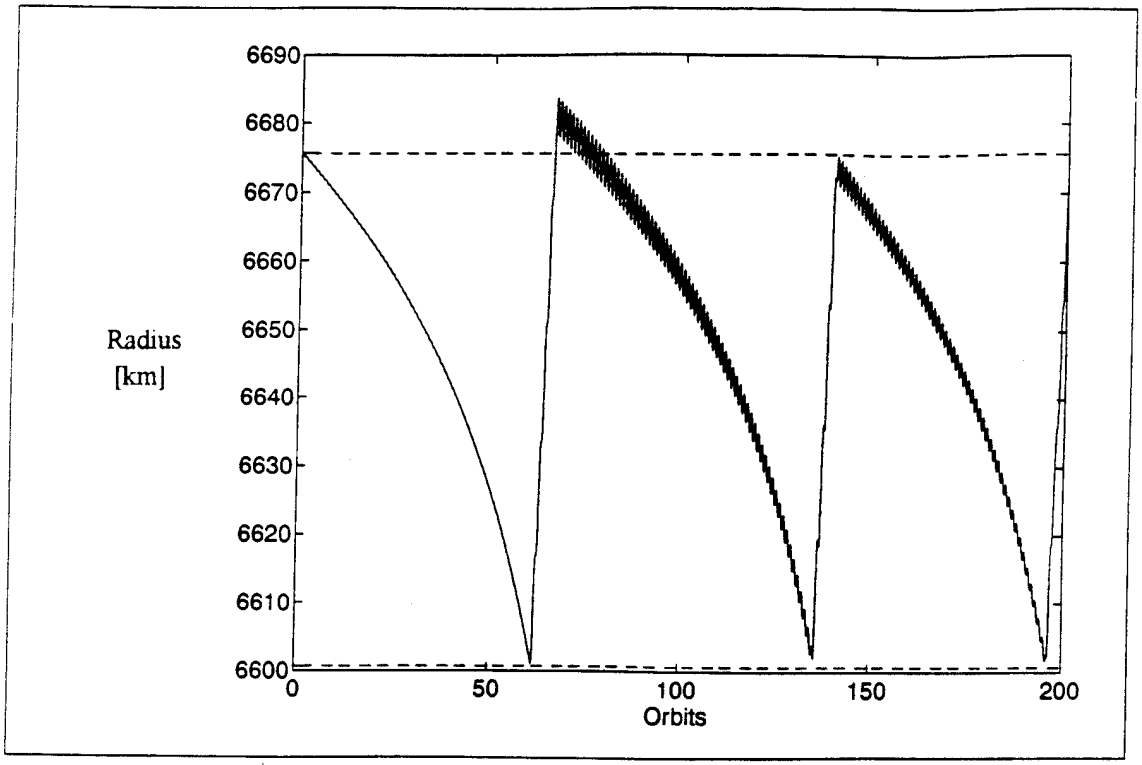

Figure 60. Dual Burn Strategy Orbital Radius (75 km Bandwidth, 40 N Thrust)

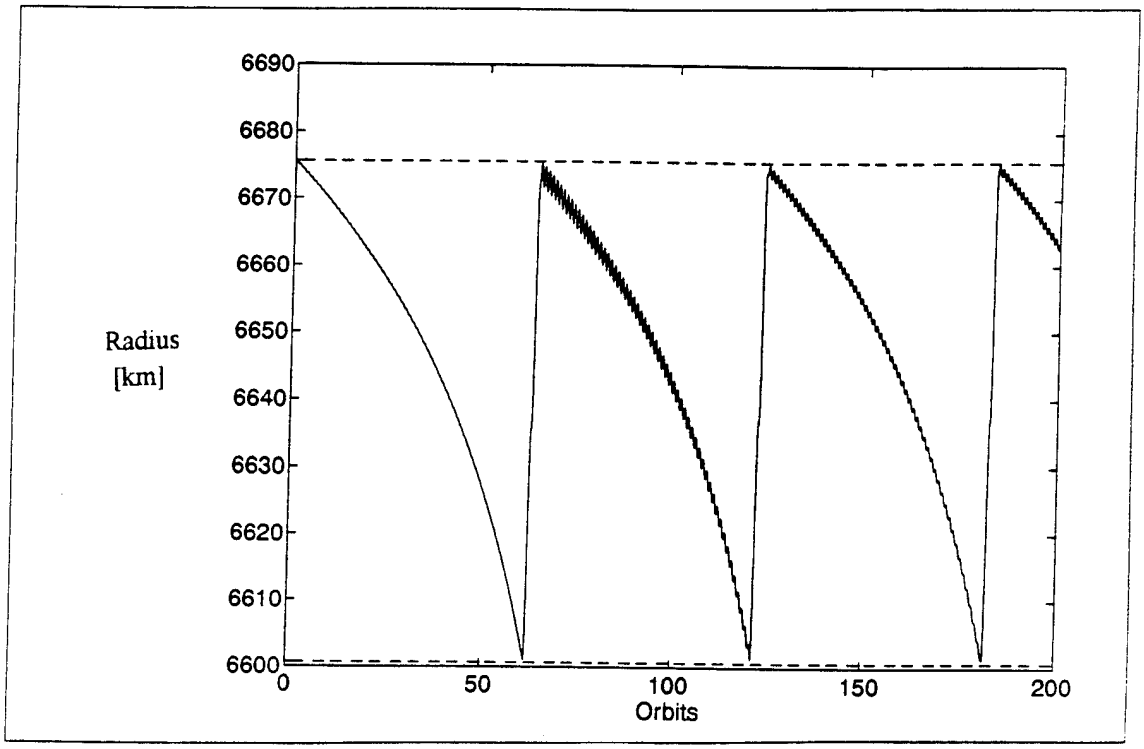

Figure 61. Dual Burn Strategy Orbital Radius (75 km Bandwidth, 80 N Thrust)

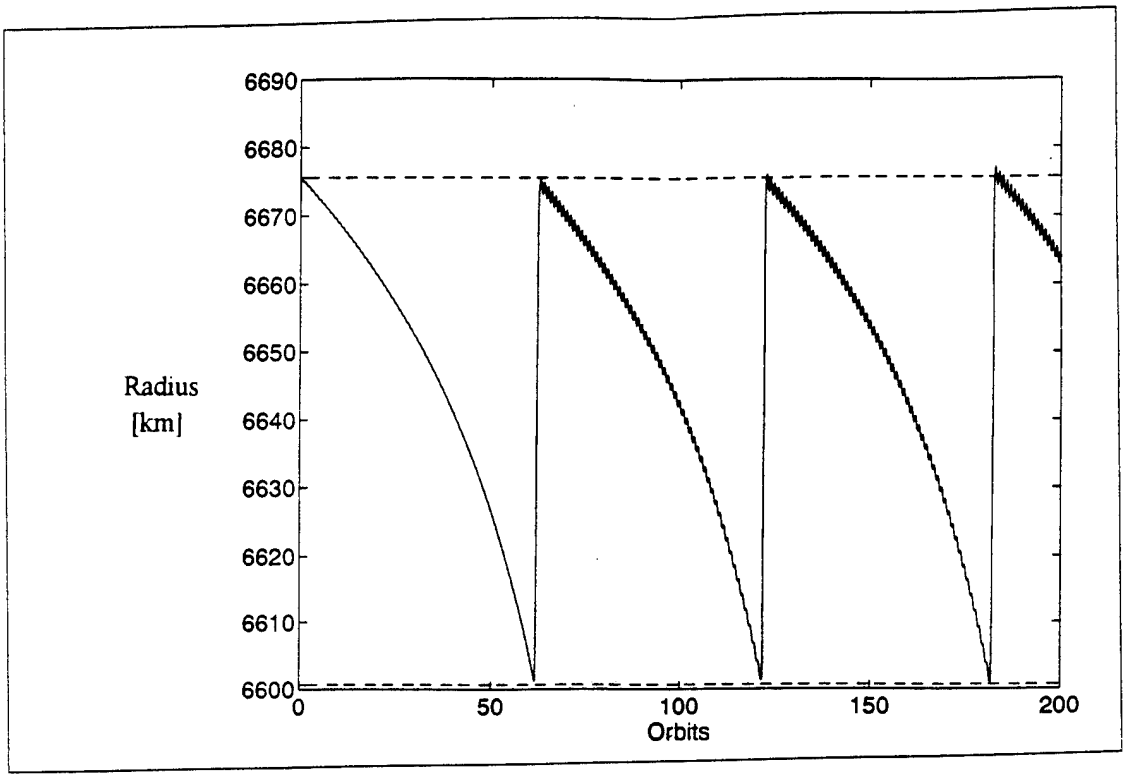

Figure 62. Dual Burn Strategy Orbital Radius (75 km Bandwidth, 160 N Thrust)

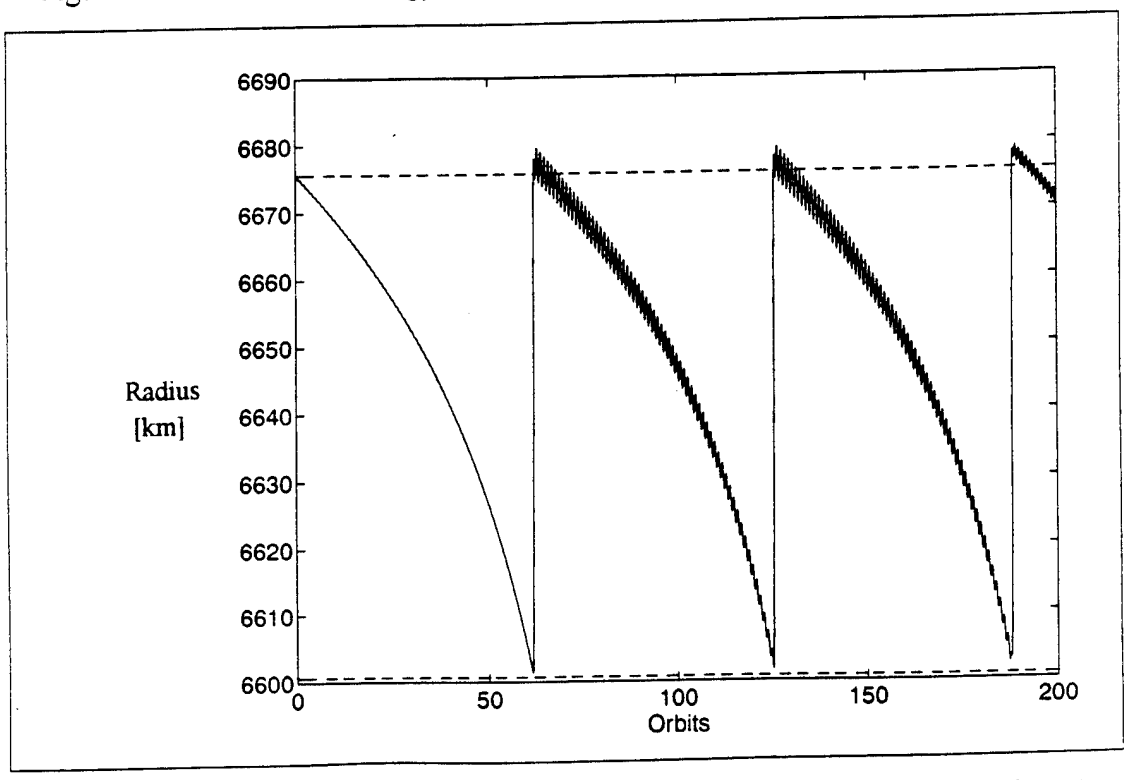

Figure 63. Dual Burn Strategy Orbital Radius (75 km Bandwidth, 320 N Thrust)

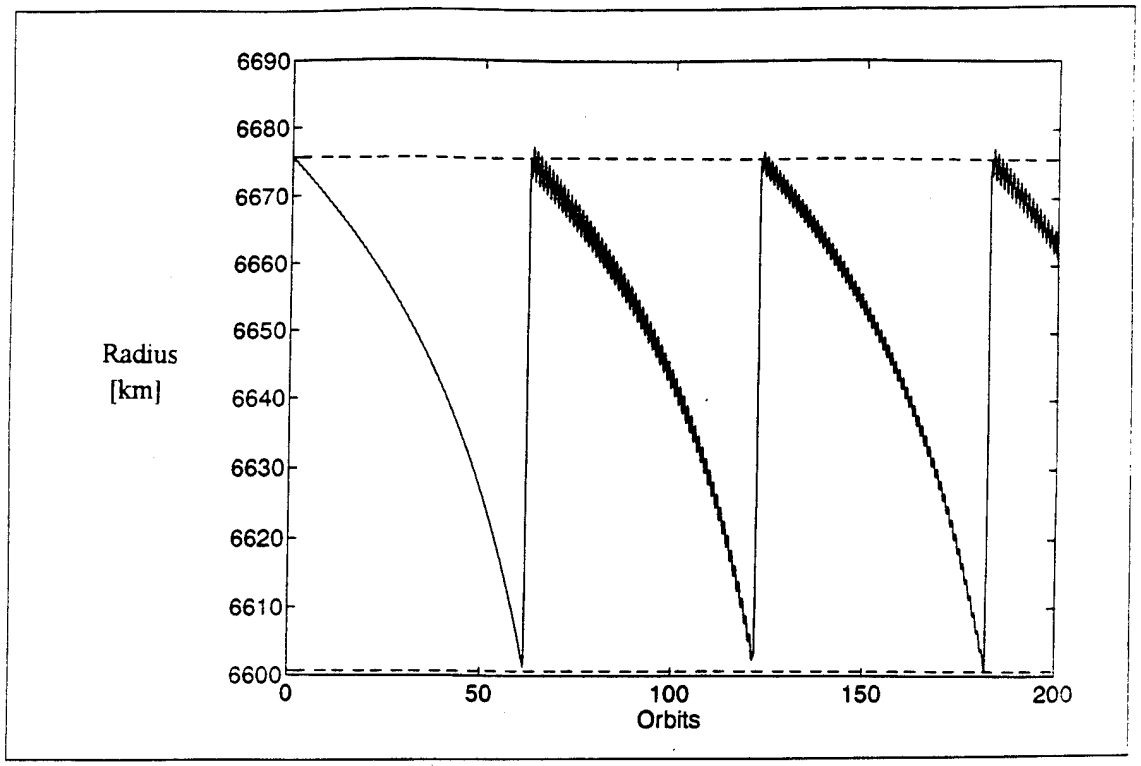

Figure 64. Dual Burn Strategy Orbital Radius (75 km Bandwidth, 640 N Thrust)

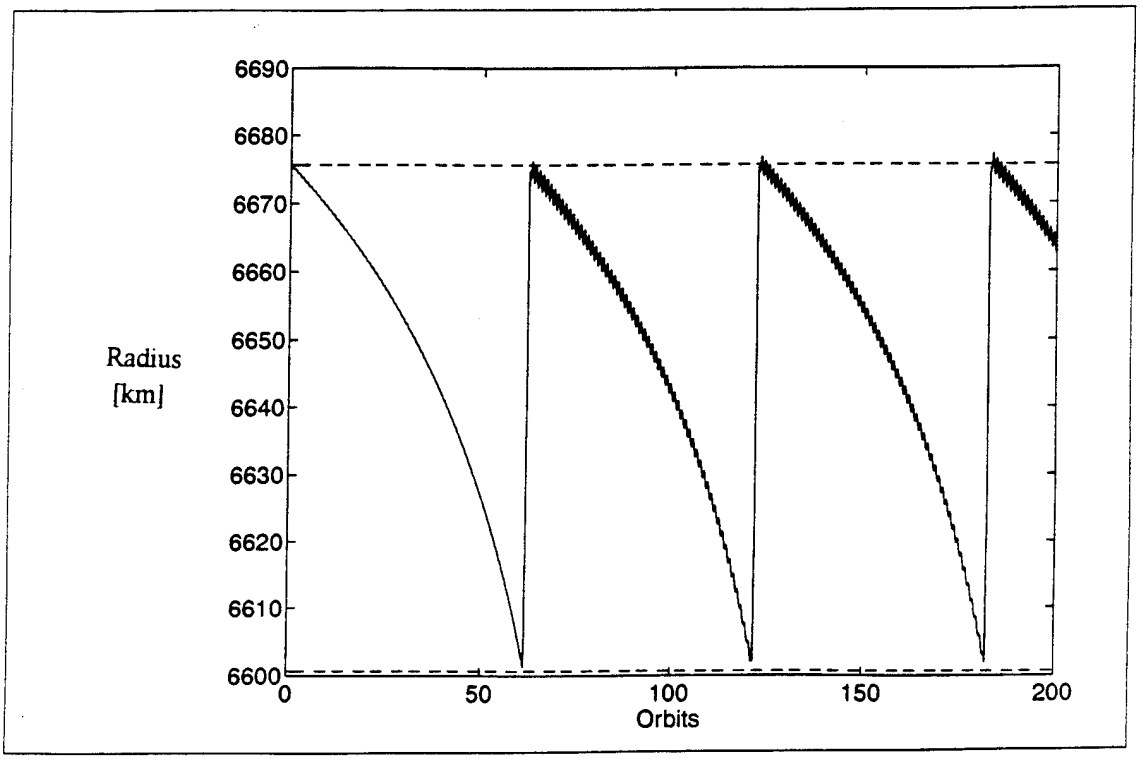

Figure 65. Dual Burn Strategy Orbital Radius (75 km Bandwidth, 1280 N Thrust)

2. Orbital Path

The orbital trajectory for the dual burn maneuver was significantly smoother than that of the single burn. Raising the perigee radius with the additional thrusting sufficiently reduced the eccentricity to enable a near-circular decay pattern to evolve in most cases. In those where the burn started early the eccentricity was decreased enough to prevent the wide range of apogee and perigee experienced in the single burn maneuver.

Bandwidth	Thrust [N]					
[km]	40	80	160	320	640	1,280
2	SAT	SAT	SAT	SAT	+10%	UNSAT
10	SAT	SAT	SAT	SAT	+2%	+12%
25	+30%	+24%	SAT	SAT	SAT	+4%
75	+10%	SAT	+3%	+5%	+3%	+3%
SAT = Satisfactorily Maintains Band UNSAT = Unsatsifactory			+_% = _% Above Maximum Radius Limit (% of Bandwidth)			

Table 4. Dual Burn Strategy Band Maintenance Summary

C. PROPELLANT CONSUMPTION

Propellant consumption is calculated for each variation of the single and dual burn maneuvers, as well as for an FKT at the maximum radius, midband radius, and minimum radius. An additional consideration involves the strategy of using a FKT to keep the satellite at the upper radial limit until the time when removing any thrusting would cause the orbit to decay to the minimum radius by the end of the run period. TFCL consumption is compared against these four base usage patterns.

Consumption for both the single and dual burn strategies is approximately the same. The exact value at any given instant may be higher for one or the other, but the average values overall are generally equal. Plateaus between burns are longer in the dual burn case, as expected. Burns occur more frequently in the single burn maneuver because

the perigee radius may not be sufficiently raised by any given burn to preclude drag quickly decaying it below the minimum limit.

Comparison of the two methods with the four baselines described above provides insight into their efficiency. In all cases considered the propellant required by either TFCL strategy is slightly less than or roughly equal to the midband FKT counterpart. As the bandwidth gets very large the TFCL values appear to drop away from the midband ones. The low altitude FKT consumes more, significantly more in cases of larger bandwidths, than the midband FKT. The upper radius FKT and its modified version use less that the midband FKT. Both TFCL models seem to be bounded above by the midband FKT and below by the high altitude FKT, as indicated in Figures 66 through 89. This suggests that although TFCL is better than attempting an FKT at the middle of the radial bandwidth, it is less efficient than either an FKT at the maximum radius or the modified maneuver described previously.

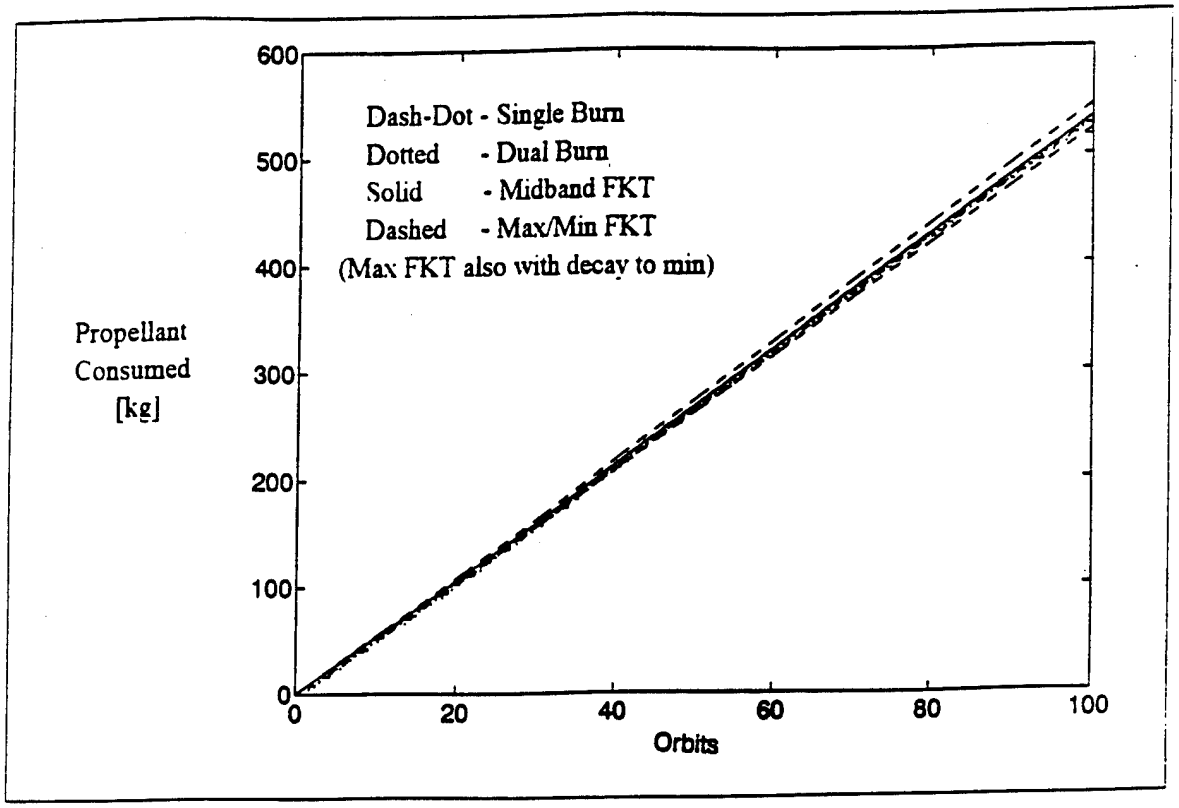

Figure 66. Propellant Consumption (2 km Bandwidth, 40 N Thrust)

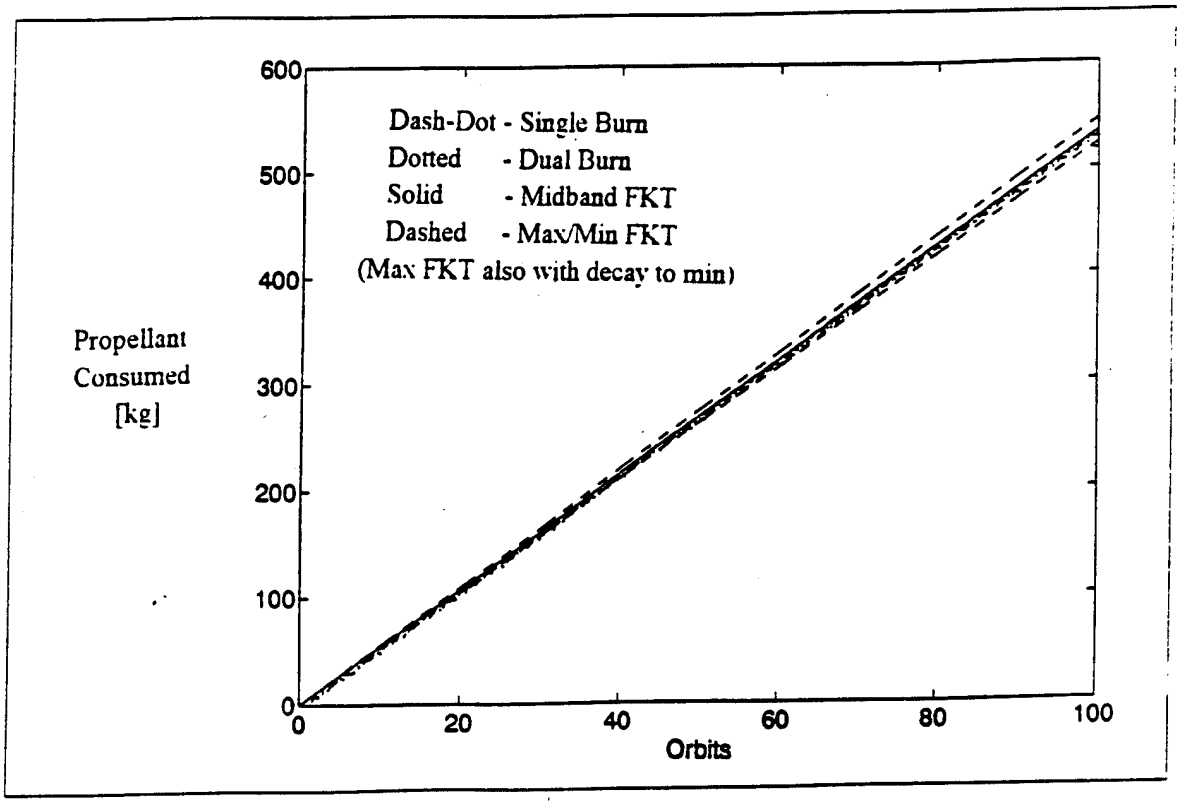

Figure 67. Propellant Consumption (2 km Bandwidth, 80 N Thrust)

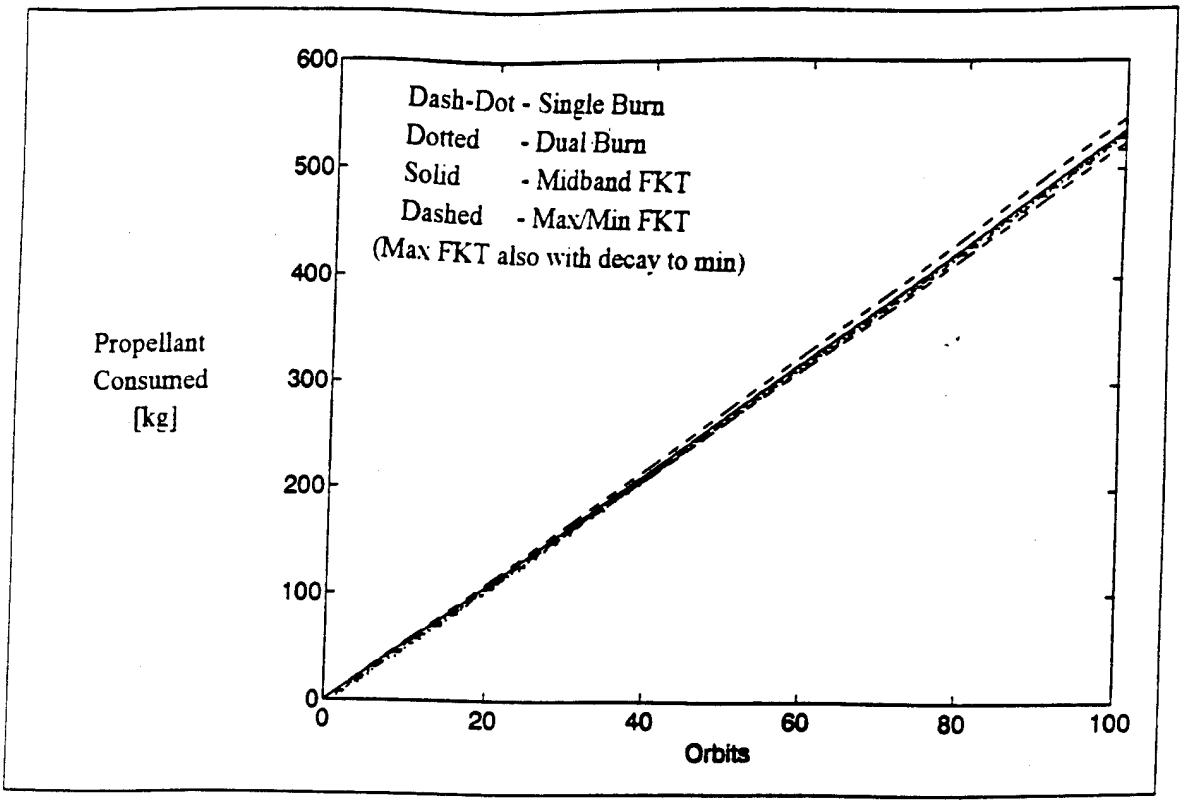

Figure 68. Propellant Consumption (2 km Bandwidth, 160 N Thrust)

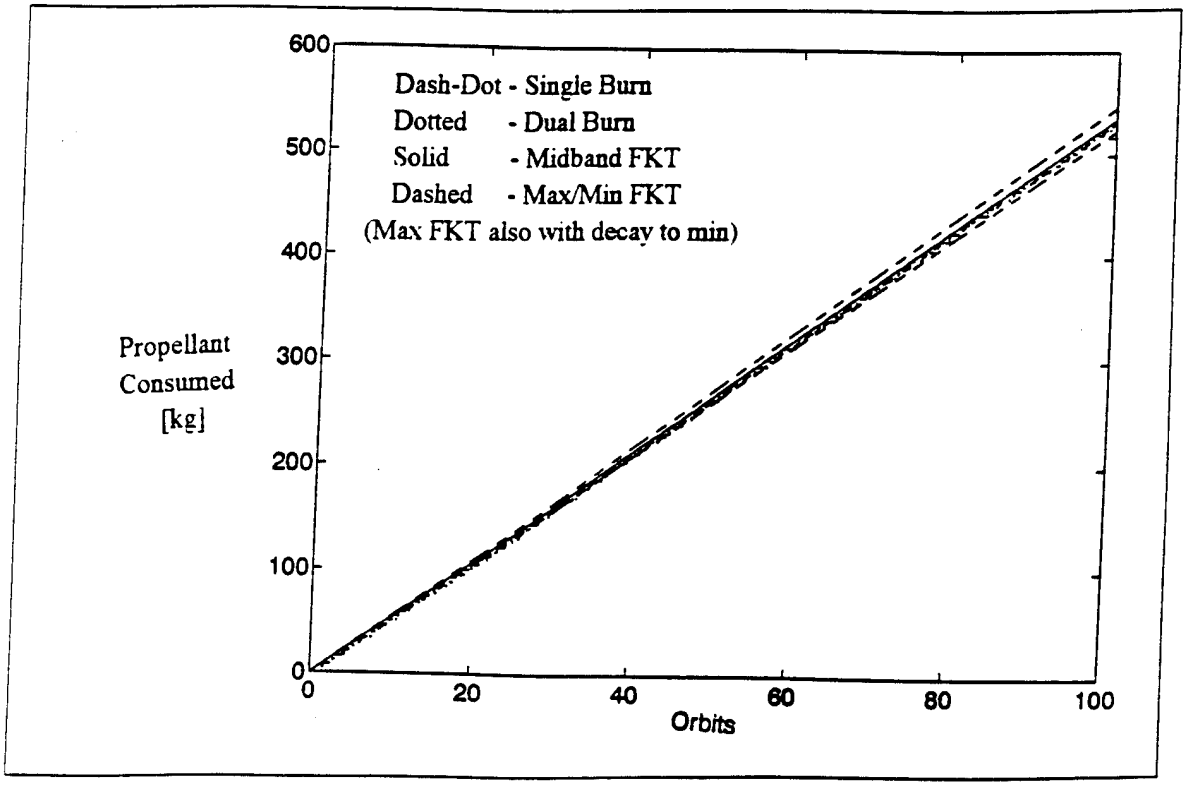

Figure 69. Propellant Consumption (2 km Bandwidth, 320 N Thrust)

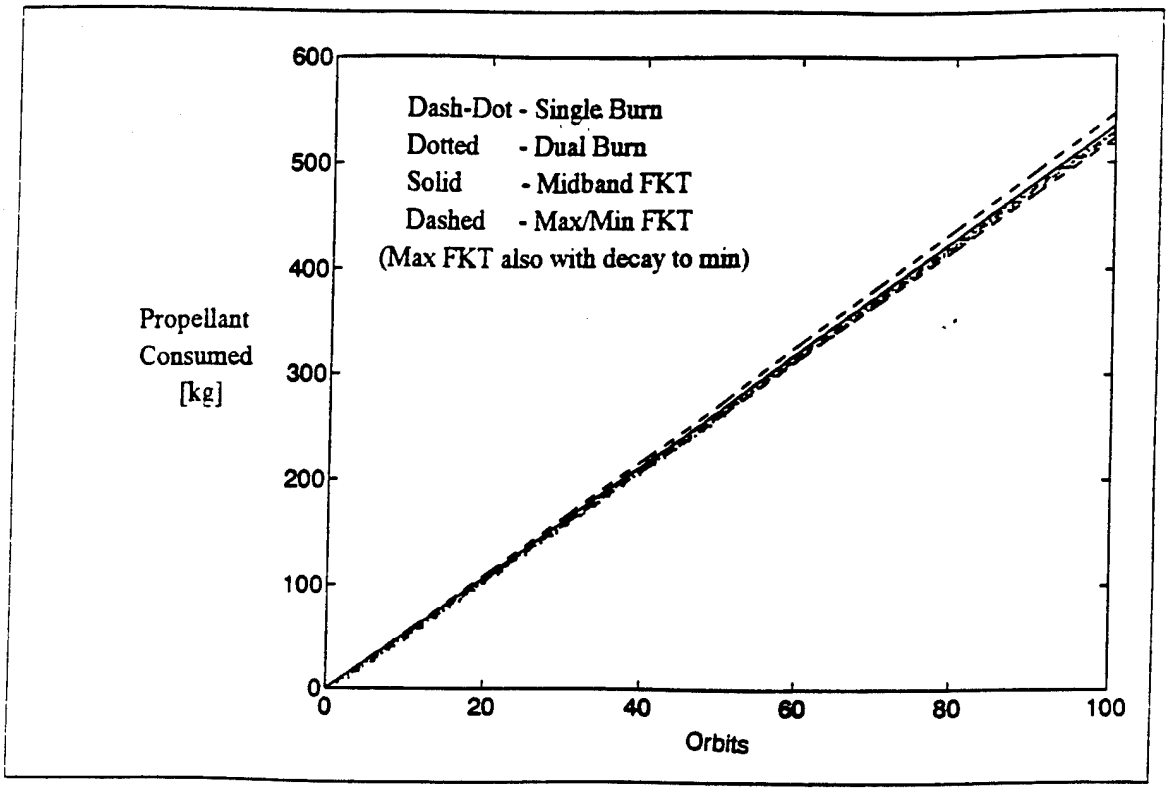

Figure 70. Propellant Consumption (2 km Bandwidth, 640 N Thrust)

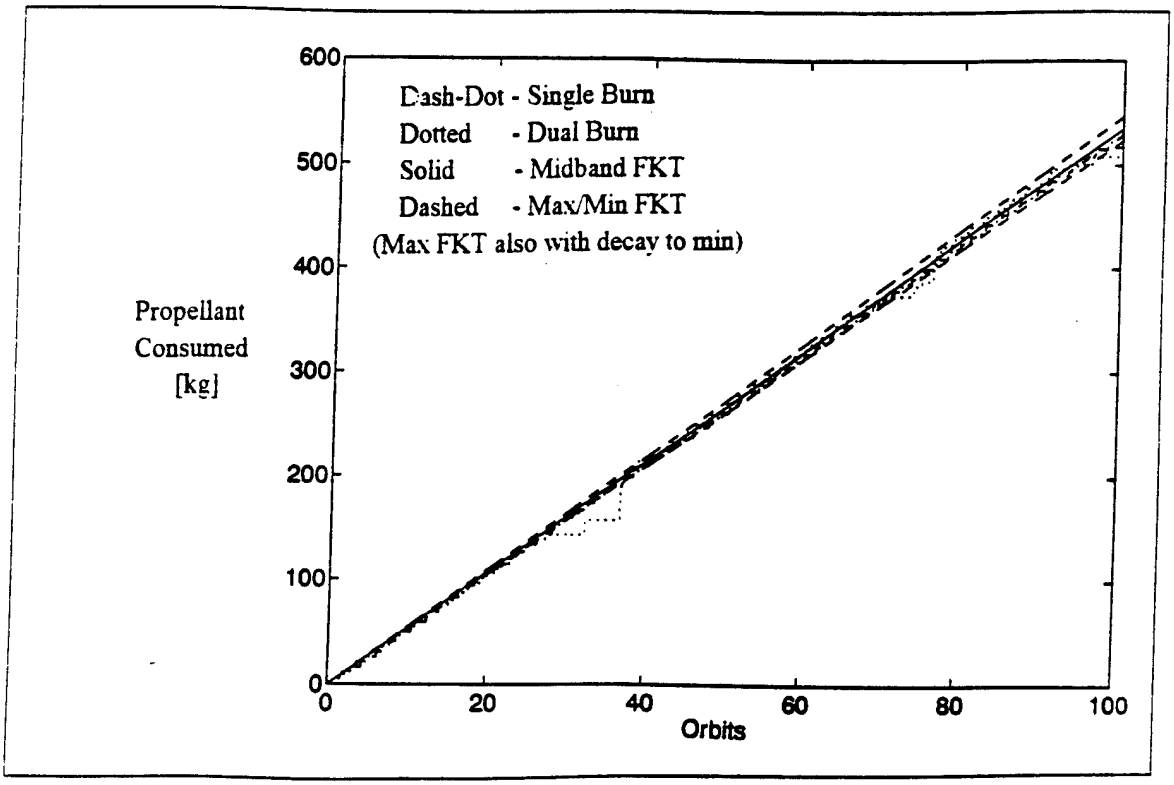

Figure 71. Propellant Consumption (2 km Bandwidth, 1280 N Thrust)

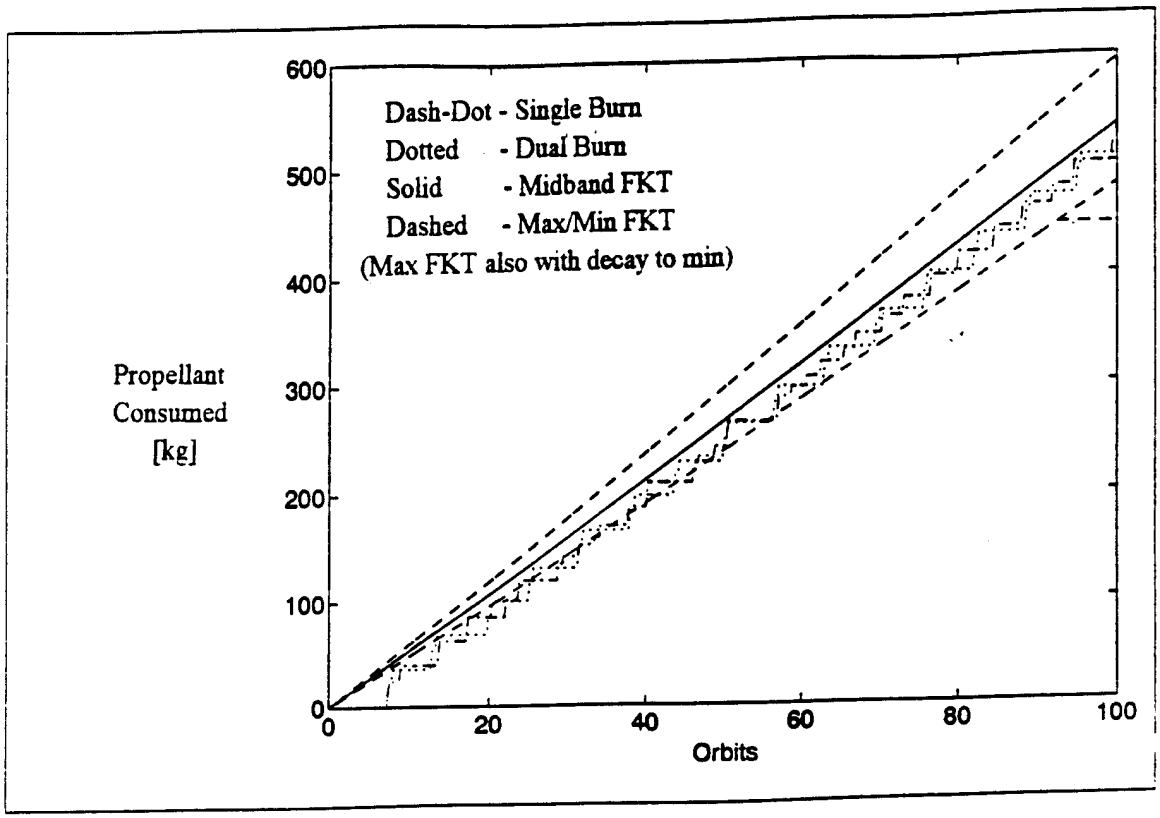

Figure 72. Propellant Consumption (10 km Bandwidth, 40 N Thrust)

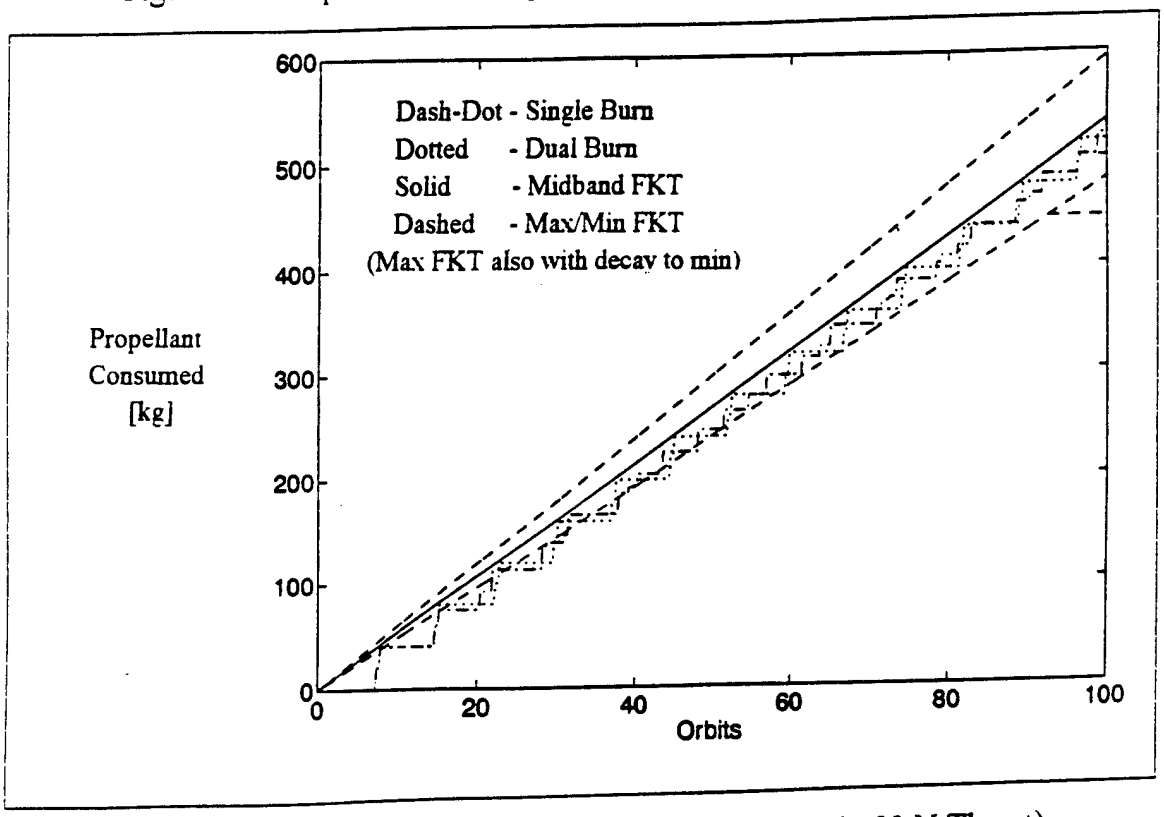

Figure 73. Propellant Consumption (10 km Bandwidth, 80 N Thrust)

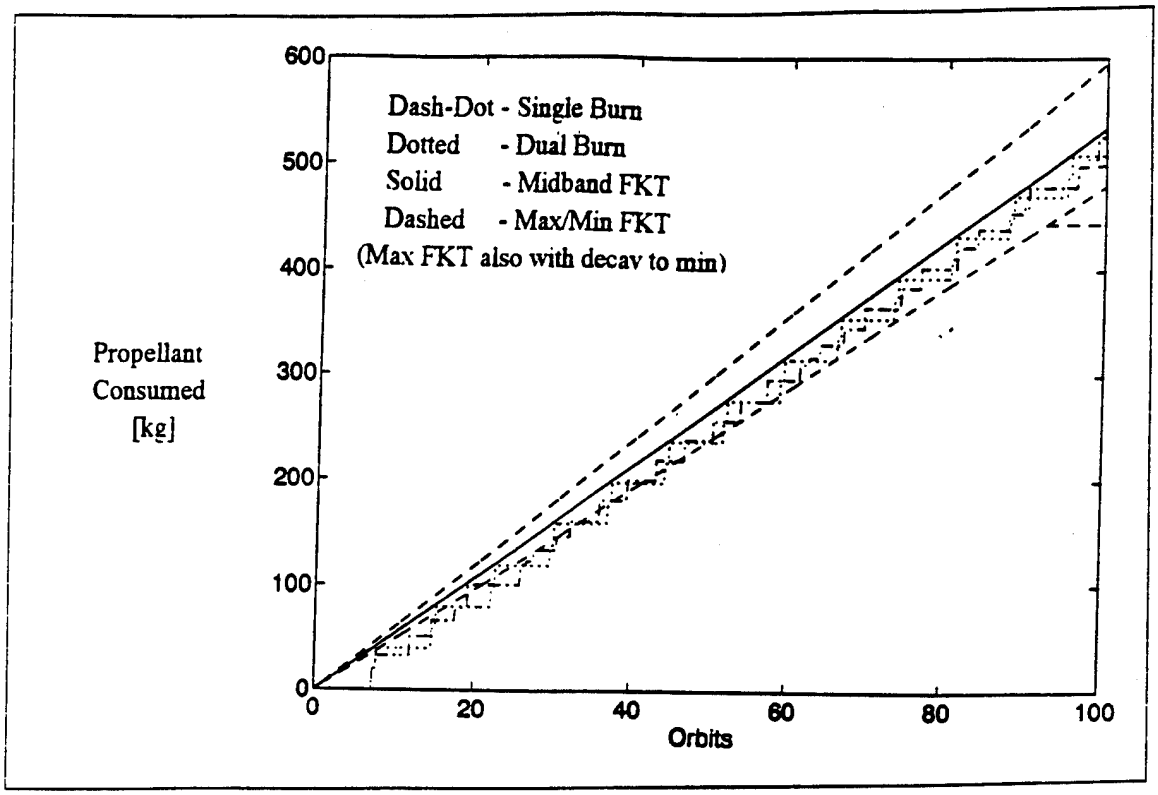

Figure 74. Propellant Consumption (10 km Bandwidth, 160 N Thrust)

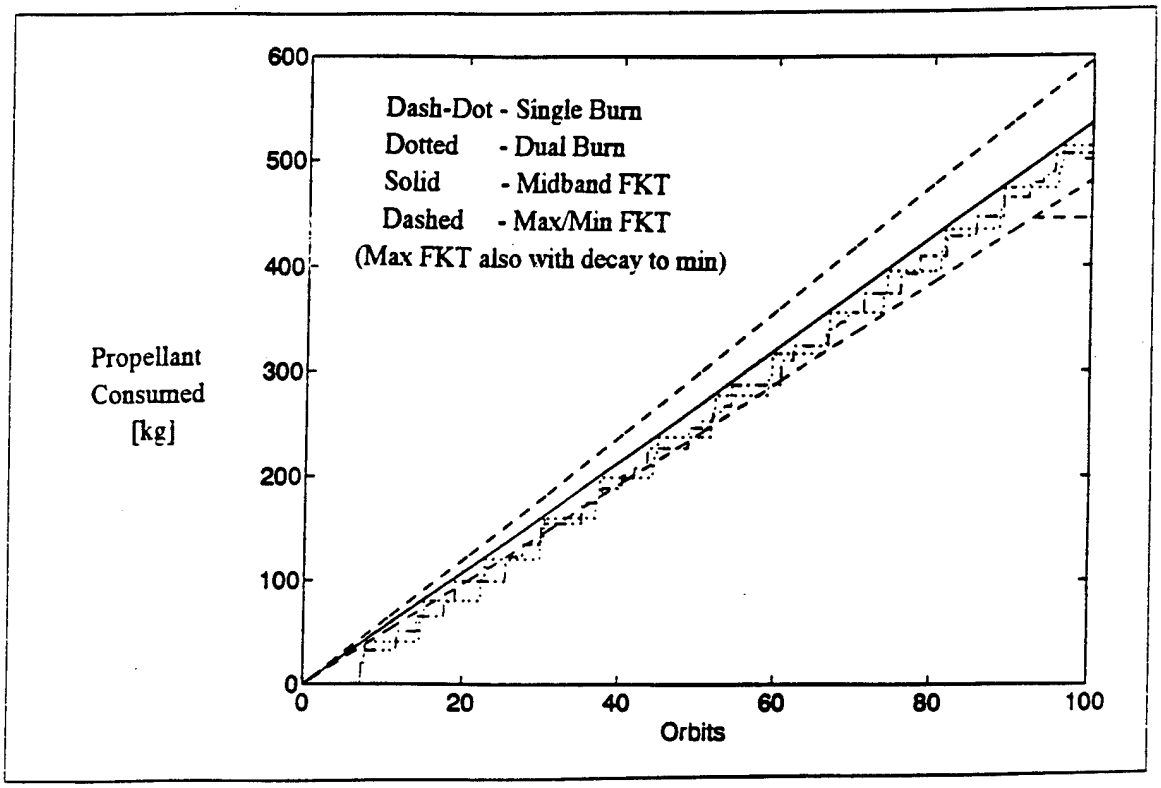

Figure 75. Propellant Consumption (10 km Bandwidth, 320 N Thrust)

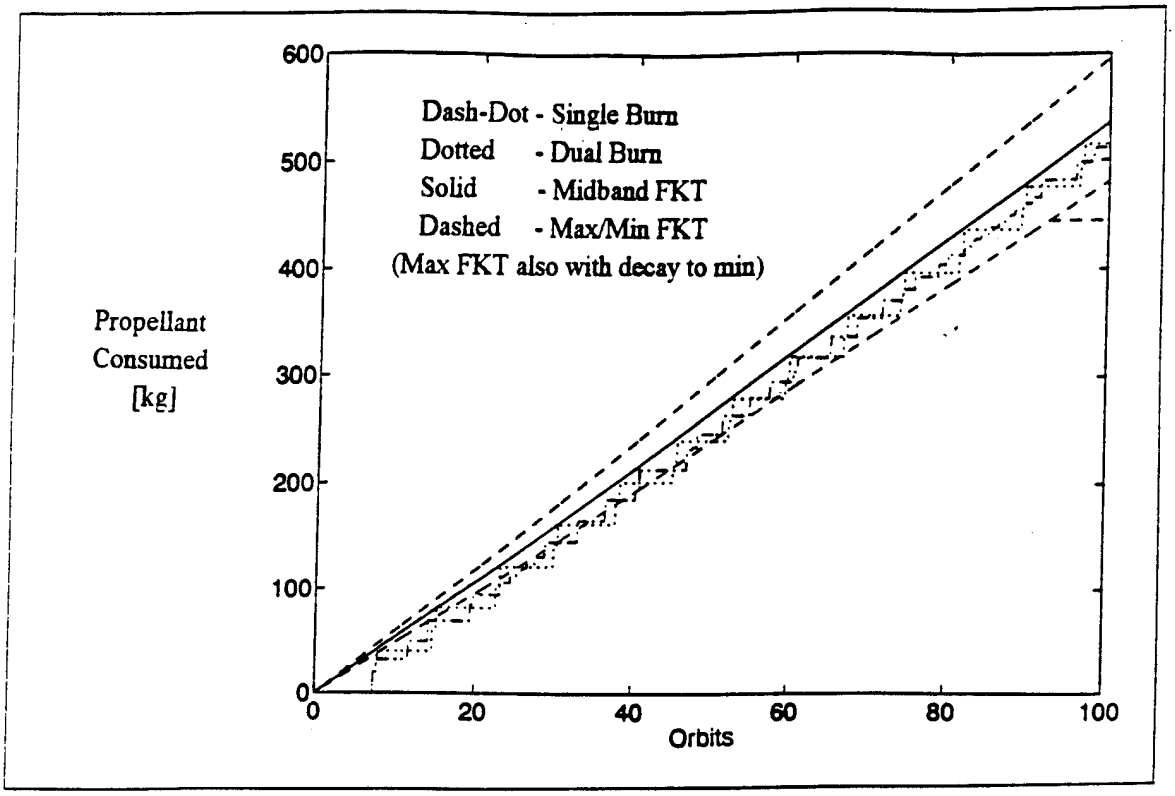

Figure 76. Propellant Consumption (10 km Bandwidth, 640 N Thrust)

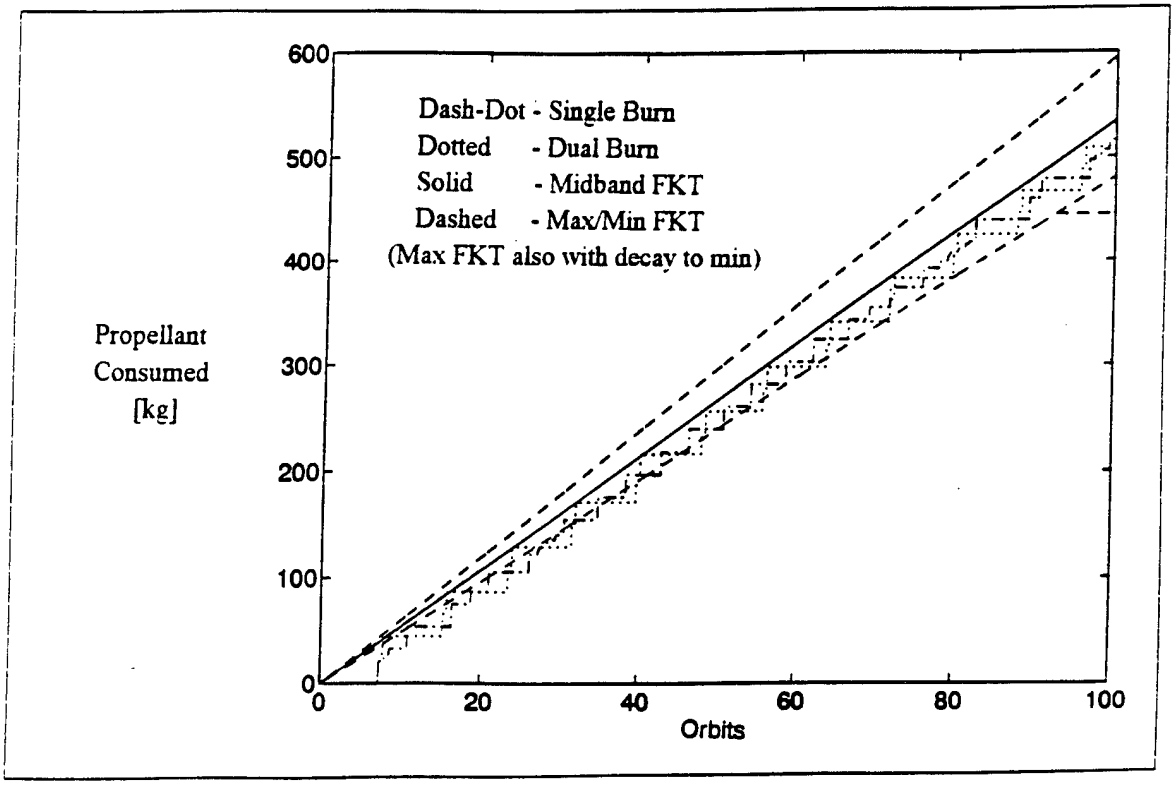

Figure 77. Propellant Consumption (10 km Bandwidth, 1280 N Thrust)

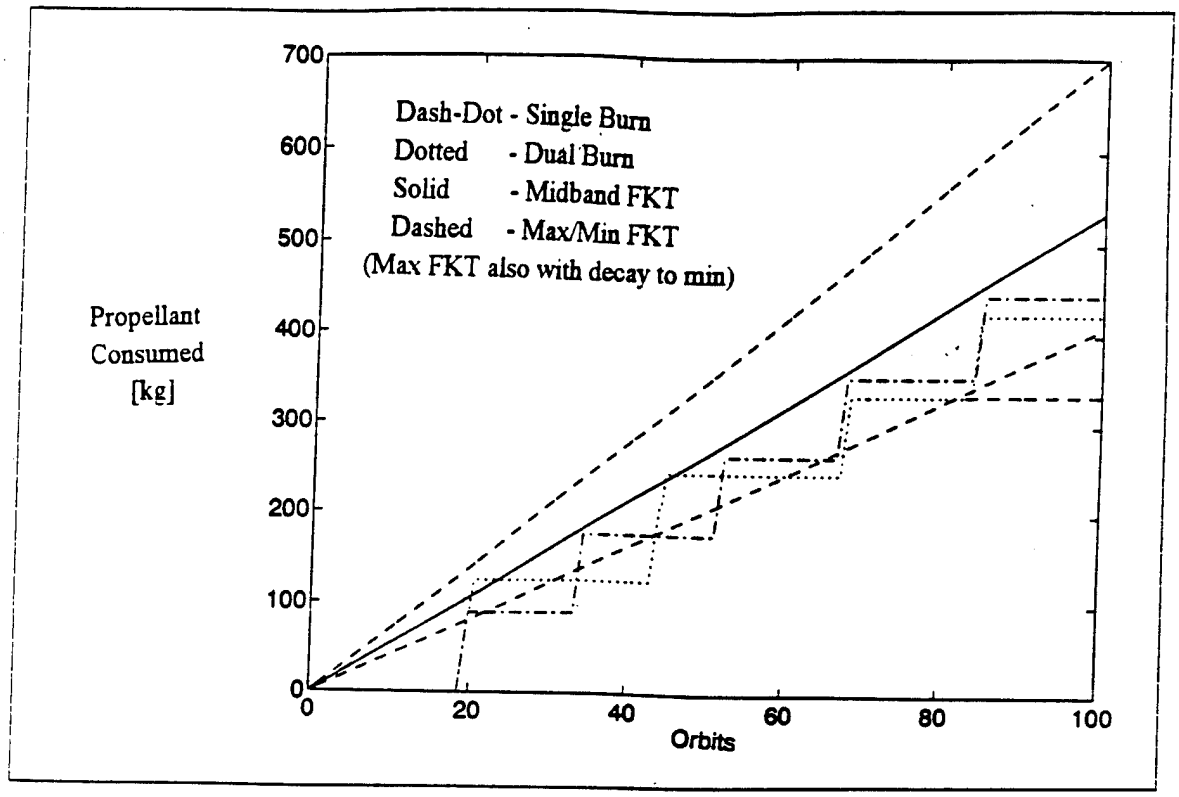

Figure 78. Propellant Consumption (25 km Bandwidth, 40 N Thrust)

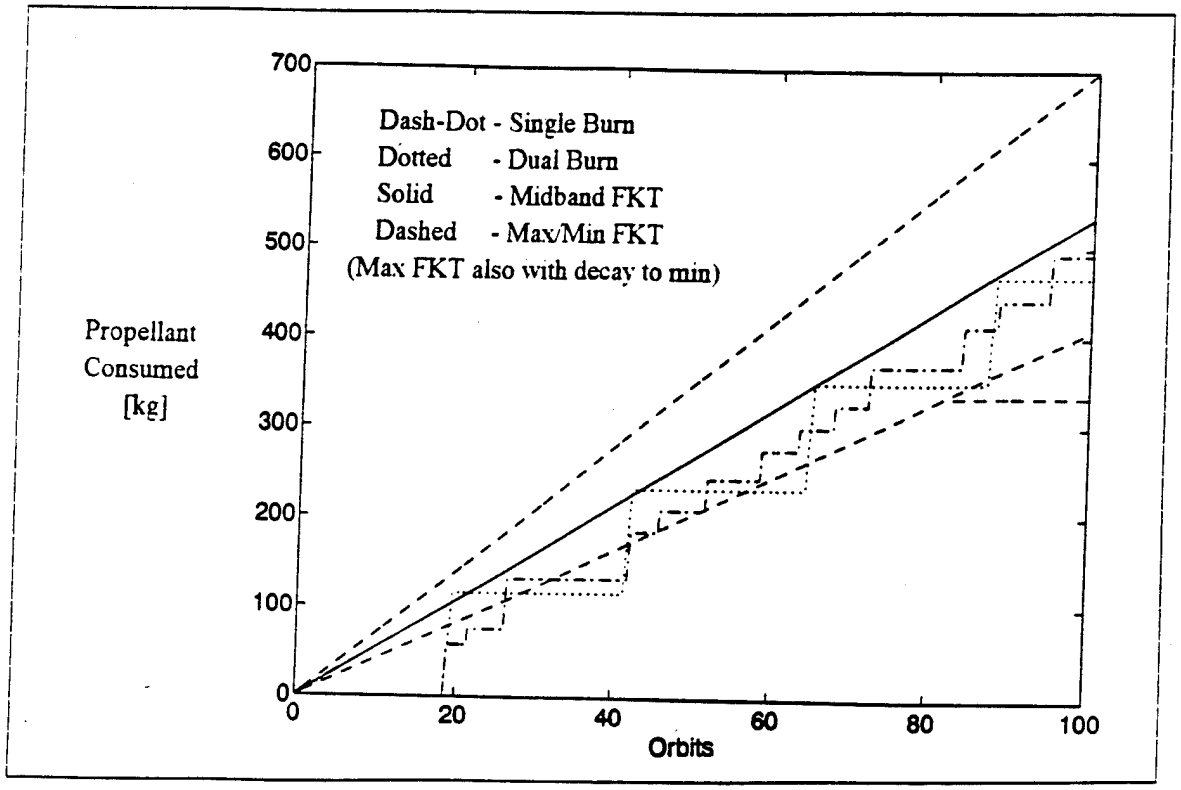

Figure 79. Propellant Consumption (25 km Bandwidth, 80 N Thrust)

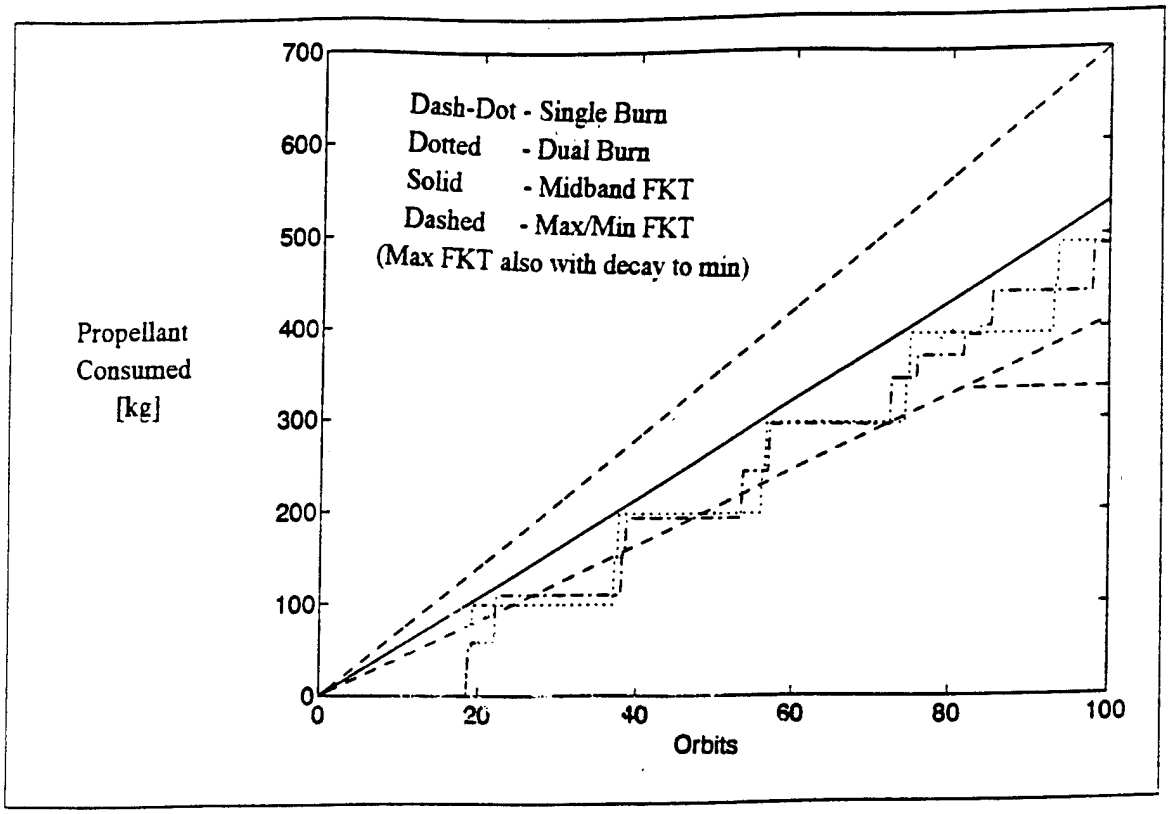

Figure 80. Propellant Consumption (25 km Bandwidth, 160 N Thrust)

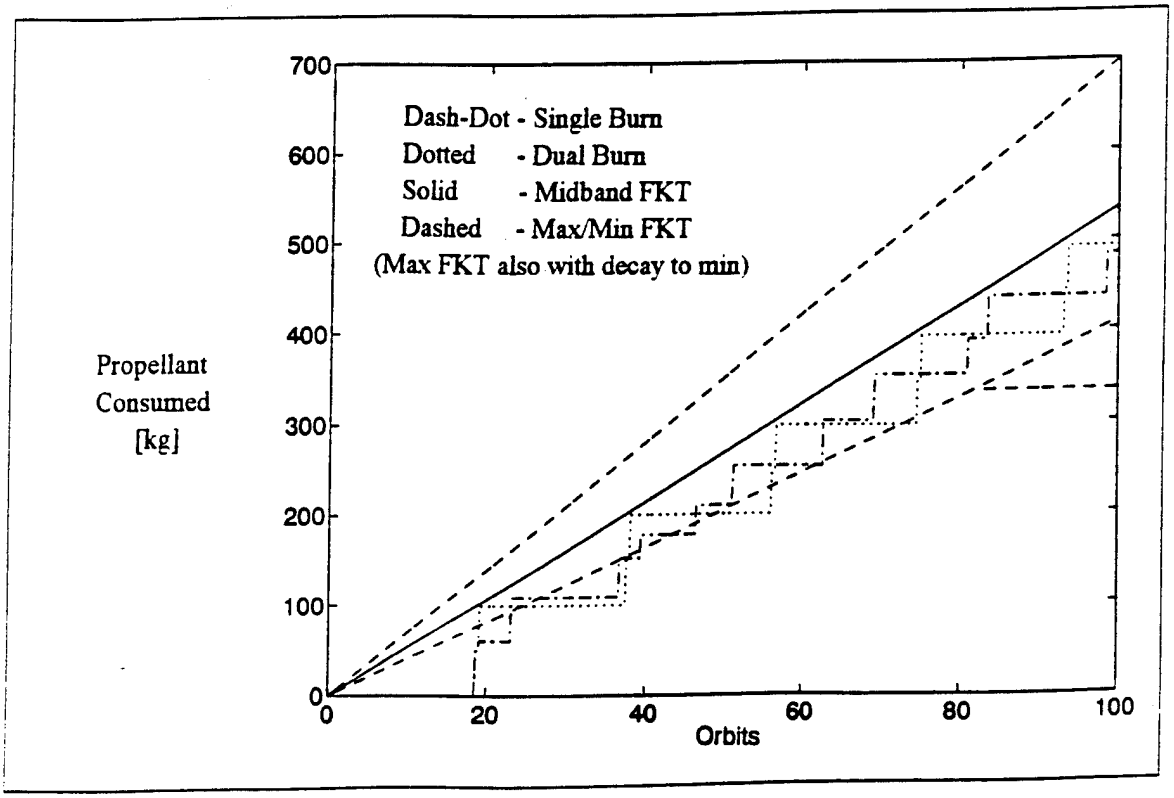

Figure 81. Propellant Consumption (25 km Bandwidth, 320 N Thrust)

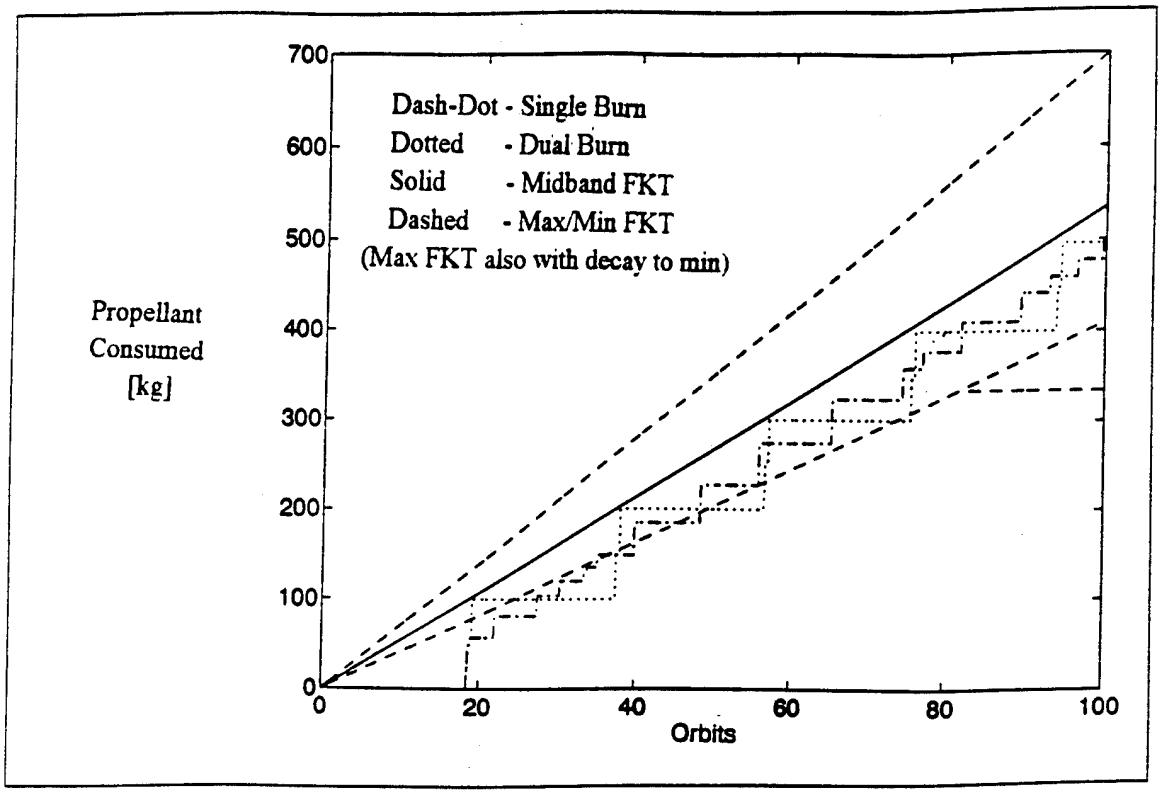

Figure 82. Propellant Consumption (25 km Bandwidth, 640 N Thrust)

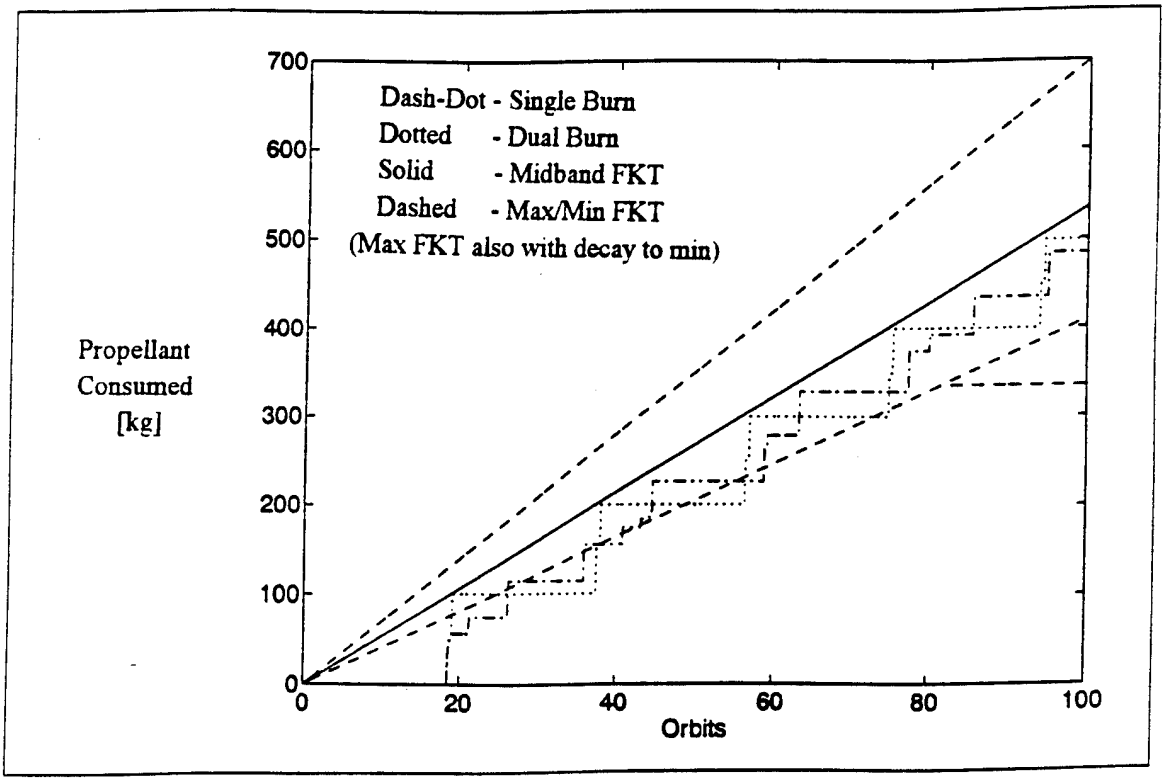

Figure 83. Propellant Consumption (25 km Bandwidth, 1280 N Thrust)

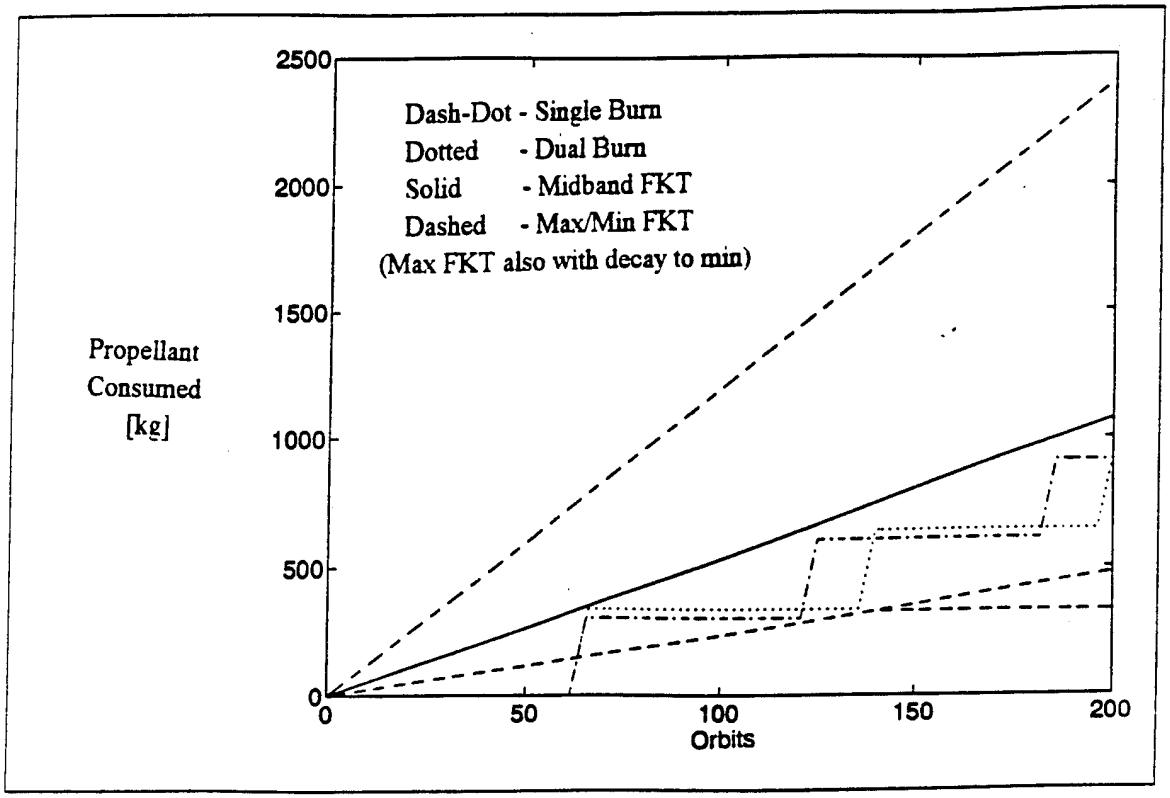

Figure 84. Propellant Consumption (75 km Bandwidth, 40 N Thrust)

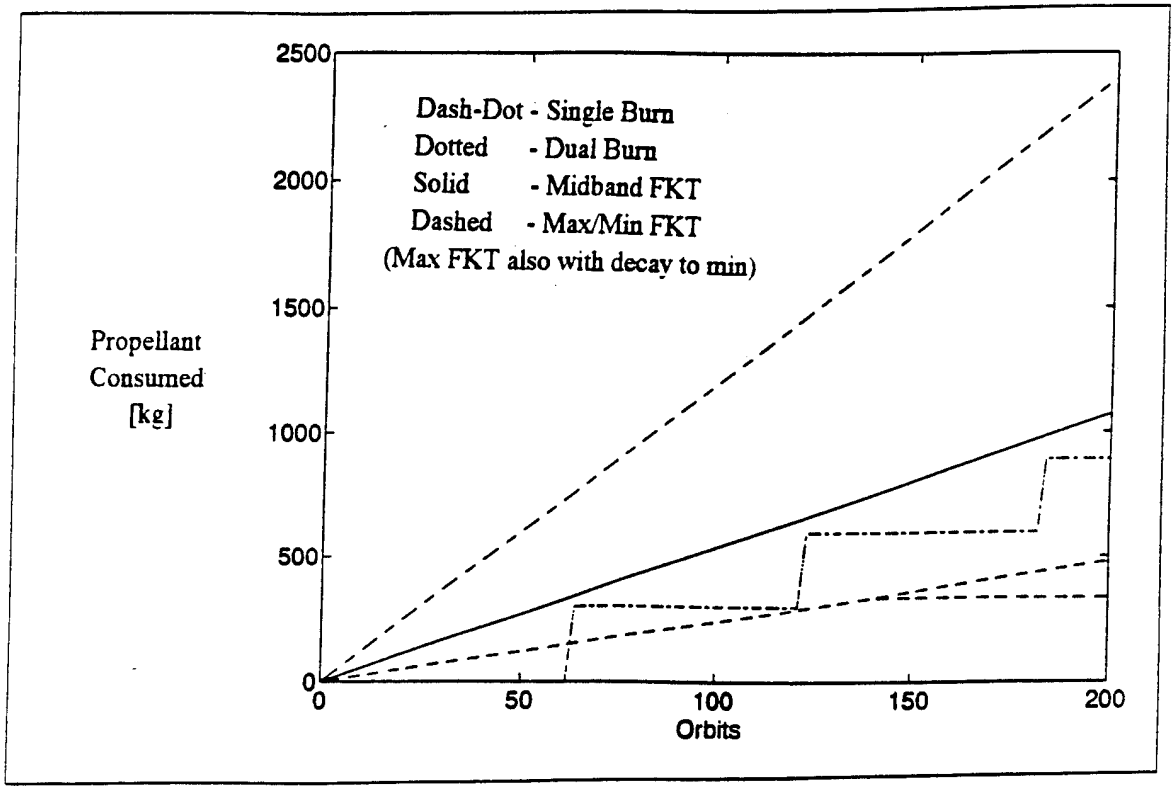

Figure 85. Propellant Consumption (75 km Bandwidth, 80 N Thrust)

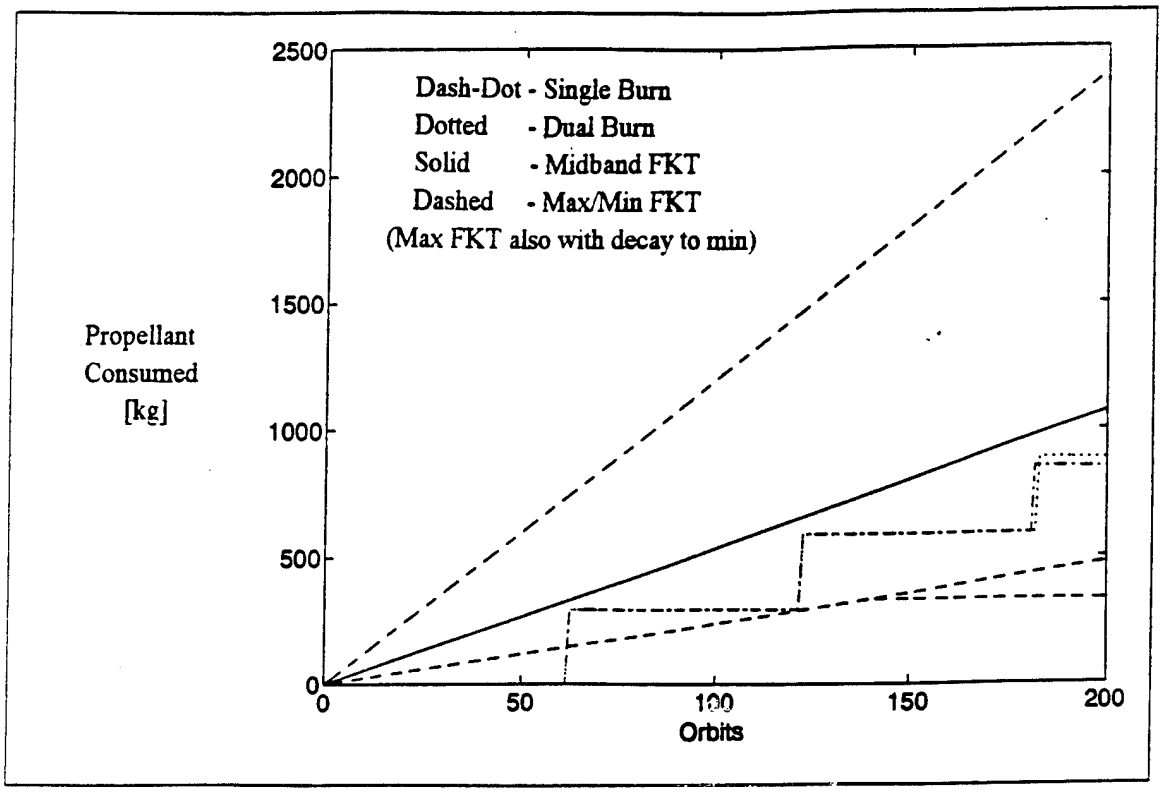

Figure 86. Propellant Consumption (75 km Bandwidth, 160 N Thrust)

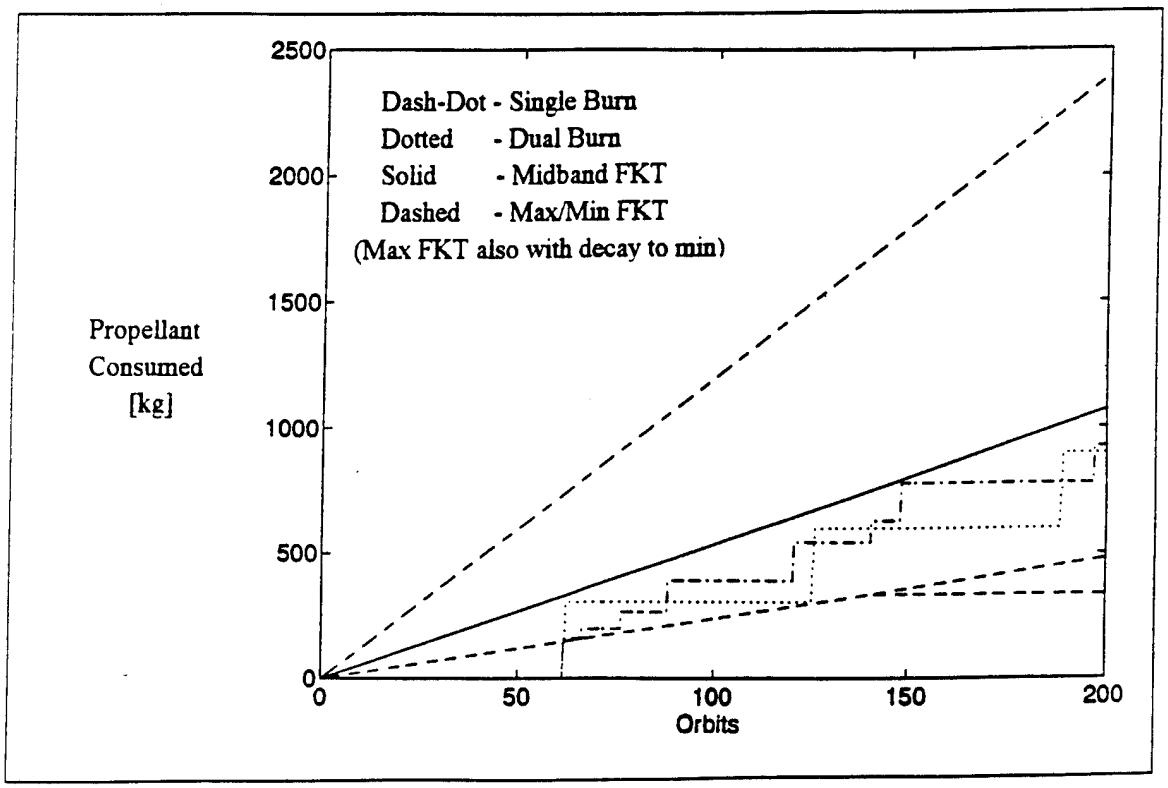

Figure 87. Propellant Consumption (75 km Bandwidth, 320 N Thrust)

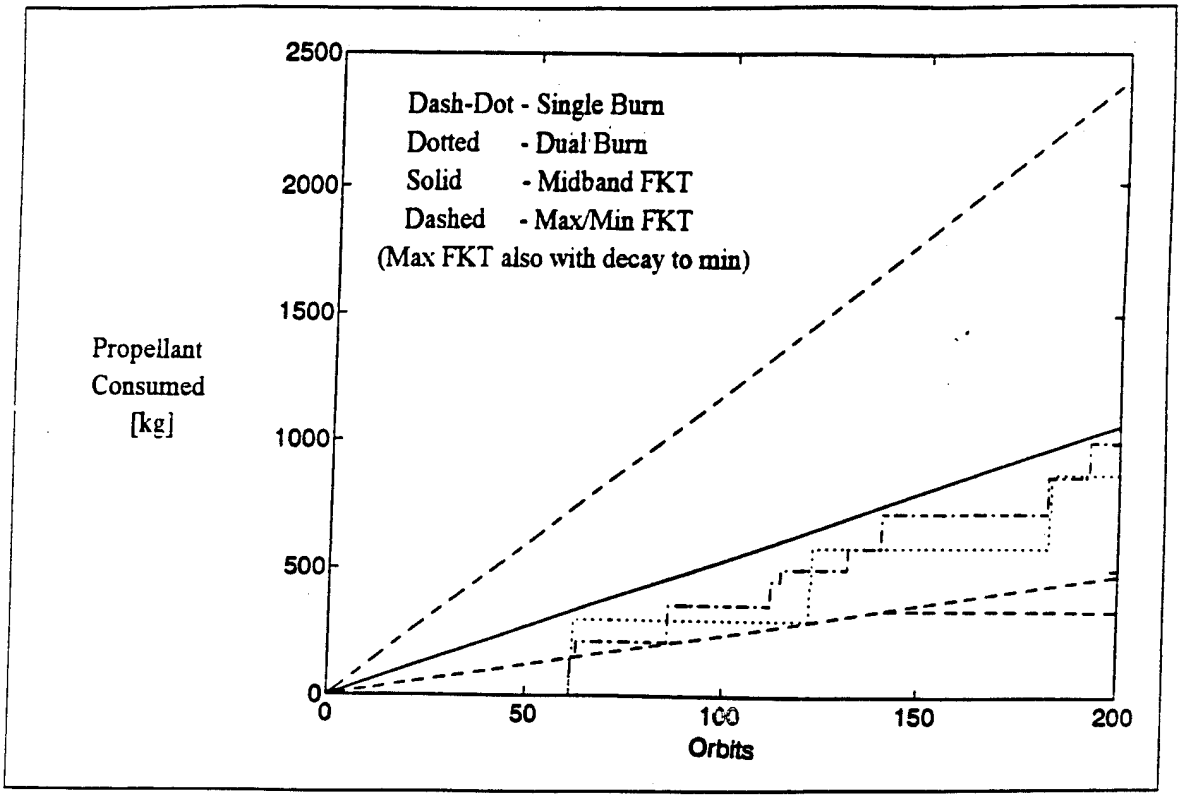

Figure 88. Propellant Consumption (75 km Bandwidth, 640 N Thrust)

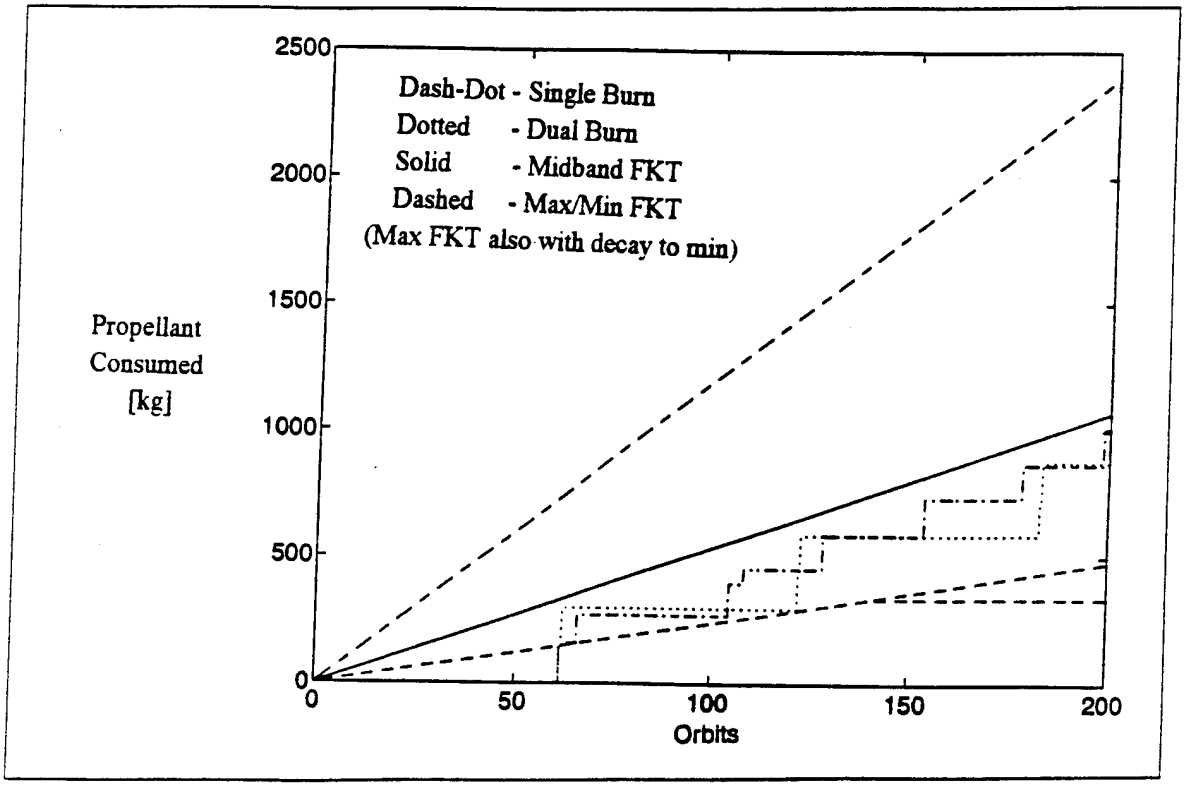

Figure 89. Propellant Consumption (75 km Bandwidth, 1280 N Thrust)

VI. CONCLUSIONS AND RECOMMENDATIONS

The purpose of this thesis was to develop a new thruster firing control logic for either a single burn or dual burn maneuver that successfully maintained an orbital band while achieving propellant efficiency approaching or exceeding that of forced Keplerian motion. Nondimensionalization of the equations permitted more accurate computation and easier visualization in variation of parameters. Results indicate that both strategies are roughly as efficient as a midband FKT, but less efficient than an upper limit FKT or an upper limit FKT with decay to minimum radius at end of life. Reducing the eccentricity with a second burn increases the period between boosting burns, but does not reduce propellant consumption.

The question of optimality of thrust cant angle is opened again, based on the new thruster firing control logic. Earlier efforts using the instantaneous radius and osculating specific energy indicated that a high angle was required to keep a vehicle within a radial band, and that low angles were incapable of constraining the radius. Thrusting along the transverse axis using the osculating perigee and apogee radii as initiator and terminator, respectively, is capable of orbital band maintenance and significantly more efficient than previous methods.

In a separate but related strategy an additional burn, based on the flight path angle as the vehicle approaches apogee, reduces the osculating orbital eccentricity, allowing a near-circular decay pattern to develop. The additional thrusting raises the perigee radius, enabling a longer time between orbit boosting maneuvers. The single and dual burn maneuvers are equally effective at band maintenance and propellant consumption, but the second method provides a potentially more desirable orbital pattern.

It is unclear which FKT model is the appropriate baseline to compare orbital band maintenance maneuvers on. At the low altitude of the band the FKT solution consumes more propellant because it is fighting a denser atmosphere. Likewise, the high altitude case and any derivatives from it have the benefit of having a significantly rarefied medium

to travel through, and require less propellant. The midband version is not the most efficient, thus its validity as the basis for comparison is also questionable.

The results of this thesis indicate several areas for future research:

(1) For apogee rasing burns fire the thruster only when the satellite is at perigee. The initial burn in both methods takes place when the osculating perigee reaches the minimum radial limit, regardless of the position of the vehicle with respect to perigee. Examining at each occurring perigee the radial decay from the previous perigee, and firing the thruster if the drop in altitude is larger than the remaining distance to the lower altitude limit could reduce propellant consumption.

(2) Refining the thruster initiation for the second burn. Modification of the scaling factor or exploration of other controlling functions could improve the performance.

(3) Coupling EITAG with a control logic and an orbital propagator. The resulting propellant consumption and band maintenance could then be compared with FKT, Pauls-Wilsey and this method.

(4) The effect varying the specific impulse has on band maintenance and propellant consumption.

Finally, additional control strategies not discussed here possibly exist that could provide the answer to the optimal control of orbital band maintenance.

APPENDIX

A. MAIN PROGRAM LISTING

```
% MAIN PROGRAM


% Variable Definitions

% a        = Semi-Major Axis
% alphad   = Thrust Angle wrt LH [degrees]
% alphar   = Thrust Angle wrt LH [radians]
% alto     = Midband Altitude [km]
% B        = Ballistic Coefficient [kg/m^2]
% Bbar     = Nondimentionalized Ballistic Coefficient
% beta     = Atmospheric Scale Height
% D        = Drag [N]
% Dbar     = Nondimentionalized Drag
% df       = Drag Factor
% dv       = Change in Velocity [m/s]
% dz       = Orbital Bandwidth [km]
% DK       = FKM Drag [N]
% e        = Eccentricity
% Esmax    = Maximum Specific Energy at Maximum Radius [J/kg]
% Esmin    = Minimum Specific Energy at Minimum Radius [J/kg]
% Es       = Specific Energy [J/kg]
% Eso      = Initial Specific Energy [J/kg]
% Et       = Total Energy [J]
% g        = Standard Earth Gravity [m/s^2]
% gammad   = Flight Path Angle wrt LH [degrees]
% gammar   = Flight Path Angle wrt LH [radians]
% Gnot     = Base Flight Path Firing Angle [radians]
% Gto      = Modified Flight Path Firing Angle [radians]
% h        = Angular Momentum [km^2/s]
% Isp      = Specific Impulse [s]
% L        = Local Computational Variables
% lambda   = Modified Thrust Firing Scaling Factor
% lfactor  = Length Conversion Factor [1000 m/km]
% m        = Spacecraft Mass [kg]
% mbar     = Nondimentionalized Mass
% mf       = Mass of Fuel Burned in Time Increment [kg]
% mfK      = FKM Mass of Fuel Burned in Time Increment [kg]
% mft      = Total Mass of Fuel Burned [kg]
% mftK     = FKM Total Mass of Fuel Burned [kg]
% mnd      = Arbitrary Mass Used for Nondimentionalization [kg]
% mo       = Initial Spacecraft Mass [kg]
% orbits   = Number of Orbits Completed
% ra       = Apogee Radius [km]
% rho      = Calculated Atmospheric Density [kg/m^3]
% rhoalt   = Reference Atmospheric Density Altitude [km]
% rhofac   = Density Variation Factor
% rhonot   = Reference Atmospheric Density [kg/m^3]
% rhostd   = Standard Earth Density [kg/m^3]
% Rmax     = Maximum Radius of Band [km]
% Rmin     = Minimum Radius of Band [km]
```

```
% Rminb     = Nondimentionalized Minimum Radius of Band
% ro        = Initial Orbital Radius [km]
% rp        = Perigee Radius [km]
% t         = Time [orbits]
% TBW       = Base Thrust-Bandwidth Scale Factor
% Te        = Earth's Surface Rotational Period [s]
% tf        = Final Step Time [s]
% tfl       = Thrust Firing Logic Selector
% Th        = Thrust [N]
% Thbar     = Nondimentionalized Thrust
% thetad    = Angle from Reference Axis [degrees]
% thetar    = Angle from Reference Axis [radians]
% ThK       = FKM Thrust [N]
% Thm       = Maximum (Blowdown) Thrust [N]
% Thmbar    = Nondimentionalized Maximum (Blowdown) Thrust
% tinc      = Increment of Time (Step Size) [s]
% tol       = Tollerance Value for Computation
% Tpo       = Initial Orbital Period [s]
% Tp        = Orbital Period [s]
% tstart    = Start Time [s]
% tstop     = Stop Time [s]
% V         = Velocity [km/s]
% Vbar      = Nondimentionalized Velocity
% Vimax     = Maximum Velocity at Present Orbit [km/s]
% Vimin     = Minimum Velocity at Present Orbit [km/s]
% Vmax      = Maximum Velocity at Maximum Radius [km/s]
% Vmin      = Minimum Velocity at Minimum Radius [km/s]
% Vprev     = Previous Velocity [km/s]
% x(1)      = Orbital Radius [km]
% x(2)      = Orbital Radial Velocity [km/s]
% x(3)      = Orbital Theta
% x(4)      = Orbital Angular Velocity [1/s]
% xbar(1)   = Nondimentionalized Orbital Radius
% xbar(2)   = Nondimentionalized Orbital Radial Velocity
% xbar(3)   = Nondimentionalized Orbital Theta
% xbar(4)   = Nondimentionalized Orbital Angular Velocity
% xbdot(1)  = Time Derivative of xbar(1)
% xbdot(2)  = Time Derivative of xbar(2)
% xbdot(3)  = Time Derivative of xbar(3)
% xbdot(4)  = Time Derivative of xbar(4)


clear all


% Constants

mu       = 3.98601208133E5; % Earth's Gravitational Parameter
                            % [km^3/s^2]
g        = 9.806;           % Gravity at Earth's Surface
                            % [m/s^2]
Re       = 6378.145;        % Earth's Radius
                            % [km]
dtor     = pi/180;          % Change Degrees to Radians
lfactor  = 1000;            % Convert km to m
tol      = 1e-6;
```

```
icount    = 1:4;              % State Variable Numbers


% Independent Variable Initialization

alto      = 260.0;
dz        = 25.0;
a         = Re+alto+dz/2;
alphad    = 0.0;
B         = 150.0;
betal     = 46.9;
df        = 1.0;
dv        = 0.0;
e         = 0.00;
Isp       = 300.0;
index     = 1;
mo        = 20000.0;
mnd       = 20000.0;
rhoalt    = 250.0;
rhostd    = 7.248e-11;
rhofac    = 12.47;
rhonot    = rhofac*rhostd;
Te        = 2*pi*(((Re^3)/mu)^0.5);
thetad    = 180.0;
Thm       = 320.0;
Thfact    = 1.0;
tinc      = 0.001;
tstart    = 0.0;
tstop     = 100;
t         = tstart;
tfl       = 0;
Gnot      = 20e-6
TBW       = 10;
lambda    = TBW/(Thm/dz^2);
Gto       = lambda*Gnot;
tol       = 1e-14;
shoodi    = 0;
doozit    = 100;


% Initialize Orbital Element Variables

thetar    = thetad*dtor;
ra        = a*(1+e);
ro        = (a*(1-e^2))/(1+e*cos(thetar));
rp        = a*(1-e);
Tpo       = 2*pi*sqrt((a^3)/mu);
V         = sqrt((2*mu/ro)-(mu/a));
ao        = a;
x(1)      = ro;
x(2)      = e*(sin(thetar))*sqrt(mu/(a*(1-e^2)));
x(3)      = thetar;
x(4)      = (sqrt(a*mu*(1-e^2)))/(x(1)^2);
xbar(1)   = x(1)/ao;
```

```
xbar(2)   = (Tpo*x(2))/ao;
xbar(3)   = x(3);
xbar(4)   = (Tpo*x(4));
Eso       = ((V^2)/2-mu/ro);
Et        = mo*Eso;
Es        = Eso;

% Initialize Satellite Variables


m         = mo;
alphar    = alphad*dtor;
mbar      = m/mnd;
Thmbar    = (Thm*Tpo^2)/(mnd*ao*lfactor);
Bbar      = B/(rhonot*ao*lfactor); % m/km
Thbar     = 0.0;
mft       = 0.0;
mftK      = 0.0;


% Initialize Altitude Band Constraint Variables

Rmax      = ro+dz/2;
Rmin      = ro-dz/2;
Rminb     = Rmin/ao;
Vmax      = (mu/Rmax)^0.5;
Vmin      = (mu/Rmin)^0.5;
Esmax     = ((Vmax^2)/2)-(mu/Rmax);
Esmin     = ((Vmin^2)/2)-(mu/Rmin);
gammar    = atan(xbar(2)/(xbar(1)*xbar(4)));
norbs(1)  = 0;
Vimax(1)  = Vmax;

orad(1)   = ro;
oV(1)     = V;
ogr(1)    = 0.0;
oh(1)     = ro^2*x(4);
oEs(1)    = Es;
oe(1)     = e;
oa(1)     = a;
ora(1)    = ra;
orp(1)    = rp;
oTp(1)    = Tpo;
tflm(1)   = 0;


% Set Forced-Keplerian Motion Drag

rK(1)          = (ro-dz/2)/ao;
vK             = Tpo*sqrt((2*mu/(rK(1)*ao))-(mu/(rK(1)*ao)))/a0;
[rho, Dbar]    = leodrag(rK, ao, rhoalt, Re, beta, vK, Bbar, df);
DK             = Dbar*mnd*ao*lfactor/(Tpo^2); % 1000 m/km
```

```
% Main Program

while t <= tstop,

  while index <= 4,

    % Determine Nondimentionalized Velocity

    [Vbar] = leovel(xbar);

    % Determine Nondimentionalized Drag

    [rho, Dbar] = leodrag(xbar, ao, rhoalt, Re, beta, Vbar, Bbar, df);

    % Determine Local Variables

    [L(1), L(2), L(3), L(4), L(5), L(6), L(7)] = leolocal(xbar, mbar,
         Vbar, Thbar, Dbar, alphar);

    % Determine Positional Differential Values

    [xbdot(1), xbdot(2), xbdot(3), xbdot(4)] = leoxdot(xbar, L);

    % Perform RK4

      if index == 1

         [xbt, xbdt, xbart] = leork4a(icount, xbar, xbdot, tinc);

      elseif index == 2

         [xbdt, xbart] = leork4b(icount, xbt, xbdt, xbdot, tinc);

      elseif index == 3

         [xbdt, xbart] = leork4c(icount, xbt, xbdt, xbdot, tinc);

      else

         [xbart] = leork4d(icount, xbt, xbdt, xbdot, tinc);

      end

      xbar(icount) = xbart(icount);

   if rem(index, 2) == 1

      t = t+0.5*tinc;
```

```
  end

  index = index+1;

end

% Reset index value

index = 1;


% Compute Propellant Consumption

Th    = Thbar*mnd*ao*lfactor/(Tpo^2);
mf    = Th*tinc*Tpo/(Isp*g);
m     = m-mf;
mft   = mft+mf;
mfK   = DK*tinc*Tpo/(Isp*g);
mftK  = mftK+mfK;
mbar  = m/mnd;


% Increment Output Counter

shoodi = shoodi+1;


% Store Propellant Consumption


if rem(shoodi,doozit) == 0

   mtv(fix(shoodi/doozit)+1) = mft;
   mtKv(fix(shoodi/doozit)+1) = mftK;
   mrat(fix(shoodi/doozit)+1) = mft/mftK;
   tflm(fix(shoodi/doozit)+1)=tfl;

 end


% Determine Orbit Parameters

eprev = e;
grp=gammar;
Vprev = V;
[r, V, gammar, h, Es] = leoparm1(xbar, Tpo, ao, mu);
[e, a, ra, rp, Tp] = leoparm2(Es, h, mu);


% Thruster Firing Evaluation

  if tfl == 2

     if ra-r < r-rp
```

```
            tfl = 3;
         end
      end
      if tlf == 3
         if Thbar > 0
            if gammar-grp >= 0
               tfl = 1;
            end
         end
      end
      if tfl == 0
         [Thval, tfl] = leotflph(rp, Rmin, ra, Rmax, Thbar, Thmbar);
      elseif rem (tfl,2) == 1
         [Thval, tfl] = leotflapn(gammar, grp, V, Thbar, Thmbar, tfl,
                     Gto);
      end
      Thbar = Thval*Thfact;

   if tfl == 4
      tfl = 0;
   end
   if e < tol
      e = 0;
   end

% Output
if rem(shoodi,doozit) == 0
   orad(fix(shoodi/doozit)+1)    = r;
   oV(fix(shoodi/doozit)+1)      = V;
   ogr(fix(shoodi/doozit)+1)     = gammar;
   oh(fix(shoodi/doozit)+1)      = h;
```

```
    oEs(fix(shoodi/doozit)+1)     = Es;
    oe(fix(shoodi/doozit)+1)      = e;
    oa(fix(shoodi/doozit)+1)      = a;
    ora(fix(shoodi/doozit)+1)     = ra;
    orp(fix(shoodi/doozit)+1)     = rp;
    oTp(fix(shoodi/doozit)+1)     = Tp;
    Thrst(fix(shoodi/doozit)+1)   = Thbar;
    oang(fix(shoodi/doozit)+1)    = xbar(3);

  % Increment Number of Orbits

     norbs(fix(shoodi/doozit)+1)=(xbar(3)-x(3))/(2*pi);

     end

if rem(shoodi,10*doozit) == 0

   norbs(fix(shoodi/doozit)+1)

end

end
end
```

B. VELOCITY SUBROUTINE LISTING

```
% NONDIMENTIONALIZED VELOCITY COMPUTATION

% Establish as Function

function [Vbarest] = leovel(xbar)

% Compute Nondimentionalized Velocity

Vbarest      = ((xbar(2))^2+(xbar(1)*xbar(4))^2)^0.5;

return

end
```

C. DRAG SUBROUTINE LISTING

```
% NONDIMENTIONALIZED DRAG COMPUTATION

% Establish as Function

function [rhogess, Dbarest] = leodrag(xbar, ao, rhoalt, Re, beta, Vbar,
                  Bbar, dfact)

% Determine Density Exponential Term

rhogess = exp(-((xbar(1)*ao-Re)-rhoalt)/beta);
```

```
% Compute Nondimentionalized Drag

Dbarest      = (dfact*rhogess*Vbar^2)/(2.0*Bbar);

return

end
```

D. LOCAL CONTRIBUTION SUBROUTINE LISTING

```
% LOCAL CONTRIBUTION SUBROUTINE

% Establish as Function

function [L1, L2, L3, L4, L5, L6, L7] = leolocal(xbar, mbar, Vbar,
                  Thbar, Dbar, alphar)

% Define Local Computational Variables

L1      = xbar(1)*xbar(4)*xbar(4);
L2      = 4.0*pi*pi/(xbar(1)*xbar(1));
L3      = (Dbar*(xbar(2)/Vbar))/mbar;
L4      = (Thbar*sin(alphar))/mbar;
L5      = (2.0*xbar(4)*xbar(2))/xbar(1);
L6      = (Dbar/(xbar(1)*mbar))*((xbar(1)*xbar(4))/Vbar);
L7      = (Thbar*cos(alphar))/(mbar*xbar(1));

return

end
```

E. DIFFERENTIAL VALUES SUBROUTINE LISTING

```
% POSITIONAL DELTA VALUES ROUTINE

% Establish as Function

function [dx1, dx2, dx3, dx4] = leoxdot(xbar, L)


% Compute Positional Delta Values

dx1     = xbar(2);
dx2     = L(1)-L(2)-L(3)+L(4);
dx3     = xbar(4);
dx4     = -L(5)-L(6)+L(7);

return

end
```

F. RUNGE-KUTTA SUBROUTINE LISTINGS

```
% RUNGE-KUTTA 4TH ORDER COMPUTATION

% Establish as Function

function [xbtemp, xbdtemp, nxbar] = leork4a(count, txbar, txbdot, tminc)

% Perform first part of RK4

xbtemp(count)   = txbar(count);
xbdtemp(count)  = txbdot(count);
nxbar(count)    = xbtemp(count)+0.5*tminc*txbdot(count);


% RUNGE-KUTTA 4TH ORDER COMPUTATION

% Establish as Function

function [xbdtemp, nxbar] = leork4b(count, txbar, txbdot, xbdot, tminc)

% Perform second part of RK4

xbdtemp(count)   = txbdot(count)+2.0*xbdot(count);
nxbar(count)     = txbar(count)+0.5*tminc*xbdot(count);


% RUNGE-KUTTA 4TH ORDER COMPUTATION

% Establish as Function

function [xbdtemp, nxbar] = leork4c(count, txbar, txbdot, xbdot, tminc)

% Perform third part of RK4

xbdtemp(count)   = txbdot(count)+2.0*xbdot(count);
nxbar(count)     = txbar(count)+tminc*xbdot(count);


% RUNGE-KUTTA 4TH ORDER COMPUTATION

% Establish as Function

function [nxbar] = leork4d(count, txbar, txbdot, xbdot, tminc)

% Perform fourth part of RK4

nxbar(count)     = txbar(count)+tminc*(xbdot(count)+txbdot(count))/6;
```

G. ORBITAL PARAMETER SUBROUTINE LISTINGS

```
% ORBITAL PARAMETERS

% Define as Function
```

```
function[Pr, PV, Pgammar, Ph, PEs] = leoparm1(xbar, Tpo, ao, mu)
% Compute Orbital Parameters
% Radius
Pr = xbar(1)*ao;
% Velocity
PV = (ao*(((xbar(2))^2+(xbar(1)*xbar(4))^2)^0.5))/Tpo;
% Flight Angle
Pgammar = atan(xbar(2)/(xbar(1)*xbar(4)));
% Angular Momentum
Ph = Pr*PV*cos(Pgammar);
% Specific Energy
PEs = (((PV^2)/2)-(mu/Pr));
return
end

% ORBITAL PARAMETERS
% Define as Function
function[Pe, Pa, Pra, Prp, PTp, PVimin, PVimax] = leoparm2(Es, h, mu)
% Compute Orbital Parameters
% Eccentricity
etest = 1.0+2.0*Es*((h/mu)^2);
Pe = sqrt(etest);
% Semi-major Axis
Pa = (-mu/(2.0*Es));
% Apogee Radius
Pra       = Pa*(1+Pe);
% Perigee Radius
Prp       = Pa*(1-Pe);
```

```
% Period
PTp        = 2.0*pi*(sqrt((Pa^3)/mu));
% Minmum Velocity
PVimin     = ((mu*(1+Pe))/(Pa*(1-Pe)))^0.5;
% Maximum Velocity
PVimax     = ((mu*(1-Pe))/(Pa*(1+Pe)))^0.5;
return
end
```

H. THRUSTER CONTROL SUBROUTINE LISTINGS

```
% THRUSTER FIRING DETERMINATION ROUTINE
% Establish as Function
function [Thrust, tfl] = leotflph(Rp, Rmin, Ra, Rmax, Th, Thmax)
% Thruster Firing Law
% Initialize Thrust Logic
tl = 0;
% Turn Thrusters Off
  if Thcheck == Thmax
%    Check Apogee Radius
      if Ra >= Rmax
         Thcheck = 0.0;
         tl = 2;
      end
  end

% Turn Thrusters On
  if tl == 0
     if Rp <= Rmin
        Thcheck = Thmax;
```

```
    end
  end
Thrust = Thcheck;
tfl = tl;
return
end

% THRUSTER FIRING DETERMINATION ROUTINE
% Establish as Function
function [Thrust, tfl] = leotflapn(gammar, grp, V, Thcheck, Thmax, tl,
                  Gval)
% Thruster Firing Law
% Turn Thrusters Off
  if tl == 1
%    Check Flight Angle
%      Turn Thrusters Off
       if gammar >= grp
          Thcheck = 0.0;
          tl = 4;%0
       end
  end

% Turn Thrusters On
  if tl == 3
    if gammar >=0
       if gammar <= Gval
           Thcheck = Thmax;
       end
    end
  end
```

```
Thrust = Thcheck;
tfl = tl;

return
end
```

LIST OF REFERENCES

1. Ross, I. M. and Melton, R. G., *Singular Arcs For Blunt Endoatmospheric Vehicles,* Proceedings of the AIAA/AAS Astrodynamics Conference, Portland, Oregon, August 20-22, 1990, AIAA Paper # 90-2974.

2. Gottlieb, R. G. , *Eccentricity-Intercept Targeting and Guidance (EITAG),* Reboost Guidance and Targeting Algorithm, TM-FM9-LA-42, 8/14/89.

3. Pauls, D. D., *Orbital Maintenance of Endoatmospheric Low Earth-Orbiting Satellites,* Master's Thesis, Naval Postgraduate School, Monterey, California, December 1991.

4. Wilsey, M. S., *A Parametric Analysis of Endoatmospheric Low-Earth-Orbit Maintenance*, Master's Thesis, Naval Postgraduate School, Monterey, California, March 1993.

5. Gardner, P. A., *An Analysis of a Single-Burn Algorithm for Low-Earth Orbit Maintenance,* Master's Thesis, Naval Postgraduate School, Monterey, California, June 1994.

6. Wertz, J. R., and Larson, W. J. (Eds), *Space Mission Analysis and Design*, Kluwer Academic Publishers, 1991.

7. Zeleny, W. B., *Orbital Mechanics*, Lecture Notes, Naval Postgraduate School, Monterey, California, January 1993.

INITIAL DISTRIBUTION LIST

1.	Defense Technical Information Center Cameron Station Alexandria, Virginia 22304-6145	2
2.	Library, Code 52 Naval Postgraduate School Monterey, California 93943-5101	2
3.	Chairman, Code SP Space Systems Academic Group Naval Postgraduate School Monterey, California 93943-5000	1
4.	Commander, Naval Space Command ATTN: N112 5280 4th Street Dahlgren, Virginia 22448-5300	1
5.	I. M. Ross, Code AA/Ro Naval Postgraduate School Monterey, California 93943-5000	9
6.	T. K. Alfriend, Code SP/Al Naval Postgraduate School Monterey, California 93943-5000	1
7.	Andrew A. Hernandez 100 Carissa Drive Satellite Beach, Florida 32937	1